2014

The Optimization of Offshore Wind Turbine Towers Using Passive Tuned Mass Dampers

ONUR CAN YILMAZ
Mech. and Industrial Eng. Dept., oyilmaz@engin.umass.edu

THE OPTIMIZATION OF OFFSHORE WIND TURBINE TOWERS USING PASSIVE TUNED MASS DAMPERS

A Thesis Presented

by

ONUR CAN YILMAZ

Submitted to the Graduate School of the
University of Massachusetts Amherst in partial fulfillment
of the requirements for the degree of

MASTER OF SCIENCE IN MECHANICAL ENGINEERING

May 2014

Mechanical and Industrial Engineering

THE OPTIMIZATION OF OFFSHORE WIND TURBINE TOWERS USING PASSIVE TUNED MASS DAMPERS

A Thesis Presented

by

ONUR CAN YILMAZ

Approved as to style and content by:

Matthew A. Lackner, Chair

Sanjay R. Arwade, Member

James F. Manwell, Member

Donald. L. Fisher, Department Chair
Mechanical and Industrial Engineering

ABSTRACT

THE OPTIMIZATION OF OFFSHORE WIND TURBINE TOWERS USING PASSIVE TUNED MASS DAMPERS

MAY 2014

ONUR CAN YILMAZ

B.Sc., MARMARA UNIVERSITY

M.S.M.E., UNIVERSITY OF MASSACHUSETTS AMHERST

Directed by: Professor Matthew A. Lackner

Increasing energy demand and carbon emissions have driven the development of alternative energy solutions. One promising technology is wind energy. Wind energy technology developments has advanced substantially since the 1980s. Offshore wind turbines have become a major research focus, due to the promising offshore wind resource. However, challenges in offshore wind energy have arisen due to the additional wave loading and strong wind loads. Structural control systems have been implemented and researched in order to decrease dynamic response of these systems. The previous studies were successful at decreasing fatigue loads in the tower and support structure of offshore wind turbines. Giving these results, it is still unknown if the reduced loading enabled by structural control systems can allow for reduced material costs in the major structural components. This research examines on an offshore wind turbine's tower-monopile structure by adding several configurations of passive tuned mass dampers, while simultaneously reducing the thickness of the structure in

order to reduce costs. A range of candidate tower-monopile systems are created, and simulated in FAST-SC with and without passive tuned mass dampers. Fatigue and ultimate loads are calculated and analyzed. A variety of design criteria are considered including fatigue and ultimate loads, as well as local and global buckling. The results demonstrate that the tower-monopile thickness may be reduced up to 6.2% and still satisfy all design criteria.

TABLE OF CONTENTS

LIST OF TABLES

LIST OF FIGURES

Figure **Page**

CHAPTER 1

INTRODUCTION

1.1 Motivation

Discoveries in science have impacted our world greatly, but as technology advances, the need for energy has grown. Fossil fuels have been consumed during industrialization, but it is known that they have negative effects on our environment, especially with carbon emissions causing global climate change. As a result of this, engineers and entrepreneurs have started to research alternative energy resources.

Wind energy has become more important in the last decade with increasing investment rates compared to other types of alternative energy sources. Wind energy can be classified into two different categories: Onshore wind energy and offshore wind energy. Onshore wind energy costs less than offshore wind energy. However, land limitations and comparably lower wind speeds have lead engineers towards offshore wind energy as well.

Offshore wind energy is a promising technology that could supply a large portion of many countries' energy demand. However turbine, platform, operation and maintenance costs are higher than onshore systems. One of the most expensive part of an ordinary wind turbine is the support structure. It is even more expensive for offshore wind turbines due to the additional substructure below water and the additional loading from the environmental conditions. An offshore wind turbine with a monopile substructure is considered for this study. Since a tower and a monopile substructure have similar physical properties, cost reduction of a tower-monopile might be achieved by minimizing the tower-monopile's mass, but is constrained by the need

to support the rotor-nacelle assembly and resist the combined loading of wind and waves.

Structural control is a method to reduce external loads on a mechanical system. The use of a passive structural control method with tuned mass dampers (TMDs) into a monopile offshore wind turbine has been researched by Lackner and Stewart [44]. Fore-aft fatigue loads were reduced by 10% and side-side fatigue loading was reduced by 66%. With these large reductions of fatigue loading, a new research question arises: Can the cost of a wind turbine tower be reduced when TMD systems that reduce structural vibrations are included in the system?

1.2 Objective

The research presented in this thesis aims to reduce the cost of an offshore wind turbine tower-monopile structure by decreasing its thickness. A structural control subsystem is implemented in order to reduce structural loads, thus potentially enabling the mass and cost reduction of the tower-monopile structure. In particular, the research analyzes whether the increased structural loading due to the mass reduction in a tower-monopile structure can be offset by the reduction in structural loading provided by a passive structural control system.

1.3 Thesis Outline

This thesis is organized as follows. In Chapter 2, a literature review is presented providing background on offshore wind energy and structural control systems. Information from previous studies are utilized to provide context for this study. Chapter 3 explains the IEC Design Standards for an offshore wind turbine. In Chapter 4, the simulation software used in this thesis, FAST-SC, is introduced. An explanation for how a TMD is coupled into the offshore wind turbine system is also provided. Previous studies about tower support structures are then summarized. Next, simulation

parameters are outlined including the details of the process utilized in this research. Chapter 5 presents the results of the study including different design load cases. A conclusion chapter is presented at the end of this thesis.

CHAPTER 2

LITERATURE REVIEW

2.1 Wind Energy Systems

2.1.1 History

The source of wind energy is the sun. The sun's radiation heats different parts of the Earth, which creates temperature differences on the Earth's surface resulting in hot air rising and reducing the atmospheric pressure at those areas. Cooler air replaces the rising hot air and creates wind.

Wind energy has been used by people for centuries. Windmills were the first type of wind machines which were used to convert wind energy into mechanical energy. The history dates back to 644 AD with the findings of vertical axis windmills in Seistan (currently eastern Iran) [32]. Horizontal axis windmills were employed later in 1300-1875 AD in the Netherlands and the Mediterranean regions [26].

Wind turbines that were aimed to generate electricity instead of mechanical power were first used towards the end of 19^{th} century with the innovation of electrical generators. One of the most important development in this transition period was the attempt of Charles Brush to convert an electrical generator into a windmill with a rotor in the United States in 1888. Even though this attempt did not create a new trend, small electrical generators became common in the next several decades. These small turbines were the inspiration of the design of Marcellus Jacobs [32]. The Jacobs turbine had three blades and a real airfoil shape which resembled today's wind turbines, and can be seen in Figure 2.1.

Figure 2.1. The Jacob's wind turbine [32]

The construction of a number of larger wind turbines was seen most notably in Danish wind turbines constructed by Poul La Cour in 1891-1918. He constructed approximately 100 wind turbines in size range of 20-35 kW each. La Cour wind turbines were not used in wind farms, but the electricity that was produced by these turbines was used to produce hydrogen which was used for lighting later [32].

The most notable early large scale wind turbine that was ever built was the Smith-Putnam wind turbine. It was built in Vermont in 1930s with a rotor diameter of 53.3 m, and a rated power of 1.25 MW [32].

Large scale commercial utilization of wind turbines was first investigated by NASA in the 1970s. In 1980, the world's first wind farm consisting of twenty turbines was built in New Hampshire, United States [36]. Although the turbines broke down due to unexpected wind loading, this project was a good experience for the coming years. On the other hand, the first commercial offshore wind farm in the world was built in Denmark in 1991 [36].

Wind technology has experienced an exponential growth in recent years. Wind turbine sizes have been getting larger and technology costs have been decreasing with new improvements. Countries have been developing strategies to switch to wind energy.

2.1.2 Market overview

Wind energy is a growing energy source that is expected to provide 20% of US Energy Demand by 2030 [49]. Other countries have also been investing in wind energy in recent years. The cumulative global installed capacity of wind energy reached 282.5 GW by the end of 2012. Figure 2.2 shows how the installed capacity changed in recent years.

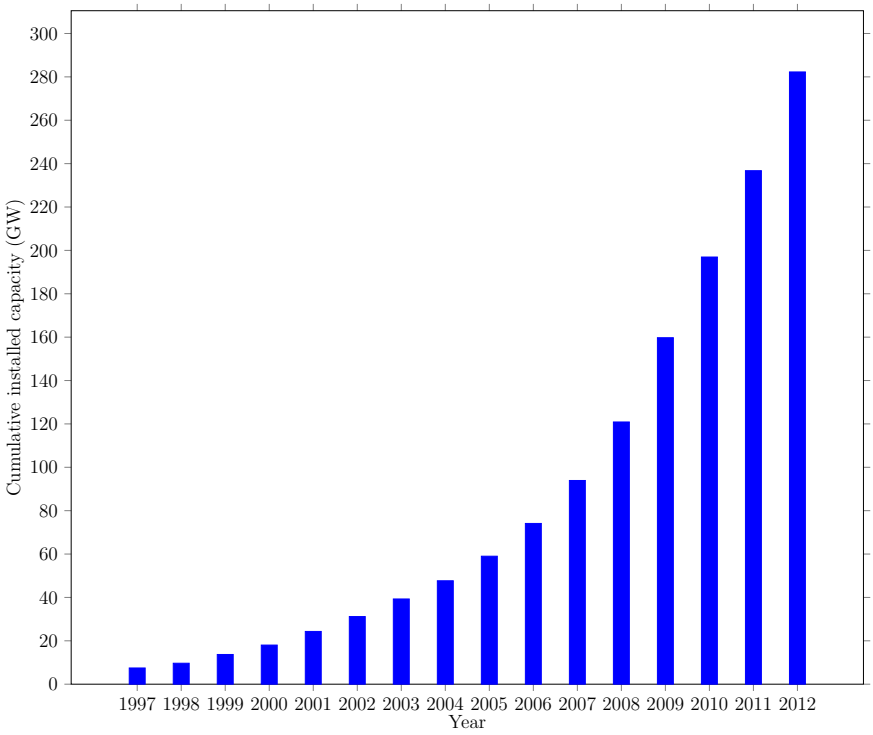

Figure 2.2. Total installed capacity by year [13]

In 2012, 44,609 MW of installed capacity were added in the world which is more than in previous years.

Figure 2.3 shows the distribution of total installed capacity in the world.

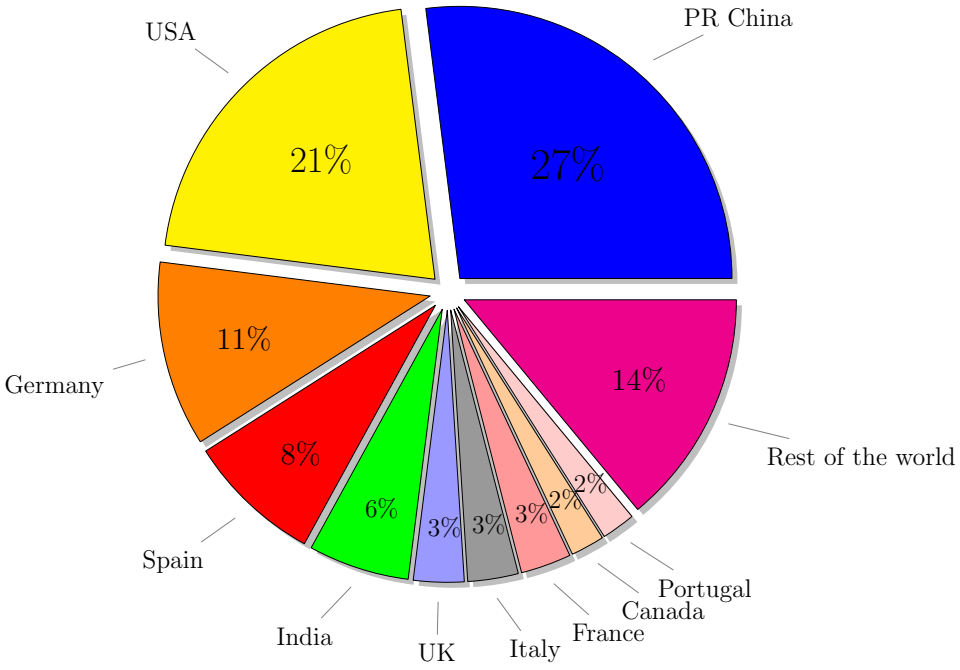

Figure 2.3. Total installed capacity distribution [11]

China leads with a total installed capacity of 75,324 MW followed by the United States with 60,007 MW. Germany, Spain, and India follow with 31,308 MW, 22,796 MW, and 18,421 MW respectively. The share of other countries can be seen in the above figure.

Estimation of the future of wind energy is important for market and product development. Forecasts guide companies and decision makers. Global Wind Energy Council forecasts that total installed capacity will approximately double itself reaching 535.1 GW at the end of 2017 [13]. Figure 2.4 and Table 2.1 shows expected growth by region.

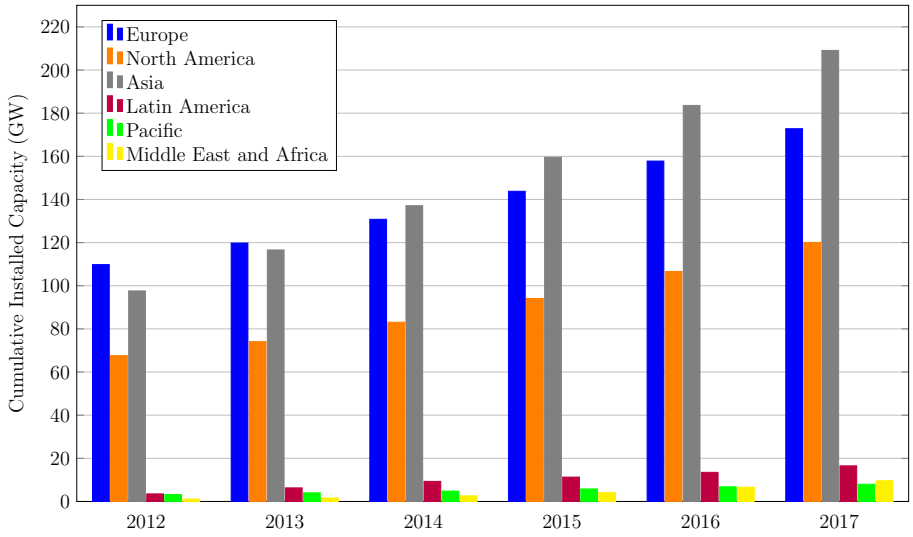

Figure 2.4. Cumulative market forecast by region 2012-2017 [14]

According to Table 2.1, Asia will be the leader with a cumulative installed capacity of 209.1 GW. Europe will follow with a capacity of 172.8 GW. North America will be the third largest market in the world with a total installment of 120.1 GW.

	2012	**2013**	**2014**	**2015**	**2016**	**2017**
Europe	109.8	119.8	130.8	143.8	157.8	172.8
North America	67.6	74.1	83.1	94.1	106.6	120.1
Asia	97.6	116.6	137.1	159.6	183.6	209.1
Latin America	3.5	6.3	9.3	11.3	13.5	16.5
Pacific	3.2	4.0	4.8	5.8	6.8	8.0
Middle East and Africa	1.1	1.6	2.6	4.1	6.6	9.6
Total	**282.8**	**322.4**	**367.7**	**418.7**	**474.9**	**536.1**

Table 2.1. Cumulative market forecast by region 2012-2017 (GW) [14]

When we take a look at offshore wind energy specifically, we see that it has been twenty-two years since the world's first offshore wind turbines were built in Denmark, the Vindeby Project [48]. Offshore wind energy now forms 2% of global wind energy installed capacity. Projections show that 80 GW of offshore wind energy could be

installed globally (mostly in Europe) by 2020. The total installed capacity of offshore wind energy can be seen in Figure 2.5.

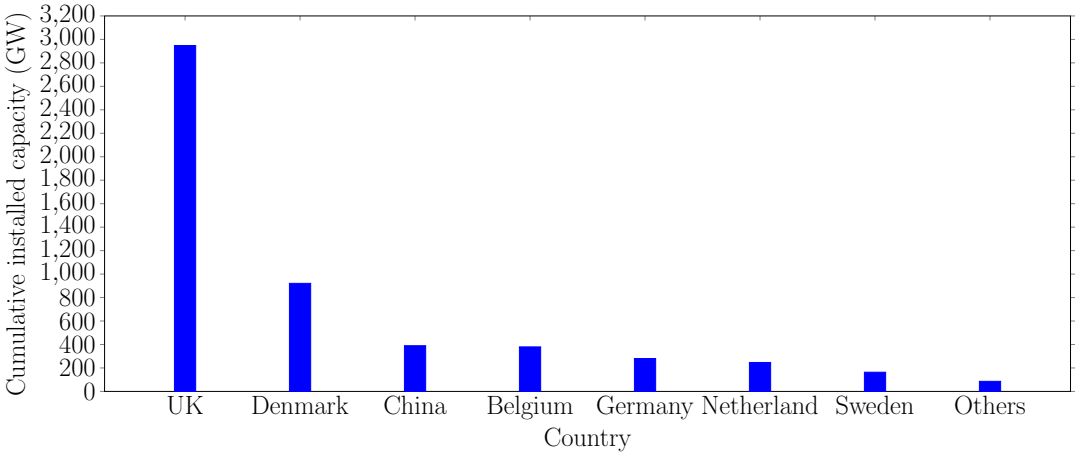

Figure 2.5. Offshore installed capacity by country [13]

The United Kingdom is leading with 2947.9 MW, Denmark and China are following with 921.0 and 389.6 MW, respectively. In the United States offshore wind farms have not been operational yet, but several projects are potential developments. Figure 2.6 shows the projects that are being developed in the US.

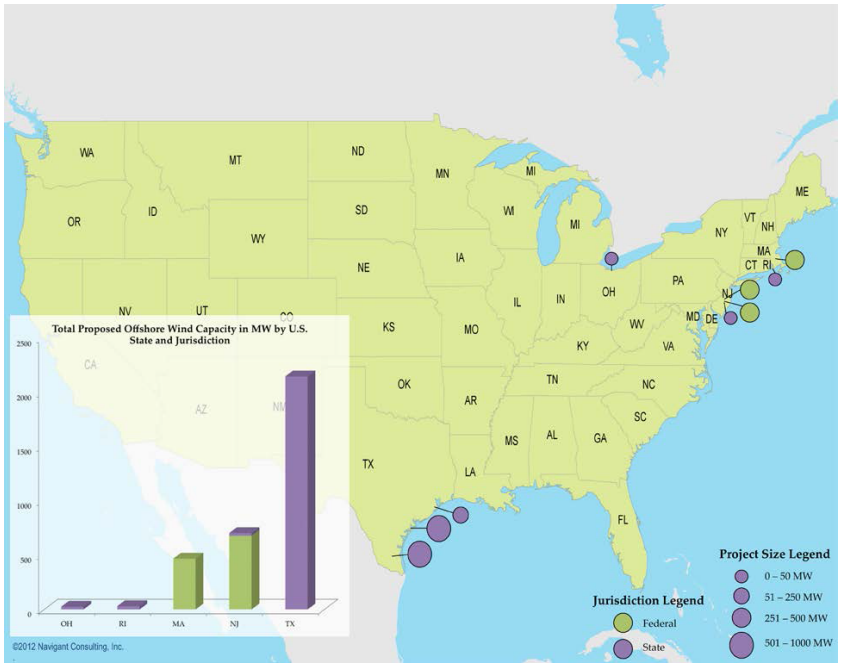

Figure 2.6. Proposed U.S. offshore wind energy projects [34]

Thirty-three offshore wind farm projects have been proposed for the United States. Nine of them with a total of 3,380 MW capacity are in advanced stage when compared to others. However, some difficulties exist for these projects before becoming operational.

2.1.3 Characteristics of a wind turbine

A typical onshore wind turbine's components are the blades, nacelle, generator, gear box, tower, and base. Figure 2.7 illustrates a modern onshore wind turbine.

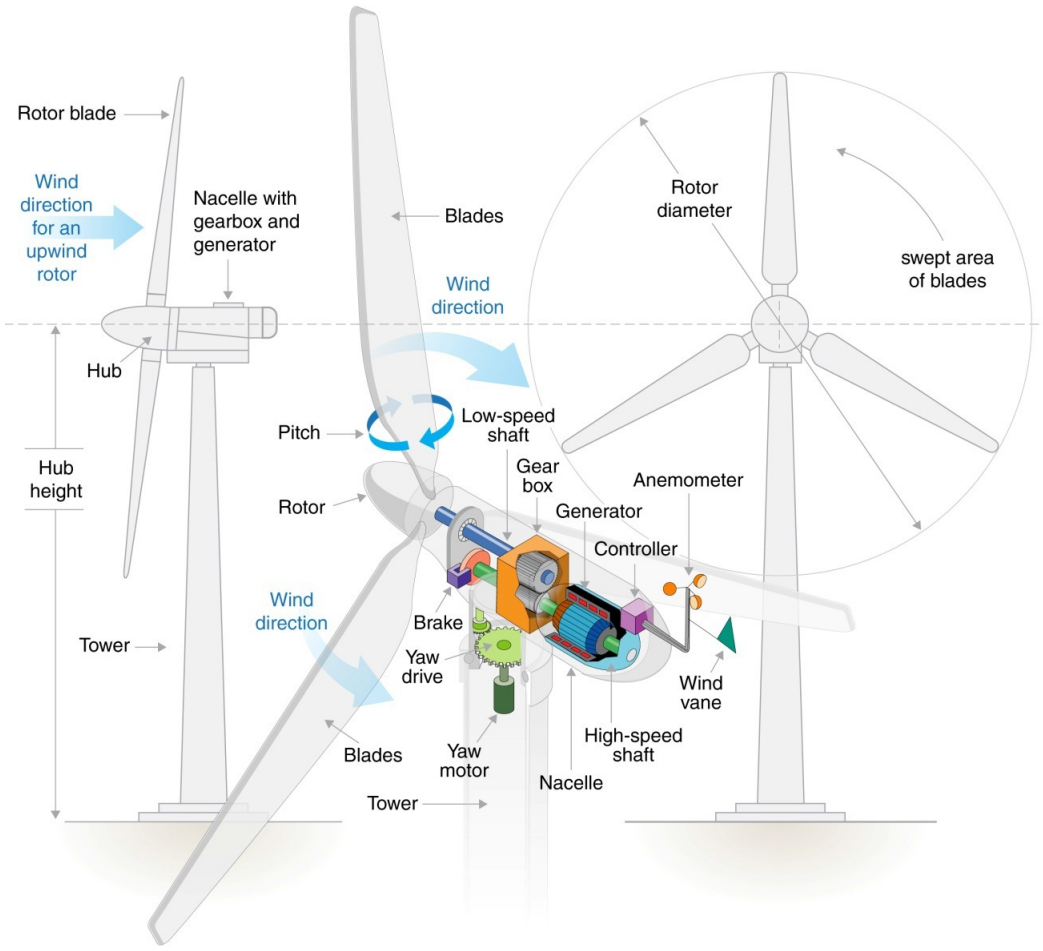

Figure 2.7. Wind turbine components [34]

Blades capture the wind with their aerodynamical design converting kinetic energy in the wind into rotational kinetic energy of the rotor. The nacelle is a place that houses the generator, gearbox and other components. The gearbox increases the rotation speed of the rotor and delivers power to the generator as low torque and high speed. The tower supports the rotor-nacelle assembly and is made of steel in

the shape of a tapered hollow cylinder. It plays a key role in elevating the turbine to higher heights as well.

Conventional wind turbines are three-bladed horizontal axis machines with variable diameters. A modern onshore wind turbine has a diameter range of 70 to 120 meters with a power generation rate of 1.5 MW to 3.0 MW. On the other hand, an offshore wind turbine ranges from 3.0 MW to 6.0 MW with a rotor diameter of around 120 m. The rotor diameter is expected to get larger as the technology and transportation opportunities improve [15]. Figure 2.8 shows the past and future of the rotor diameters sizes.

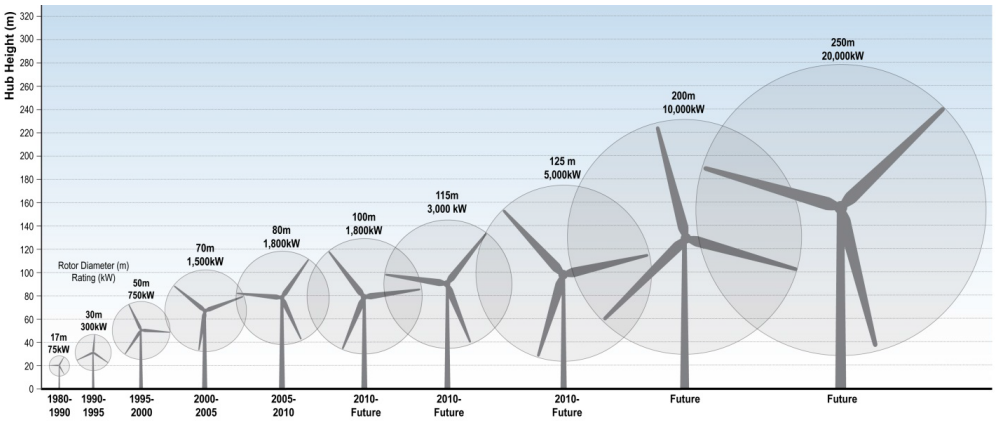

Figure 2.8. Evolution of wind turbine sizes over time [34]

An offshore wind system contains similar parts as an onshore wind system, but requires additional components like substructures and foundations. Parts of an offshore wind turbine can be seen in Figure 2.9.

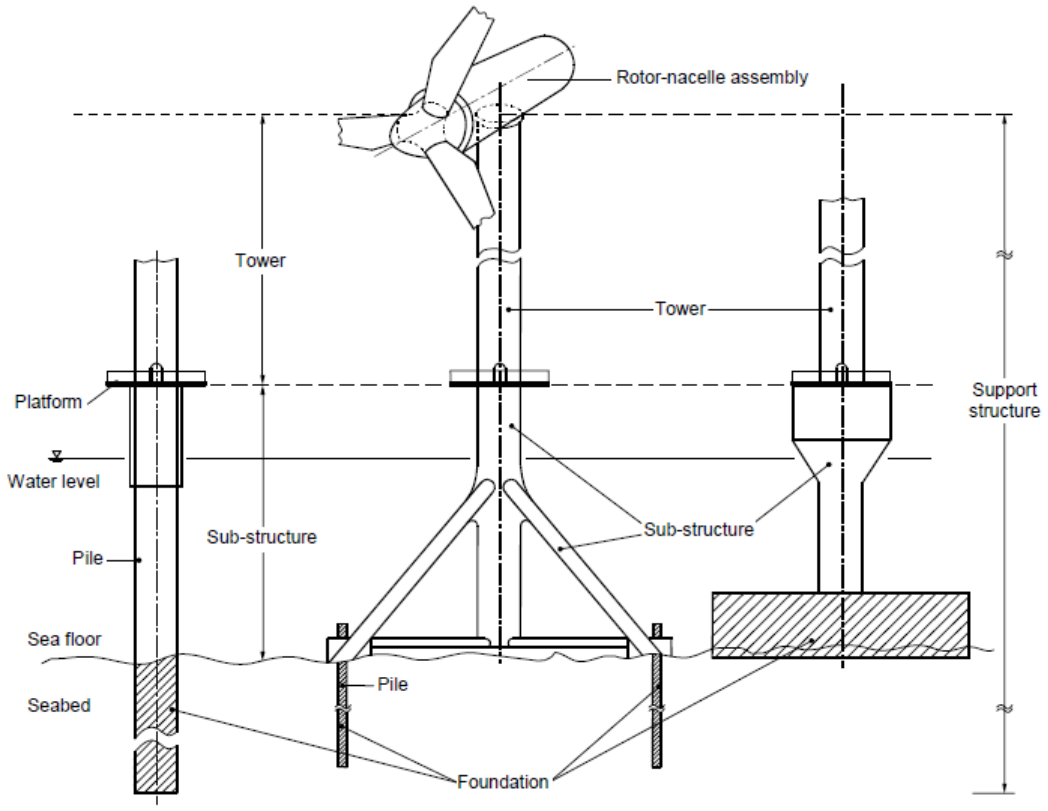

Figure 2.9. Parts of an offshore wind turbine [19]

A foundation is defined as the part that is in contact with soil. A substructure forms the part that is in between the mudline and the tower. A support structure includes the tower, substructure, and foundation. The types of the substructures will be explained in Section 2.2.2.

2.1.4 A brief comparison of onshore and offshore wind energy

While onshore wind energy forms 98% of current installed wind energy capacity, researches and investments focus on offshore wind energy because of its promising capacity. A generalized comparison can be made between onshore and offshore wind energy [48]:

- Large turbine sizes might be more difficult to transport by road for onshore wind energy than offshore wind energy in which the delivery is done by a barge or ship.

- The wind strength is generally reduced over land except in higher elevations. On the other hand, wind is stronger and less turbulent over sea. This leads to higher capacity factors for offshore wind turbines.

- Wind farms are affected by land characteristics in onshore wind turbines. The siting might encounter obstacles including land ownership, hills and mountains. However, offshore wind energy has a freedom in siting when it is compared to onshore. This also affects wind farm capacity. A typical onshore wind farm is probably smaller than 50 MW, while offshore wind farms are almost unlimited and might be larger than 1,000 MW.

Offshore wind energy also has some drawbacks.

- There is less practical experience with offshore wind energy.

- Logistics and foundations are complex and expensive.

- Erection of the turbines is more complicated and can only be done during calm weather.

- Electrical connection challenges exist.

- Maintenance is complex and weather dependent.

2.1.5 Cost breakdown analysis for wind energy systems

The following section presents cost breakdown data for onshore and offshore wind systems. The reference study has been performed by Tegen et.al. [46]. A detailed analysis on the cost of energy calculation has been performed by taking historical trends and future projections into account.

Figure 2.10 shows the installed capital cost breakdown for an onshore wind project. The turbine itself forms 68% of the overall cost. The drivetrain has 37% of the total cost, followed by the rotor, and the tower with 16%, and 15%, respectively. It should be noted that the term "drivetrain" is assumed to include all the other components in the nacelle. The balance of station (23%), and soft costs (9%) are the other cost factors.

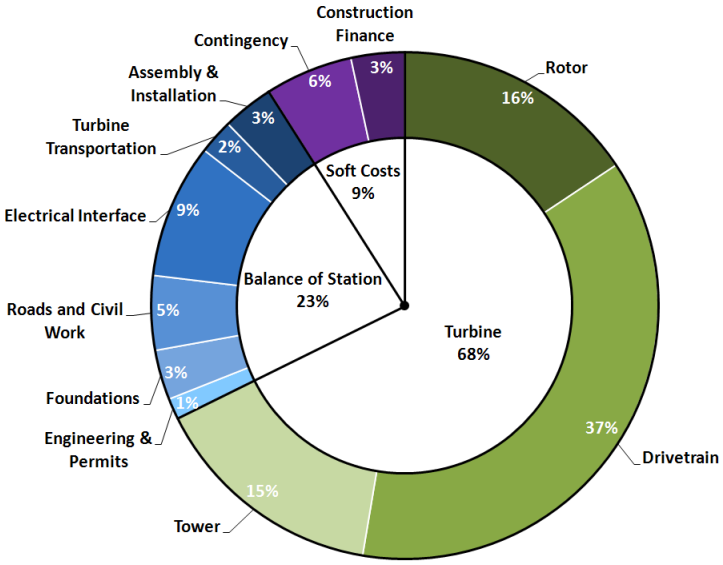

Figure 2.10. Installed capital cost for onshore wind systems [46]

On the other hand, the offshore wind system cost breakdown can be seen in Figure 2.11. It is assumed that the reference offshore wind turbine has a monopile support substructure in this case. Now, the turbine forms 32% of the overall installed cost, and it is dominated by 52% for the balance of station. Soft costs follow with 16%.

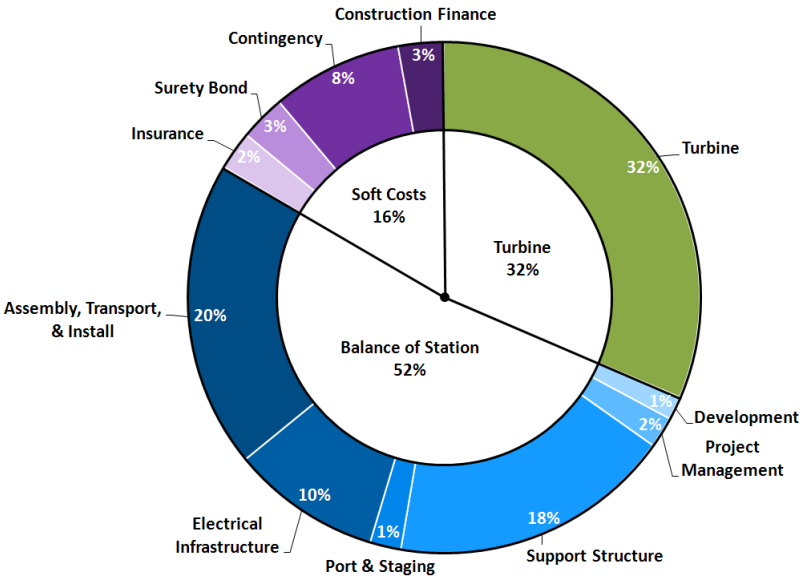

Figure 2.11. Installed capital cost for offshore wind systems [46]

IEC 61400-3 defines the support structure as the "part of an offshore wind turbine consisting of the tower, substructure and foundation", as shown in Figure 2.9. And in turn, the substructure is defined as the "part of an offshore wind turbine support structure which extends upwards from the seabed and connects the foundation to the tower." On the other hand, Tegen et. al. have a different definition in their research [46]. The term "turbine" is assumed to include the tower for both the land-based and offshore system. A simple calculation can be made in order to calculate the share of the total cost comprised by the tower-monopile structure. Using the information from Figure 2.10 and 2.11, and based on the research's definition, one can conclude that a tower represents approximately 22% of the overall installed cost of the turbine. With a 32% portion of turbine costs in offshore systems, the tower corresponds to 7% of the overall installed cost. Moreover, a support structure (monopile in this case) forms 18% of the overall installed cost. To conclude, a tower-monopile structure approximately comprises 25% of the overall installed cost in an offshore wind energy system.

2.2 Offshore Wind Energy

2.2.1 Offshore wind resource

Offshore wind energy is attractive because of the excellent wind resource. Offshore sites have higher wind speeds, less wind shear and turbulence. As can be seen in Figure 2.12, the United States has mean wind speed values at 90 m of 8 m/s or higher in most offshore regions.

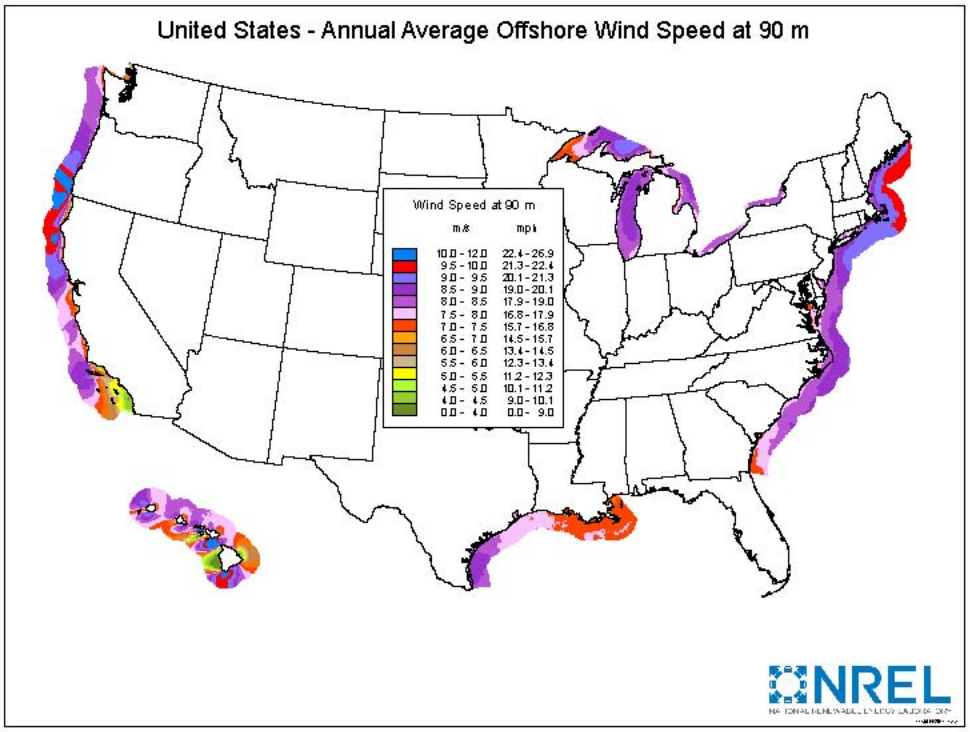

Figure 2.12. United States annual average offshore wind speed at 90 m [39]

The depth of the seabed is an important factor for selecting the right substructure for offshore wind turbines. Figure 2.13 shows the capacity by water depth in the United States.

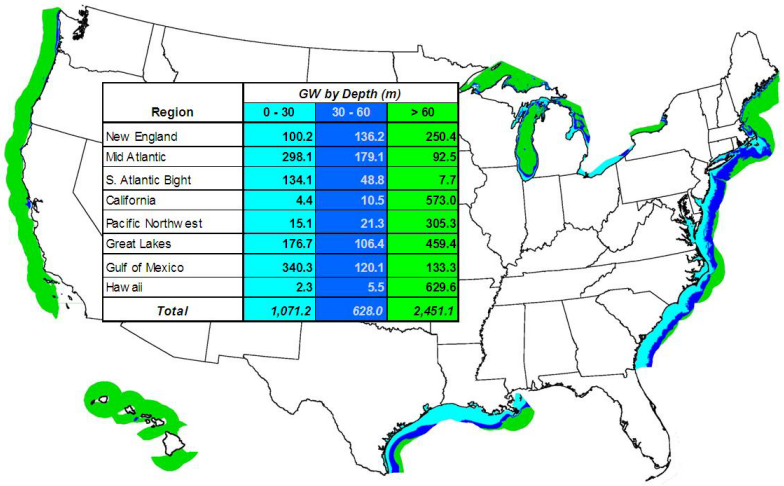

Figure 2.13. United States offshore wind resource by region and depth for annual average wind speed sites above 7 m/s

2.2.2 Wind turbine substructures

There are two main substructure types according to their connections with the seabed, fixed bottom substructures and floating substructures. While fixed bottom substructures are preferred for shallow waters, floating platforms may be used for transitional and deep water areas. As water depth increases, the cost of the substructure probably increases because of additional material and complexity. Figure 2.14 presents an overview of the cost for each depth.

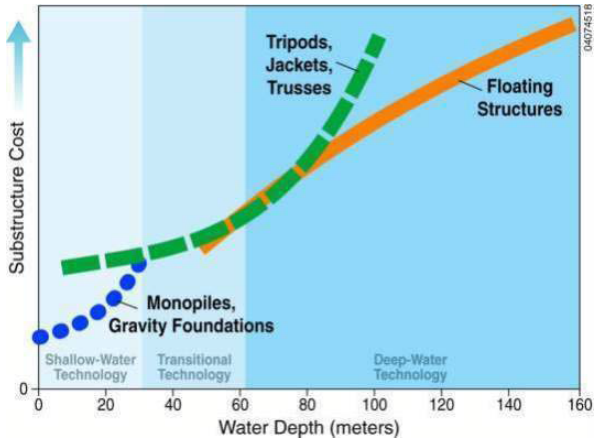

Figure 2.14. Cost of offshore wind turbine substructures with water depth [33]

Floating substructures are expected to be the most expensive substructures with the existing technology.

2.2.2.1 Fixed bottom substructures

Monopiles, gravity-base and suction-bucket substructures are the most common types in shallow waters.

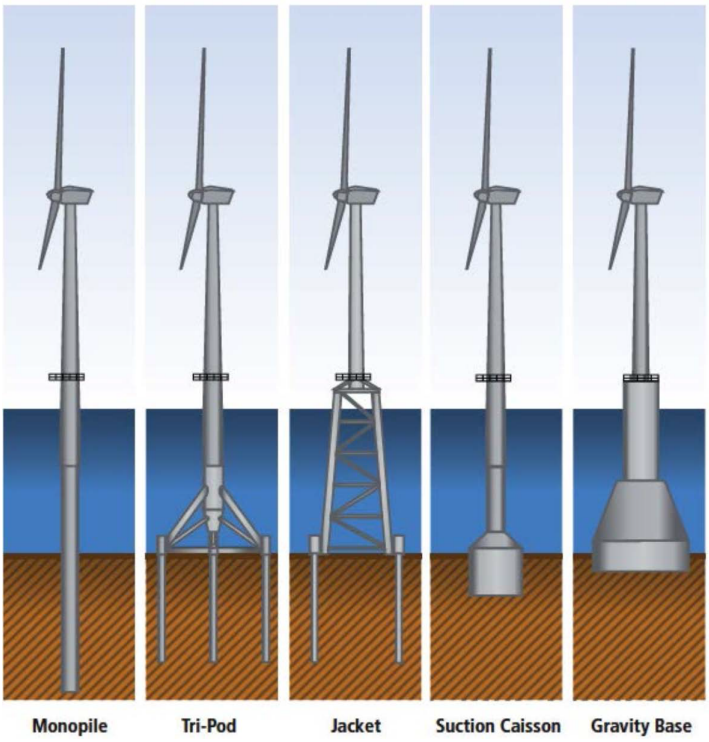

Figure 2.15. Shallow water structure technology [34]

A monopile is a simple substructure which is formed by a hollow steel cylinder driven into the seabed at one end. On the other end, a transition piece is assembled in order to connect with the turbine tower. Tripod and jacket substructures are space frame designs that are generally used for deep water areas. They are pinned into the seabed with pilings. They are often chosen for offshore oil rigs [34]. A suction caisson resembles a monopile with shorter height and larger diameter. The water inside the hollow cylinder is evacuated creating a pressure difference that drives the

caisson down into the seabed. The stability depends on the soil type resulting in limited usage in certain areas [44]. A gravity-base substructure can be preferred as an alternative to a monopile for areas where piles are not possible.

The most common offshore foundation substructure is a monopile with a usage percentage of 75% in the European market [34]. They are often cheaper and simpler than the alternatives of tripod, jacket, suction caisson, and gravity base.

A monopile substructure with a water depth of 20 m will be used in this study. The reference monopile is the monopile that is used for NREL 5MW Offshore Wind Turbine designed by the National Renewable Energy Laboratory (NREL).

2.2.2.2 Floating substructures

The long-term prospects of floating substructures are uncertain, but less foundation material usage and simplicity of installation are possible benefits. Three main floating concepts are ballast stabilized (spar-buoy), mooring line stabilized (tension leg platform), and buoyancy stabilized (semi-submersible) floating substructures. Figure 2.16 shows these concepts.

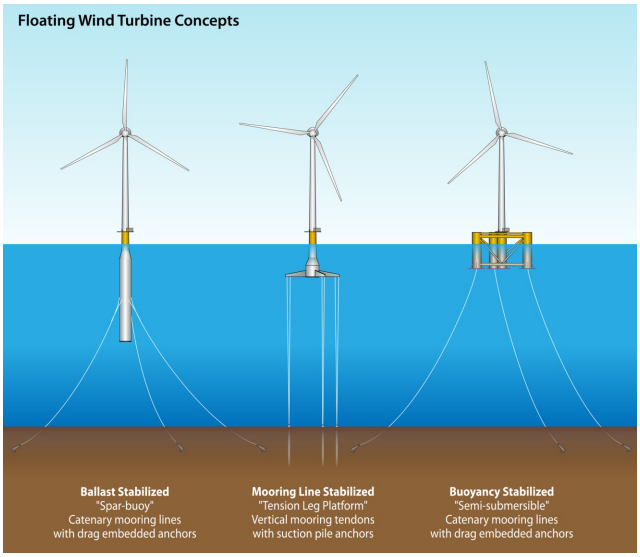

Figure 2.16. Floating water structure technology [34]

A spar-buoy is stabilized with a buoyant structure containing large ballast placed at a lower level of the platform. A tension leg platform uses vertical mooring tendons. A semi-submersible platform is stabilized with a set of buoyant structures [34].

2.3 Structural Control

Structural control is an area of civil engineering and its principles have been used successfully in many applications. Structural control mechanisms have been developed to balance dynamic forces on a system. These forces might be caused by an earthquake, waves or wind loads. These "excitation" forces affect the "structure" causing a structural "response", as shown in Figure 2.17.

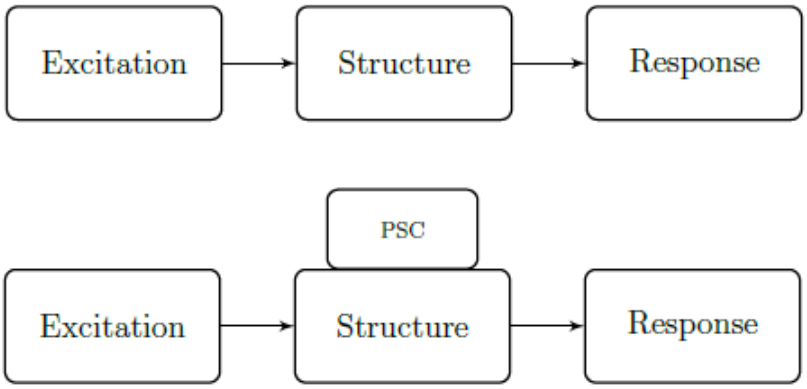

Figure 2.17. General structure type without and with an additional control mechanism [43]

Engineers have developed different designs of structural control systems to control this response of the structure. One type is a passive structural control mechanism that can be attached directly onto the structure as illustrated in Figure 2.17.

The following sections provide information about passive structural control followed by other types of structural control.

2.3.1 Passive structural control

A passive structural controller dynamically couples to the main structure with the absence of a power source. It creates forces opposite to the motion of the structure.

A passive control device might be used to dissipate energy for the system or absorb energy from the system. Passive control devices can be divided into two categories: energy dissipating devices and tuned (resonant) devices [41]. The basic characteristic of an energy dissipating device is that it does not depend on the natural frequency of the system. On the other hand, tuned devices respond relative to the natural frequency of the system. The main types of tuned damper devices are tuned mass dampers, tuned liquid dampers and tuned liquid columns dampers [41].

2.3.1.1 Tuned mass damper

A tuned mass damper (TMD) mechanism consists of a spring, a damper, and a mass. As the system vibrates with a certain natural frequency, the TMD mass vibrates simultaneously and the spring and the damper are tuned near this natural frequency. The spring absorbs the excitation in the system. The damper depletes this energy and converts it to heat energy. As a result, low vibration rates are obtained in the overall system [44].

Figure 2.18 shows the effect of a passive tuned mass damper system. The primary system has a natural frequency ω_B with an amplitude of $H(s)$ that will cause the failure of the structure. The TMD controls the response of the structure.

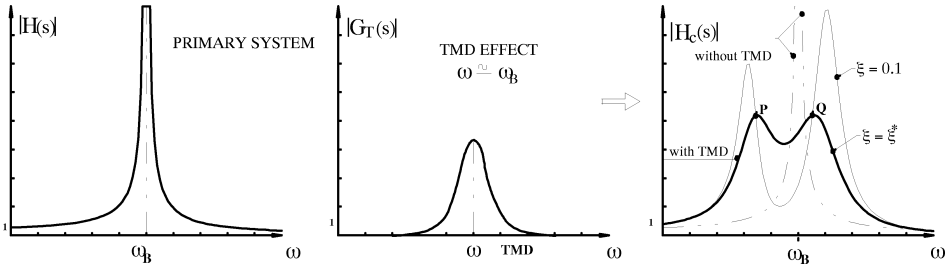

Figure 2.18. TMD effect on a system [40]

2.3.1.2 Tuned liquid damper

A tuned liquid damper (TLD) generally consists of a rigid tank with shallow water in it. It is physically placed on a structure and the frequency is tuned to the structure's natural frequency. Figure 2.19 (a) shows a schematic representation of a TLD attached to a structure, which is modeled as a single degree of freedom system. Additionally, Figure 2.19 (b) details the TLD response.

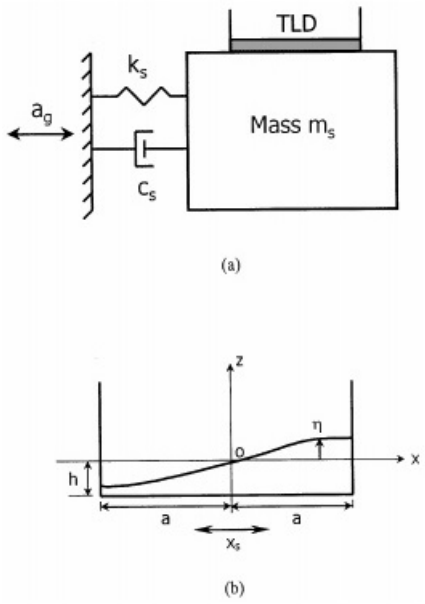

Figure 2.19. Schematic of (a) a single-degree of freedom structure with a rectangular tuned liquid damper and (b) dimensions of the rectangular tuned liquid damper [3]

As the liquid inside the TLD moves, it creates dynamic forces that absorb excitation. The effectiveness of tuned liquid dampers was investigated by Tamura et. al. Nagasaki Airport Tower was equipped with a TLD system in this study. Experiment results showed that the damping ratio of the tower was increased 4.5 times of the original value [45].

The manufacturing process of TLDs is simple and installation parameters are easy. It can also be considered cost-effective since it does not require frequent maintenance [3].

2.3.1.3 Tuned liquid columns damper

A tuned liquid columns damper works similarly to a tuned liquid damper except that it has two vertical columns. The height difference in these columns plays the role of a spring. Likewise, the fluid passing through the orifice provides a damping force [44]. Figure 2.20 shows general scheme of a tuned liquid columns damper.

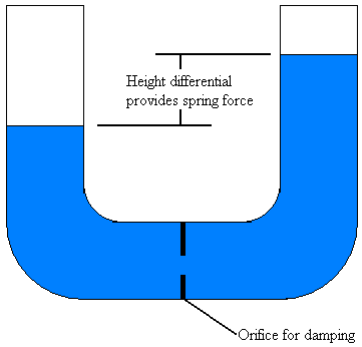

Figure 2.20. Schematic of a tuned liquid columns damper [44]

2.3.2 Active structural control

An active structural control system contains additional sensors and actuators. It collects simultaneous data from the system and controls it. Some active structural control techniques have been reviewed by Korkmaz [28]. These are:

- Active cable and tendon control
- Active strut control
- Active tuned-mass damper

Active cable and tendon control is a type of shape control mechanism that helps to prevent structural deformation. Active strut control is used with the same purpose, but struts replace cables in this case. An active tuned mass damper is similar to a passive tuned mass damper with an added control mechanism. As mentioned above, this control mechanism consists of sensors and actuators.

The first application of an active mass driver system was installed by the Kajima Corporation in the Kyobashi Building in 1989. Two active mass dampers were placed in the building. One was in the center of mass of the roof and the second was placed an eccentric distance from the center of mass in order to control torsional vibrations [31].

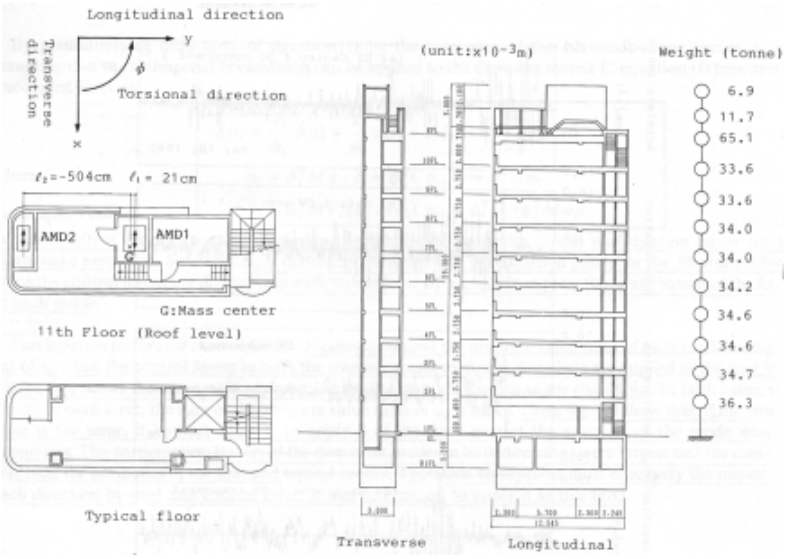

Figure 2.21. First application of active structural control in Japan [27]

2.3.3 Semi-active and hybrid structural control

A semi-active structural control device has almost the same characteristics as passive structural control, but the damping of the system can be adjusted during the operation. On the other hand, a hybrid structural control device works like an active structural control device with the addition of a passive control device also included.

2.4 Modeling of Offshore Wind Turbines

2.4.1 Basic modeling of offshore wind turbines

A turbine with a monopile support structure can be modeled as an inverted pendulum [9]. A general representation of the system can be seen in Figure 2.22.

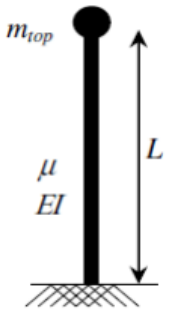

Figure 2.22. Structural model of a flexible wind turbine system [9]

$$f_{nat}^2 \cong \frac{3.04}{4\pi^2} \frac{EI}{(m_{top} + 0.227\mu L)L^3} \tag{2.1}$$

where f_{nat} is the first natural frequency, m_{top} is tower top mass, μ is tower mass per unit length, L is tower length and EI is tower bending stiffness [9].

This model is very simple. It ignores the fact that the tower is tapered and generally does not have a constant wall thickness. The diameter of the monopile may be greater than that of the tower base and in any case is likely to be thicker. Furthermore, the soil is significant and is usually taken into account.

2.4.2 Foundation modeling

The Offshore Code Comparison Collaboration (OC3) project presents an investigation of the cost effectiveness of different support structures at varying offshore sites. It also investigates the different modeling approaches for NREL's 5MW wind turbine. The same wind turbine (NREL 5MW) is used in the OC3 project for different support structures. In Phase I & II of this project, a monopile substructure is chosen with

different modeling options. In the first phase, the monopile is assumed to be rigid, but the tower is assumed to be flexible. On the other hand, the monopile is made flexible in Phase II by applying different models to represent the soil-pile interactions.

In Phase I, the monopile foundation is assumed to be rigid with a depth of 20 m under the mean sea level. The distributed tower-monopile structural properties are referenced from this study. It should be noted that these tower-monopile structural properties are used in Phase I & II, and will be introduced in Table 4.2. Phase II suggests that the flexible foundation method is designed to apply realistic soil properties and general design procedures, but the auxiliary effects (axial displacement, torsion displacement, and scouring, etc.) are neglected. The dynamic response of the system is expected to be observed sufficiently as a result of this method [24].

Figure 2.23 illustrates these models that are used for modeling a flexible monopile substructure.

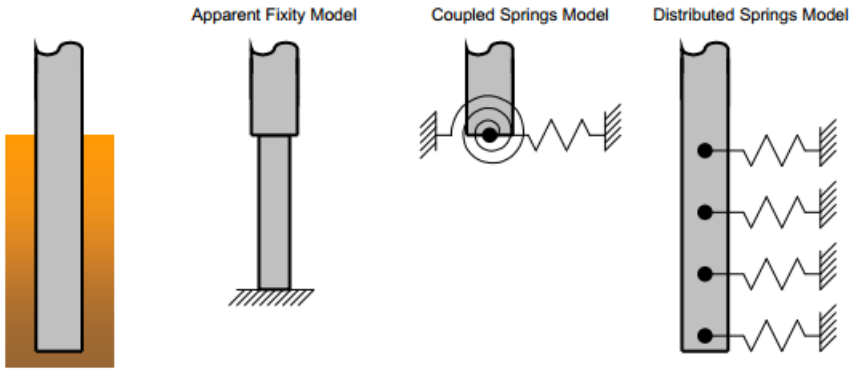

Figure 2.23. Simplified models for a monopile with flexible foundation[24]

The definitions of these models are summarized from NREL's technical report and a detailed comparison can be found in the reference [24].

The monopile with a flexible substructure is idealized as a cantilevered beam in the apparent fixity length (AF) model. In this model, the structural properties are assumed to be different above and below the mudline.

In the distributed springs (DS) model, the subsoil portion of the monopile is modeled with lateral springs that are distributed along its depth. The $p - y$ model is used to calculate the subsoil spring stiffness constants. The real properties of the monopile are used at the upper part of the beam .

The coupled springs (CS) method models the flexible monopile foundation by introducing a set of translational and rotational DOFs with coupled springs. A stiffness matrix is assumed to be positioned at the mudline for this method. The stiffness values are set up in order to get the same response with the AF method.The real properties of the monopile are used for the upper part of the substructure.

The method that is used in this thesis assumes a rigid monopile foundation. Phase I of OC3 project is referenced for the related structural properties of the substructure. The modal shapes that will be explained in the following chapter are calculated according to this method.

2.4.3 Modeling structural control in wind turbines and FAST-SC

The use of passive structural control in wind turbines has been researched, especially for offshore wind turbines because of the additional wave loads and higher wind speeds [6, 8, 10, 29, 44, 47]. Lackner and Rotea developed a new simulation tool, FAST-SC, allowing the user to add two independent tuned mass dampers into the wind turbine model within the FAST aero-elastic code, originally developed by NREL. The location of the TMDs can be defined in the nacelle or the foundation substructure, and the displacement orientation of the TMDs can also be defined. Figure 2.24 shows a TMD_x which translates in the fore-aft direction. Likewise, a TMD_y could be installed in nacelle that translates in the side-side direction.

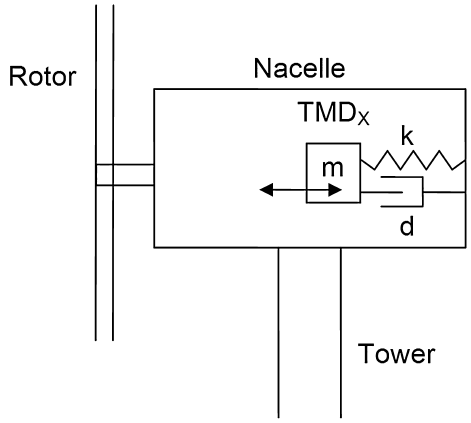

Figure 2.24. Schematic of TMD_x in turbine nacelle [29]

In the study of Stewart and Lackner, an offshore wind turbine with a monopile has been modeled. Figure 2.25 has been derived considering a two degree-of-freedom structure. One is the tower bending and the other is a passive TMD. Moreover, a genetic algorithm was developed in order to optimize the TMD spring stiffness and damping coefficient for different foundation substructures. A tuning ratio and a damping ratio were suggested for different TMD mass cases. In the following chapter of this proposal, these values will be introduced and used in calculations.

Stewart suggests that the fore-aft-direction has the highest loads formed by wind and waves. Therefore the main equations have been derived by considering the fore-aft direction.

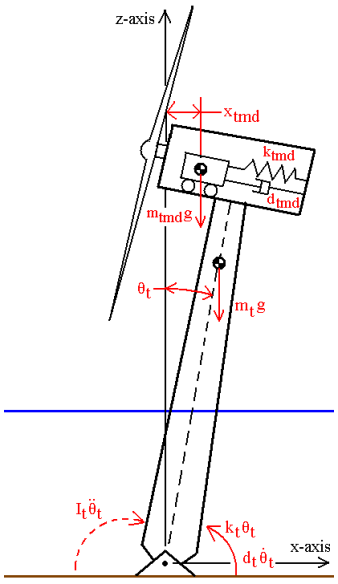

Figure 2.25. Diagram of the limited degree-of-freedom model for the monopile [44]

Equation 2.2 and 2.3 have been derived by Stewart by applying a simple dynamic analysis with small angle approximations.

$$I_t\ddot{\theta}_t = m_t g R_t\theta_t - k_t\theta_t - d_t\dot{\theta}_t - k_{tmd}R_{tmd}(R_{tmd}\theta_t - x_{tmd}) \\ -d_{tmd}R_{tmd}(R_{tmd}\dot{\theta}_{tmd} - \dot{x}_{tmd}) - m_{tmd}g(R_{tmd}\theta_t - x_{tmd}) \tag{2.2}$$

$$m_{TMD}\ddot{x}_{TMD} = k_{TMD}(R_{TMD}\theta_t - x_{TMD}) + d_{TMD}(R_{TMD}\dot{\theta}_t - \dot{x}_{TMD}) \\ +m_{TMD}g\theta_t \tag{2.3}$$

Term	Representation
k	Spring constants
d	Damping constants
m	Mass
t subscripts	Tower degree of freedom
tmd subscripts	TMD degree of freedom
θ_t	Tower bending angle from vertical
x_{tmd}	TMD displacement

Table 2.2. Explanation of the terms in Equations 2.2 and 2.3

2.5 Wind Turbine Towers

There are three main types of towers in use for horizontal wind turbines [32].

- free-standing lattice (truss)
- cantilevered pipe (tubular tower)
- guyed lattice or pole

The most common type of tower for modern horizontal axis turbines is a tubular tower. It has the advantages of fewer bolted connections, it provides a safe area to climb, and it is pleasing visually. Towers are generally made of steel, but sometimes steel reinforced concrete might be employed. It is painted or galvanized in order to protect it from environmental effects [32]. In this study, a tubular wind tower is used with a monopile substructure. The tower axes system can be seen in Figure 2.26.

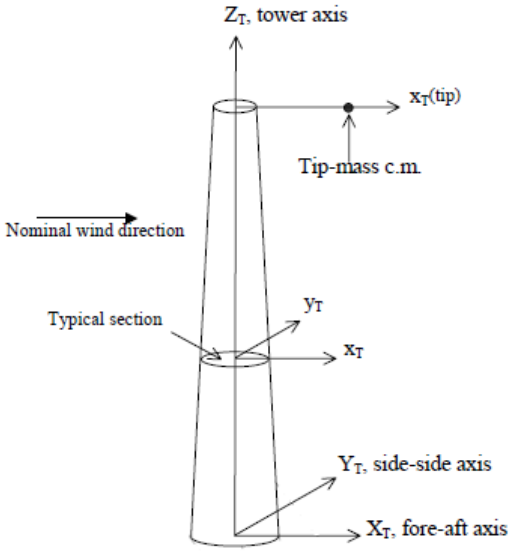

Figure 2.26. Tower axes-systems [5]

Characteristics of the tower with a monopile substructure can be seen in Table 2.3.

Property	Value
Base diameter	6 m
Base thickness	0.027 m
Top diameter	3.87 m
Top thickness	0.019 m
Young's modulus	210 GPa
Shear modulus	80.8 GPa
Effective density of the steel	8500 kg/m^3

Table 2.3. Baseline tower-monopile distributed properties [25]

The tower is the largest above-water member of a wind turbine and it is subjected to both steady and dynamic loads. Steady loads are derived from aerodynamically produced thrust and torque, as well as the weight of the rotor itself. Dynamic loads result from wind and waves (for offshore wind turbines). The effects of loading must be investigated specifically for buckling and bending [32]. Therefore, in this study, the design criteria will include the buckling and bending stresses.

The design of the tower has been studied by a number of researchers. Jamil et. al. investigated a tubular wind turbine tower and proposed a parametric study with a 250 kW wind turbine tower [20]. Lee and Bang developed a numerical solution for the prediction of the lateral buckling load for wind turbine tower structures [30]. Corbett formed a detailed optimization approach for tower and foundation systems. Tower analysis was performed by taking internal forces, displacements, and stresses into account [35]. Critical equations that are presented in the following sections are referenced from these studies.

CHAPTER 3

IEC DESIGN STANDARDS

3.1 General Overview

The International Electrotechnical Commission (IEC) is a worldwide organization that aims to promote international co-operation on all questions concerning standardization in the electrical and electronic fields [18].

IEC 61400 design standards are concerned with wind turbines. Some of the parts of the IEC 61400 are:

- Part 1: Design requirements
- Part 2: Design requirements for small wind turbines
- Part 3: Design requirements for offshore wind turbines [19]
- Part 11: Acoustic noise measurement techniques
- Part 12: Wind turbine power performance techniques
- Part 13: Measurement of mechanical loads
- Part 23: Full-scale structural testing of rotor blades

The first part of IEC 61400 (IEC 61400-1) specifies fundamental design requirements to ensure the engineering principle of wind turbines. The additional parts of the standard focus on specific subjects in the field. The design standards for offshore wind turbines are presented in IEC 61400-3 which was published in 2009 [19].

IEC 61400-1, and IEC 61400-3 are taken into consideration during this study. The following sections presents detailed information about the standards that are used.

3.2 External Conditions

IEC 61400-1 requires the use of a structural dynamics model to predict design loads. The definitions of all relevant combinations of external conditions and design situations are explained in the standard [18].

External conditions that are related to an onshore wind system can be divided into two categories: wind conditions, and other environmental conditions such as electrical conditions, and soil properties that are relevant to the design of wind turbine foundation substructures [18]. The marine conditions (waves, sea currents, water level, sea ice, marine growth, seabed movement and scour) should be considered additionally for offshore wind systems [19].

A wind turbine system can be examined under the two situations. The first one is the normal external conditions that usually affects the structural loading conditions. The second one is the extreme external conditions that defines rare external design conditions. The design load cases (DLCs) are presented in the IEC 61400-3 for an offshore wind system. Some of the load cases are presented in Table 3.1.

Design situation	DLC	Wind conditions	Waves	Wind and wave directionality	Sea currents	Water level	Other conditions	Type of analysis	Partial safety factor
1) Power production	1.2	NTM $V_{in} < V_{hub} < V_{out}$	NSS Joint prob. distribution of H_s, T_p, V_{hub}	COD, MUL	No currents	NWLR or $\geq$ MSL		F	*
	1.4	ECD $V_{hub} = V_r - 2m/s, V_r, V_r + 2m/s$	NSS (or NWH)	MIS, wind direction change	NCM	MSL		U	N
2) Power production plus occurrence of fault	2.3	EOG $V_{hub} = V_r \pm 2m/s$ and V_{out}	NSS (or NWH)	COD, UNI	NCM	MSL	External or internal electrical fault including loss of electrical network	U	A
3) Start up	3.2	EOG $V_{hub} = V_r \pm 2m/s$ and V_{out}	NSS (or NWH)	COD, UNI	NCM	MSL		U	N
4) Normal shut down	4.2	EOG $V_{hub} = V_r \pm 2m/s$ and V_{out}	NSS (or NWH)	COD, UNI	NCM	MSL		U	N
5) Parked (standing still or idling)	6.2a	EWM Turbulent wind model $V_{hub} = k_1 V_{net}$	ESS $H_s = k_2 H_{e50}$	MIS, MUL	ECM	EWLR	Loss of electrical network	U	A
	6.3a	EWM Turbulent wind model $V_{hub} = k_1 V_{net}$	ESS $H_s = k_2 H_{e1}$	MIS, MUL	ECM	NWLR	Extreme yaw misalignment	U	N

Table 3.1. Design load cases [19]

"DLC" is the design load case, "NTM" is the normal turbulence model, "ECD" is the extreme coherent gust with direction change, "EOG" is the extreme operating

gust, “EWM” is the extreme wind model, “NSS” is the normal sea state,“ESS” is the extreme sea state,“NCM” is the normal current model,“COD” is the co-directional, “H_s” is the significant wave height, “T_s” is the peak spectral period, “V_h” is the hub height wind speed, “V_r” is the rated wind speed, “F” is the fatigue, “U” is the ultimate strength, “N” is the normal, and “A” is the abnormal.

3.2.1 Wind properties

The wind is the key parameter in wind turbine design when applying dynamic forces on the wind turbine components. In the design process of the turbine design, these loads are expected to be considered. IEC 61400-1 defines wind turbine classes. Table 3.2 shows the basic parameters for wind turbine classes.

Wind turbine class		**I**	**II**	**III**	**S**
V_{ref}	(m/s)	50	42.5	37.5	Values
A	I_{ref} (-)	0,16			specified
B	I_{ref} (-)	0,14			by the
C	I_{ref} (-)	0,12			designer

Table 3.2. Wind turbine classes with basic parameters [18]

V_{ref} is the reference average wind speed over 10 min, A, B, and C are the turbulence characteristics (A is higher, B is medium, and C is lower turbulence), I_{ref} is the expected value of the turbulence intensity at 15 m/s [18]. S is the specific wind turbine class that can be defined by the designer.

TurbSim is a stochastic, full-field, turbulent-wind simulator. A physics-based statistical model is used to simulate time series of three-component wind speed vectors at points in a two dimensional vertical rectangular grid that is fixed in space [21].

IECWind is a program to generate IEC hub-height wind files. IECWind is able to generate wind files that are specific to IEC design load cases [38].

TurbSim generated wind files are used to perform fatigue analysis. On the other hand, extreme events are performed with wind files generated by IECWind.

3.2.2 Wave properties

The wind is the main cause in the creation of waves. The waves apply continuous dynamic forces on the support structure in offshore wind turbines. The amplitude of the waves can reach 30 m in deep-water locations in the Atlantic Ocean [9]. IEC 61400-3 defines wave models for the wind turbine design process.

- Normal sea state (NSS)
- Normal wave height (NWH)
- Severe sea state (SSS)
- Severe wave height (SWH)
- Extreme sea state (ESS)
- Extreme wave height (EWH)
- Reduced wave height (RWH)
- Breaking waves

The detailed information about each state can be found in the standard [19].

Normal sea state (NSS) and Normal wave height (NWH) are assumed for the purpose of this study.

Mathematical methods can be employed in order to represent the sea surface. Figure 3.1 shows a random wave height in a specific time period for a constant point, and its power spectra according to Pierson-Moskowitz method.

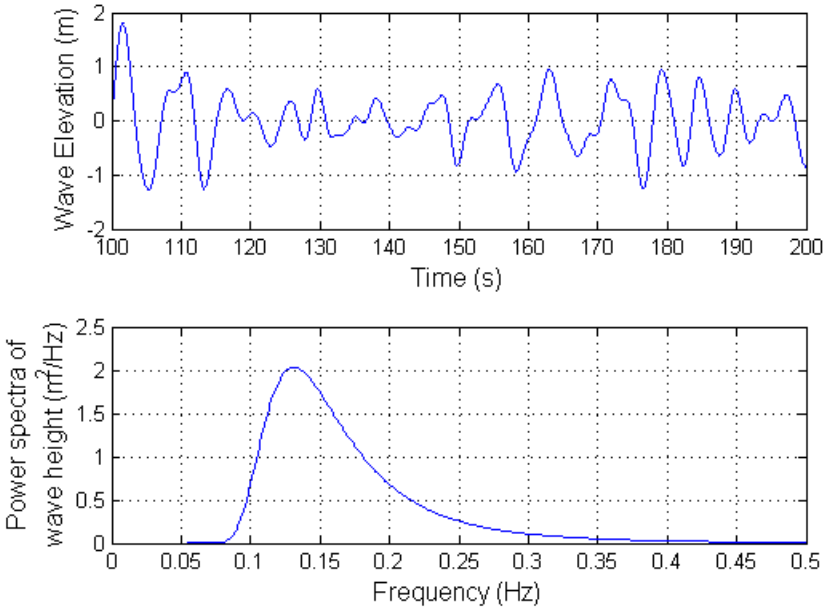

Figure 3.1. Wave elevation and Pierson-Moskowitz wave spectra for a wind speed of 10 m/s

Fourier transform of this time series presents the energy density or energy spectrum, as shown in Figure 3.1. The mean of 1/3 of the waves with the highest amplitudes in the time series is called the significant wave height. It is approximately equal to 4 times the standard deviation of the time series. It should be noted that this is a simple method to represent the real-life sea state condition, but it is assumed to be sufficient for this research.

$$H_s = 4\sigma \tag{3.1}$$

Figure 3.2 shows the expected significant wave height in normal sea state conditions at a reference site. This is an approximation derived from a technical report [22].

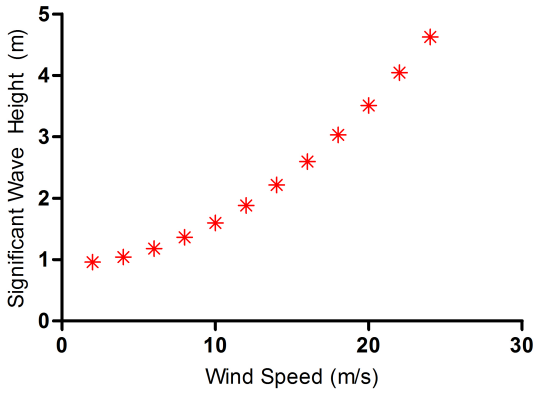

Figure 3.2. Significant wave height variation with respect to hub-height wind speed

The peak spectral period is the inverse of the frequency at which the value of the frequency spectrum is a maximum. Figure 3.3 shows the expected peak spectral period with respect to wind speed. Stewart created this data by collecting wave information for the East Coast of the United States, and evaluating it according to wind speed [44].

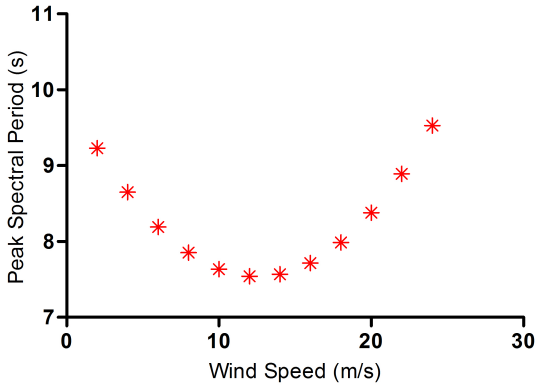

Figure 3.3. Peak spectral period variation with respect to hub-height wind speed

The expected values of the significant wave height and the peak spectral period for a given mean wind speed are updated for each simulation according to the above approximations.

3.3 Extreme Conditions

The extreme condition analysis aims to represent an extreme event that may be caused by tornadoes, hurricanes, extreme wind speeds, large tides, etc.. The IEC 61400-3 design standards requires that the designer perform these extreme condition simulations in order to take real life conditions into account during the design process. Some extreme events were chosen for evaluation in this research and are now explained.

3.3.1 Extreme operating gust

The extreme operating gust is defined as an instantaneous, sharp rise in the wind speed followed by a decrease. The IEC operating gust is assumed to have a period of 10.5 seconds. Figure 3.5 shows an example of an extreme operating gust.

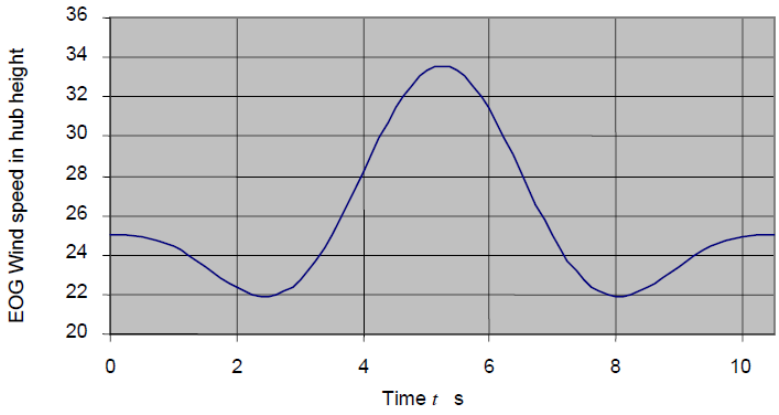

Figure 3.4. Example of extreme operating gust [18]

This sudden change in wind speed might cause failures in wind turbine creating extreme ultimate loads when it reaches critical speeds. Therefore, IEC 61400-1 requires an analysis of this event in the design process. The analyses are to be performed according to Table 3.1.

3.3.2 Extreme coherent gust with direction change

A coherent gust can be defined as a rapid rise in wind speed across the rotor. In some cases, this rise might also have a direction change simultaneously [32]. Figure 3.5 shows an example amplitude change in wind speed.

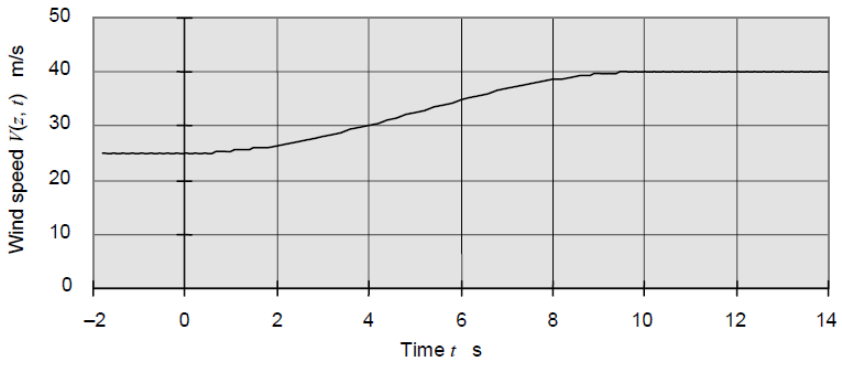

Figure 3.5. Example of extreme coherent gust [18]

The IEC 61400-1 defines the amplitude change as 15 m/s, and it is superimposed on the mean wind speed [32]. This analysis is to be performed as an extreme event during a design process of a wind turbine.

3.3.3 Extreme wind speed model

The extreme wind speed model (EWM) requires analysis of the effects of two very high wind speeds that are expected to occur, but only rarely [32].

Two extreme wind speeds can be obtained for this model. The first one is the 50-year extreme wind (U_{e50}) that represents the extreme wind speed with a recurrence

period of 50 years. On the other hand, the 1-year extreme wind (U_{e1}) is the wind speed with a recurrence period of 1-year.

The extreme wind speed model can be a steady or a turbulent wind model, but it should be based on the reference wind speed, and a fixed turbulence intensity [18].

The extreme wind model with a recurrence period of 1 year is employed at the end of this study. The related wind speed is calculated by IECWind.

CHAPTER 4

METHODOLOGY

The aim of this study is to optimize the tower and the monopile thickness of a reference wind turbine, in order to minimize tower and monopile mass while still meeting constraints on loading.

The process to develop a set of candidate tower-monopile structures is summarized here. The first step in this study is to decrease the tower and the monopile thicknesses of the reference wind turbine in increments of 5% until a 50% reduction is achieved. This strategy is used in order to consider reduced mass towers and monopiles, while still preserving the same outer diameter of the tower and the monopile over their entire lengths. Because the tower-monopile outer diameter, and the wall thickness affect the natural frequency, this approach was used to preserve an approximately constant natural frequency across all candidate tower-monopile structures. As a result of this process, eleven different tower-monopile structure thicknesses are created.

The next step is to calculate tower-monopile structural properties (mass density, inertia, stiffness) for each thickness, including the mode shapes. Passive TMD parameters for different TMD masses are calculated in the next step, for each candidate tower-monopile system. FAST-SC simulations with the candidate tower-monopile structures and TMD configurations follow and tower-monopile loads are generated. The data are then processed and maximum operational loads and fatigue damage loads are obtained. As a final step, design constraints are evaluated to determine optimal tower-monopile configurations. Spectral analysis is also included aiming to analyze the designs in terms of acceptable natural frequency range. The extreme

condition simulations are performed at the end of this study, and the results are evaluated according to the same design criteria.

4.1 Preprocessing

4.1.1 Calculation of tower-monopile structural properties

In this study, the NREL 5 MW offshore wind turbine is used as a baseline wind turbine design. A detailed technical report can be found in the bibliography of this proposal [25], and Table 4.1 provides some important specifications.

Rating	5 MW
Rotor orientation, Configuration	Upwind, 3 Blades
Control	Variable speed, Collective Pitch
Drivetrain	High speed, Multiple stage gearbox
Rotor, Hub diameter	126 m, 3 m
Hub height	90 m
Cut-in, Rated, Cut-out wind speed	3 m/s, 11.4 m/s, 25 m/s
Cut-in, Rated rotor speed	6.9 rpm, 12.1 rpm
Rated tip speed	80 m/s
Overhang, Shaft tilt, Precone	5 m, 5 deg, 2.5 deg
Rotor mass	110,000 kg
Nacelle mass	240,000 kg
Tower mass	347,460 kg
Coordinate location of overall CM	(-0.2 m, 0.0 m, 64.0 m)
Nacelle dimensions	18 m x 6 m x 6 m

Table 4.1. Physical parameters of NREL 5MW baseline turbine [44]

In order to create alternative candidate tower-monopile structures by decreasing the thicknesses of the baseline configuration, structural properties of the baseline turbine are needed. The tower-monopile structural properties are presented in Figure 4.2. The monopile structural properties are shown until a height fraction of 0.28. The tower structural properties follow up to a height fraction of 1.00.

Elevation (m)	**HtFract** ($-$)	**TMassDen** (kg/m)	**TwFAStif** ($N.m^2$)	**TwSSStif** ($N.m^2$)	**TwGJStif** ($N.m^2$)	**TwEAStif** (N)	**TwFAIner** ($kg.m$)	**TwSSIner** ($kg.m$)	**TwFAcgOf** (m)	**TwSScgOf** (m)
-20.00	0.00	9517.14	1.04E+12	1.04E+12	7.98E+11	2.35E+11	4.20E+04	4.20E+04	0.00	0.00
10.00	0.28	9517.14	1.04E+12	1.04E+12	7.98E+11	2.35E+11	4.20E+04	4.20E+04	0.00	0.00
10.00	0.28	4306.51	4.74E+11	4.74E+11	3.65E+11	1.06E+11	1.92E+04	1.92E+04	0.00	0.00
17.76	0.35	4030.44	4.13E+11	4.13E+11	3.18E+11	9.96E+10	1.67E+04	1.67E+04	0.00	0.00
25.52	0.42	3763.45	3.58E+11	3.58E+11	2.75E+11	9.30E+10	1.45E+04	1.45E+04	0.00	0.00
33.28	0.50	3505.52	3.08E+11	3.08E+11	2.37E+11	8.66E+10	1.25E+04	1.25E+04	0.00	0.00
41.04	0.57	3256.66	2.64E+11	2.64E+11	2.03E+11	8.05E+10	1.07E+04	1.07E+04	0.00	0.00
48.80	0.64	3016.86	2.25E+11	2.25E+11	1.73E+11	7.45E+10	9.10E+03	9.10E+03	0.00	0.00
56.56	0.71	2786.13	1.90E+11	1.90E+11	1.46E+11	6.88E+10	7.69E+03	7.69E+03	0.00	0.00
64.32	0.78	2564.46	1.59E+11	1.59E+11	1.23E+11	6.34E+10	6.46E+03	6.46E+03	0.00	0.00
72.08	0.86	2351.87	1.33E+11	1.33E+11	1.02E+11	5.81E+10	5.37E+03	5.37E+03	0.00	0.00
79.84	0.93	2148.34	1.10E+11	1.10E+11	8.43E+10	5.31E+10	4.43E+03	4.43E+03	0.00	0.00
87.60	1.00	1953.87	8.95E+10	8.95E+10	6.89E+10	4.83E+10	3.62E+03	3.62E+03	0.00	0.00

Table 4.2. Distributed support structure properties for the reference tower and monopile [24]

"Elevation" is the distance from the sea surface, "HtFract" is the fractional height along the tower-monopile centerline from the monopile base (0.0) to the tower top (1.0), "TMassDen" is the mass density per unit length, "TwFAStif" and "TwSSStif" are the tower-monopile fore-aft and side-side stiffnesses. Likewise, "TwGJStif" is the tower-monopile torsion stiffness, "TwEAStif" is defined as 10^7 times the average mass moments of inertia at each tower-monopile section. The tower-monopile fore-aft and side-side inertia values are represented as "TwFAIner" and "TwSSIner", respectively. "TwFAcgOf" and "TwSScgOf" are the offset distances from the CM of the tower-monopile [25].

By implementing simple algebraic operations, one can scale and calculate new property values for different thicknesses of the tower and the monopile. The thickness reduction is applied both to the tower and the monopile substructure. The monopile-tower structure is divided into 13 nodes as shown in Table 4.2. Sectional calculations are performed, and the outer radii are kept constant, but the internal radii are increased in order to decrease the thickness. It should be noted that the additional material (bolts, painting, etc.) on the tower-monopile structure is kept constant relative to the baseline turbine, since the outer radii are constant for all candidates.

The tower-monopile is assumed to be cantilevered. Therefore, the properties of the tower-monopile structure under the mudline does not need to be defined. In real life, the monopile is embedded beneath the mudline until a certain depth. Since the change in the thickness of the monopile under the mudline would affect its stiffness, the depth is needed to be increased in order to obtain the same properties that are equal to the baseline foundation. The depth of the monopile under the mudline is proportional to the installation cost of the structure. Therefore, no modifications are assumed in this study for the below mudline portion of the monopile.

The following equations are used to calculate tower-monopile structural properties per unit length.

$$A = \pi\left(r_o^2 - r_i^2\right) \qquad (m^2) \qquad (4.1)$$

$$I = \pi\left(\frac{r_o^4 - r_i^4}{4}\right) \qquad (m^4) \qquad (4.2)$$

$$J = 2I \qquad (m^4) \qquad (4.3)$$

$$Mass\,density\ /\ length = \rho A \qquad (kg/m) \qquad (4.4)$$

$$Bending\ stiffness\ /\ length = EI \qquad (N.m^2) \qquad (4.5)$$

$$Torsional\ stiffness\ /\ length = GJ \qquad (N.m^2) \qquad (4.6)$$

$$Axial\ stiffness\ /\ length = EA \qquad (N) \qquad (4.7)$$

$$Inertia\ /\ length = \mu\frac{r_o^2}{2}\left(\frac{t_w}{r_o} + \frac{1}{2}\left(\frac{t_w}{r_o}\right)^2\right) \qquad (kg.m) \qquad (4.8)$$

r_o is the outer radius, r_i is the inner radius, A is the cross sectional area, I is the polar moment of inertia, J is the torsional moment of inertia, ρ is the effective density of steel (8500 kg/m^3), μ is the mass density per unit length and, t_w is the wall thickness.

Figure 4.1 shows the change in tower-monopile mass density with respect to the thickness reduction percentage.

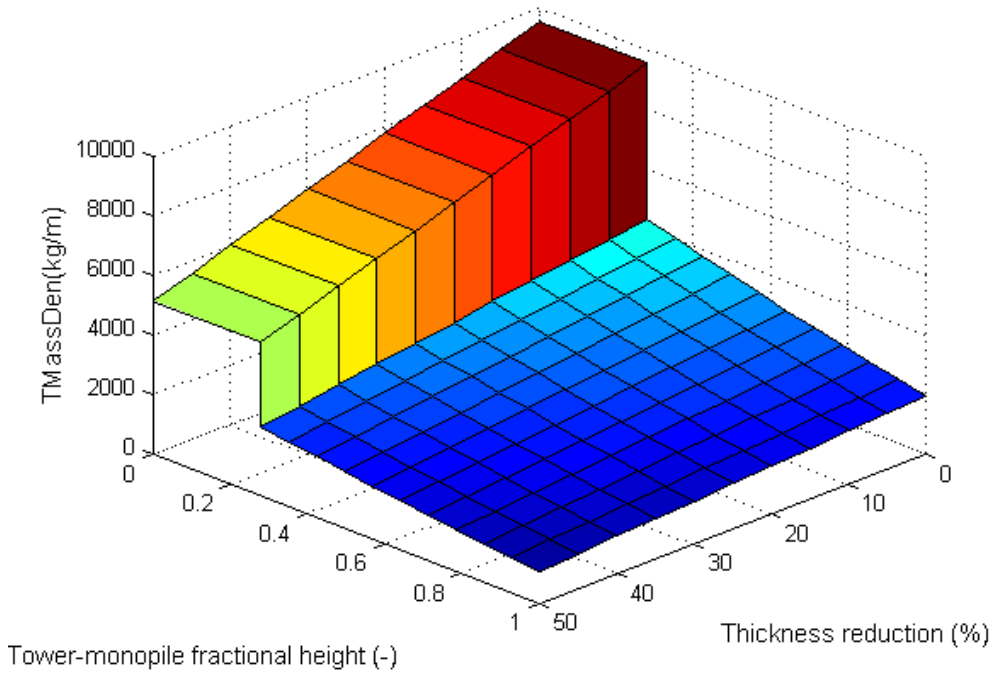

Figure 4.1. Distributed tower-monopile mass density

The thickness reduction reduces the overall mass of the tower-monopile structure as well as its natural frequency. The natural frequency is also affected by the tower-monopile top mass. Since the tower-monopile top mass also changes due to the inclusion of a TMD, each configuration's natural frequency is calculated separately and the results are listed in Table 4.3.

Thickness reduction (%)	Tower-monopile overall mass (kg)	Natural frequency (Hz)				
		Tower-monopile top additional weight				
		No TMD	5,000 kg	10,000 kg	20,000 kg	40,000 kg
0	522,617	0.2975	0.2956	0.2939	0.2904	0.2839
5	495,443	0.2907	0.2890	0.2872	0.2839	0.2774
10	474,681	0.2838	0.2821	0.2804	0.2770	0.2707
15	450,686	0.2767	0.2750	0.2733	0.2700	0.2639
20	426,672	0.2692	0.2675	0.2659	0.2627	0.2567
25	402,640	0.2614	0.2590	0.2582	0.2551	0.2492
30	378,589	0.2534	0.2518	0.2502	0.2472	0.2415
35	354,521	0.2448	0.2433	0.2418	0.2389	0.2333
40	330,434	0.2360	0.2345	0.2330	0.2302	0.2248
45	306,329	0.2267	0.2252	0.2238	0.2211	0.2159
50	282,205	0.2167	0.2153	0.2140	0.2113	0.2063

Table 4.3. Tower-monopile 1^{st} natural frequencies for different candidates

Figure 4.2 and 4.3 show the change in stiffness and inertia of the tower-monopile structure with respect to the thickness reduction percentage. It should be noted that the properties for the fore-aft and side-side directions are equal for an axi-symmetric cylinder.

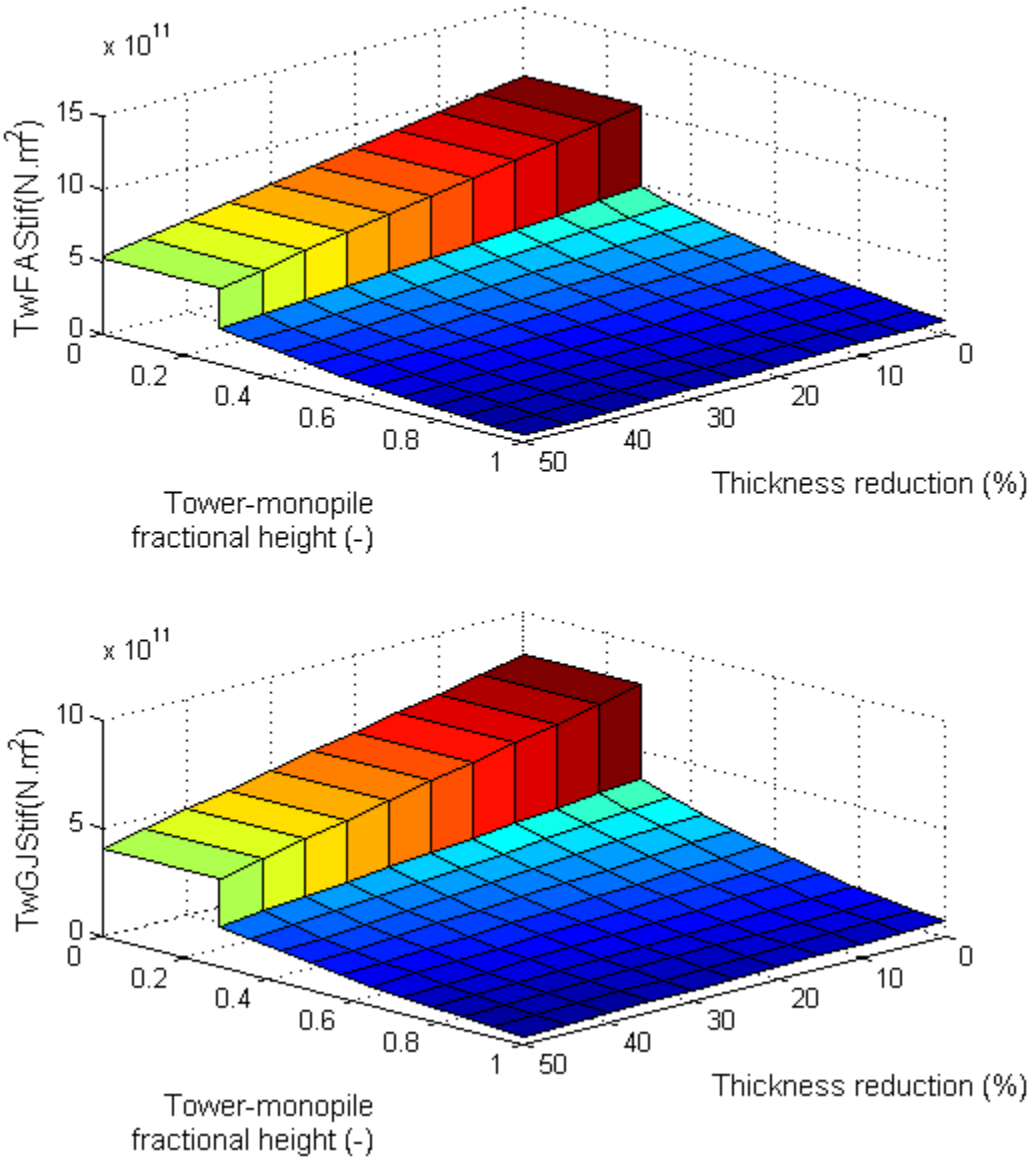

Figure 4.2. Distributed tower-monopile fore-aft and torsional stiffness

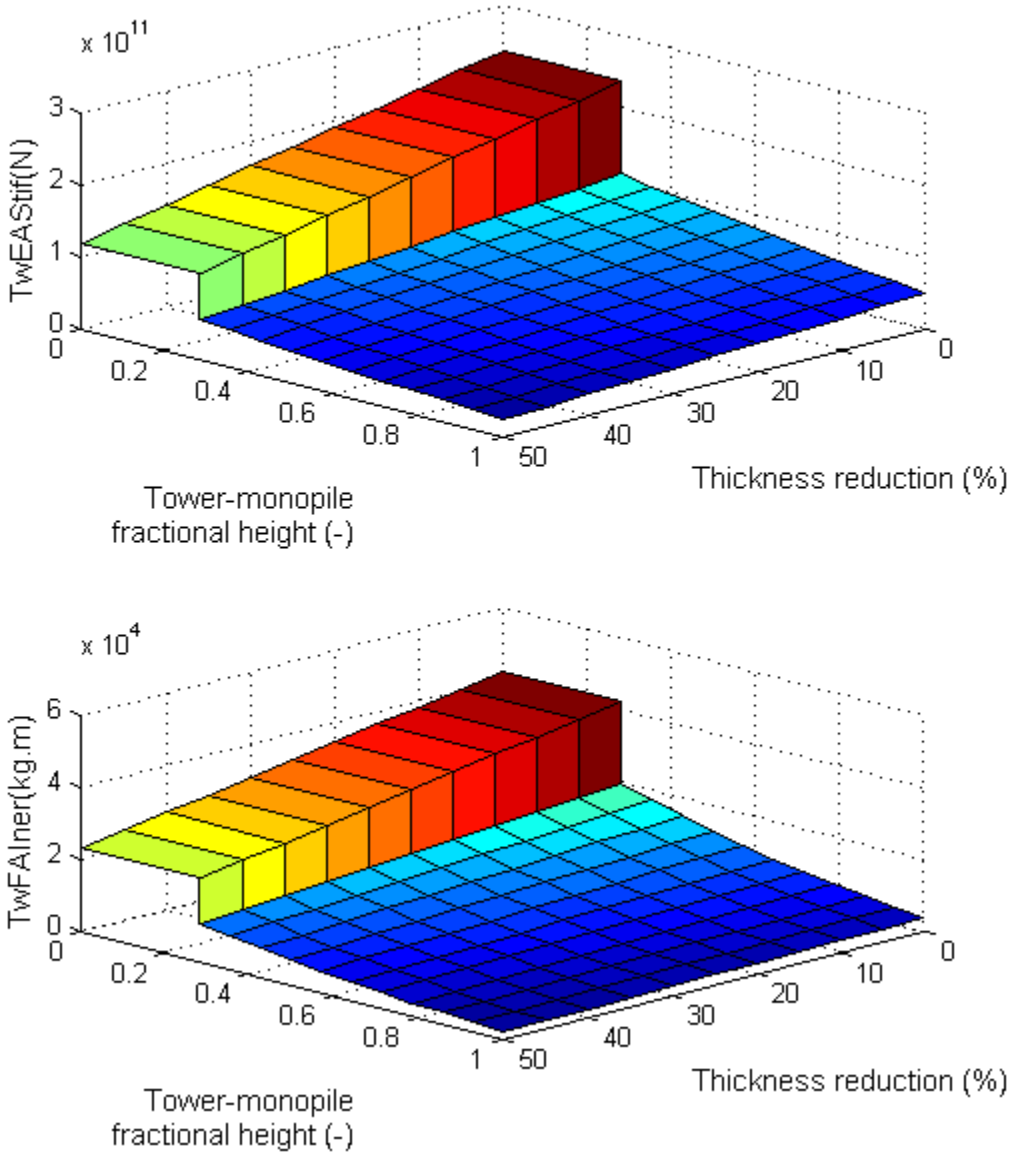

Figure 4.3. Distributed tower-monopile axial stiffness and fore-aft inertia

4.1.2 Modal shapes

FAST-SC requires the two fore-aft and the two side-side mode shapes for the tower-monopile. The modes are described in the form of a 6^{th} order polynomial with the constant, and linear terms always equal to zero because the tower-monopile is

modeled as a cantilevered beam, i.e. fixed at one end. A critical point is that the tower-monopile height is normalized to 1, so the deflection must have a normalized value of 1. As a result, the sum of polynomial coefficients must be equal to 1 [23].

A graphical representation of the tower-monopile mode shapes can be seen in Figure 4.4.

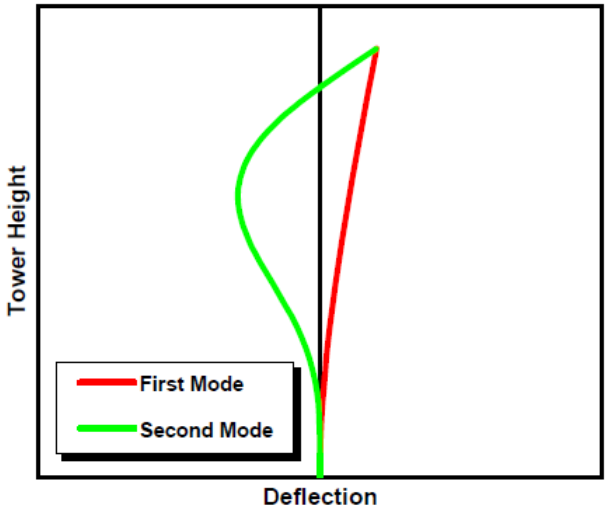

Figure 4.4. Tower mode shapes [23]

4.1.2.1 BModes

BModes, developed by NREL, is a finite-element code that provides dynamically coupled modes for a beam [5]. It can calculate mode shapes of a blade or a tower based on the structural properties, including the inertia and mass density of the system.

For this study, eleven different tower-monopile structures have been evaluated in BModes in order to calculate mode shape coefficients. It should be noted that the effect of the additional mass at the tower top due to the TMDs should be taken into account in the process. Therefore, the mode shapes are calculated by considering additional masses into the nacelle. The sample results for the baseline, 25% and 50%

thickness reduced tower-monopile structures can be seen in Figure 4.5 and 4.6. These analysis are performed without any additional tower-monopile top mass.

Figure 4.5 shows the tower-monopile mode shapes for the fore-aft direction for three different thicknesses.

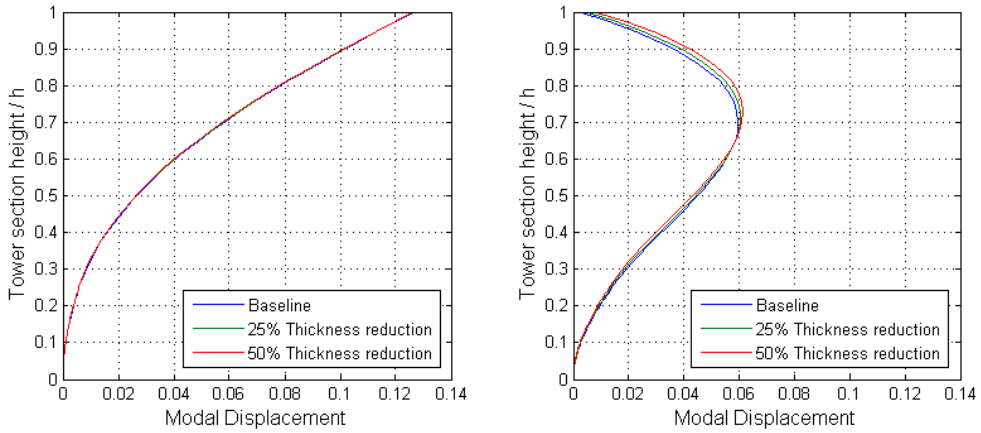

Figure 4.5. 1^{st} (left) and 2^{nd} (right) tower-monopile mode shapes in the fore-aft direction

Figure 4.6 shows the tower-monopile mode shapes for the side-side direction for three different thicknesses.

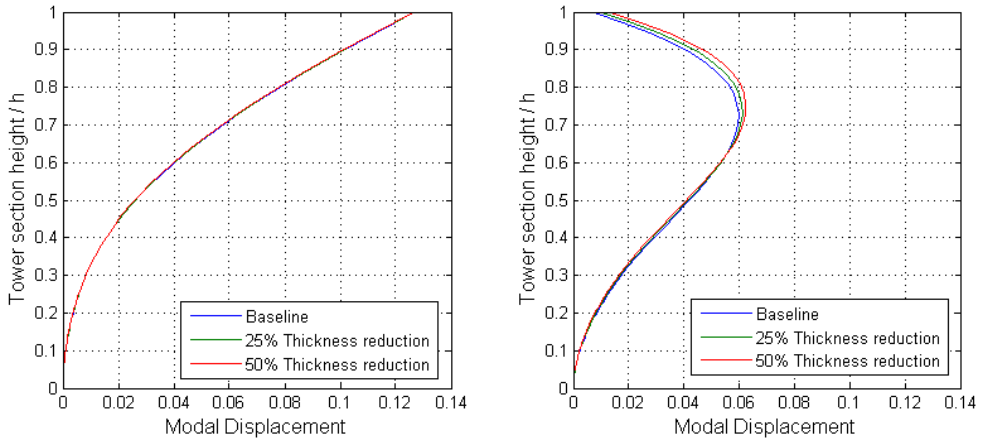

Figure 4.6. 1^{st} (left) and 2^{nd} (right) tower-monopile mode shapes in the side-side direction

It can be observed that as the thickness is decreased, higher modal displacements are obtained in the second mode shapes for both the fore-aft direction and side-side direction. It should be noted that the modal displacements are not normalized in the x-axis. The 1^{st} mode shapes are almost equal for different thicknesses. Since the center of mass of the tower-monopile top mass is not symmetric along the x, and y axises, slightly different modal shapes are observed in these two different directions.

4.1.2.2 Tower-monopile motion in real simulations

After obtaining the mode shapes of the tower-monopile structures, an analysis of deflections is performed.

In order to get the deflections of the candidate structures, the aerodynamic calculations are turned off in FAST. The degree of freedoms (DOFs) are turned off except for the tower-monopile DOFs. The initial tower-monopile top displacement is set to 1m in the fore-aft direction. The displacements at the half height and at the top of the tower-monopile are chosen as the outputs of the simulations.

Figure 4.7 shows the displacement with respect to time at the half height of the structure.

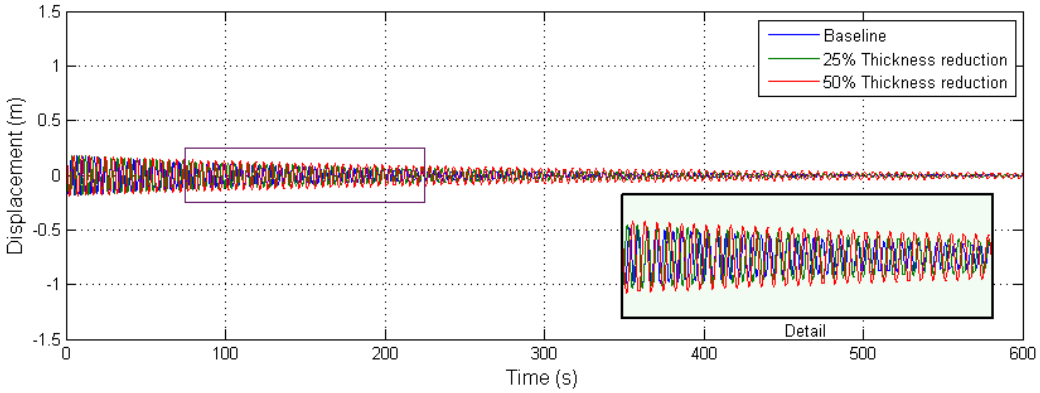

Figure 4.7. The displacement at the half height of the tower-monopile

According to the above figure, the baseline configuration experiences the lowest amplitude deflection. On the other hand, 25% thickness reduction causes more deflection of the structure, but comparably higher deflections are observed with a thickness reduction of 50%.

The power spectra of these time series present the natural frequencies of the structures which can be seen in Figure 4.8.

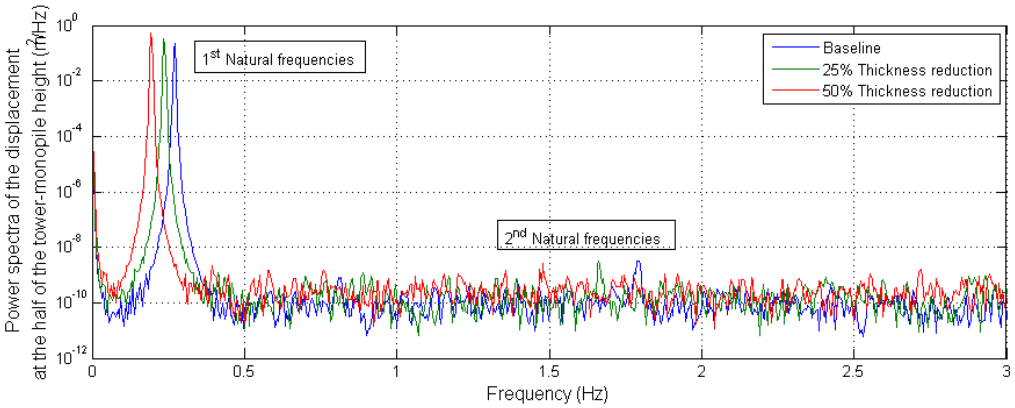

Figure 4.8. Power spectral density for deflection of half height of the tower-monopile

The peaks represent the tower-monopile vibrational frequencies. The first natural frequencies of the structure decreas as the thickness is reduced. However, the corresponding amplitude increases. Moreover, we observe that the 2^{nd} natural frequencies also decrease as the thickness is reduced. This tower-monopile height is chosen to display the second natural frequency values in the spectra, as can be seen in Figure 4.8. This peak is not expected to be observed in the next analysis which uses the tower-monopile top deflection to generate the spectra. This is due to the fact that the second natural frequency has two nodes (one at the fixed end, and the other at a location near to the free end), and one anti-node (closer to the half length of the beam) for a cantilevered beam.

The tower-monopile top displacement is presented in Figure 4.9.

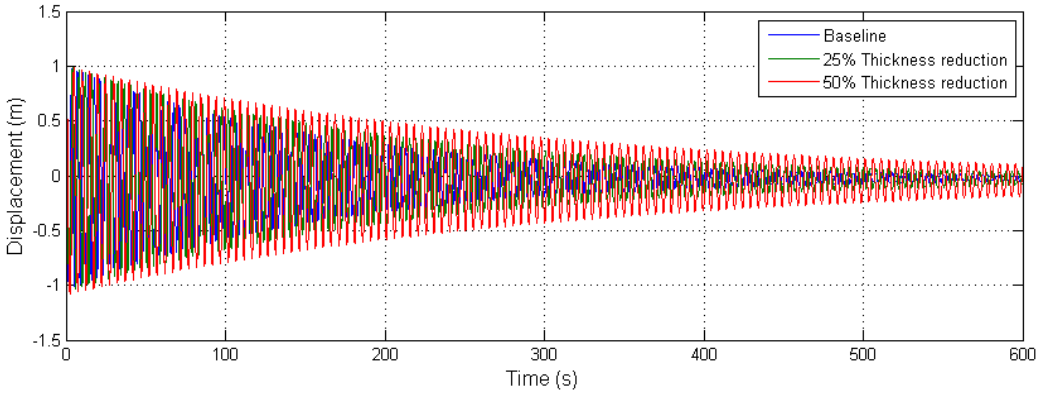

Figure 4.9. Tower-monopile top deflection for different thicknesses

Similar to the deflection at the half height of the tower-monopile structure, the deflection increases as the thickness is reduced.

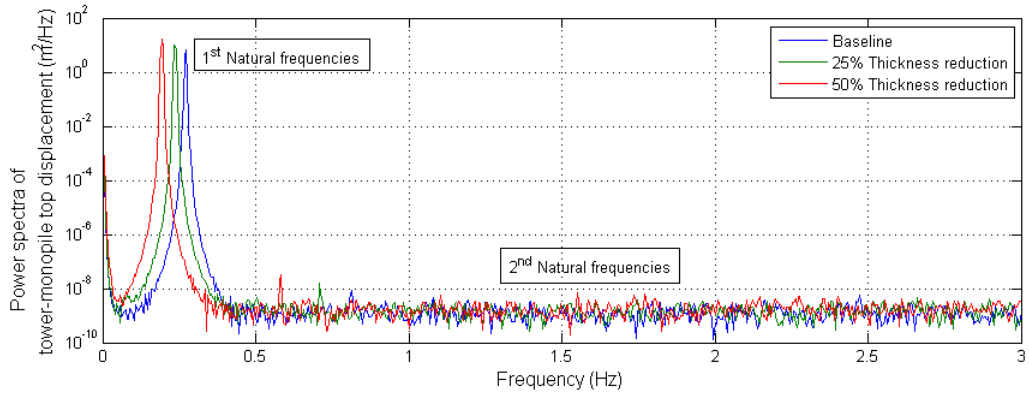

Figure 4.10. Power spectral density for tower-monopile top deflection

A decreasing trend in the first natural frequency of the structures is observed, as the thickness reduction increases. Likewise, the amplitude of the spectra for the first natural frequencies increases. The peaks at the second natural frequencies are not observed for this tower-monopile height, as expected.

To provide a comparison between the FAST-SC results and BModes results, the 1^{st} and 2^{nd} natural frequencies of the tower-monopile structure in the fore-aft direction are listed in Table 4.4.

Thickness reduction (%)	**Tower-monopile 1^{st} natural frequency (Hz)**		**Tower-monopile 2^{nd} natural frequency (Hz)**	
	BModes	**FAST-SC**	**BModes**	**FAST-SC**
0	0.2975	0.2723	1.7267	1.7930
25	0.2614	0.2348	1.5668	1.6620
50	0.2167	0.1925	1.3456	1.4740

Table 4.4. Comparison of the results of BModes and FAST for the 1^{st} and 2^{nd} natural frequencies of the tower-monopile structure in the fore-aft direction

The FAST frequency values are the frequency values at which the peaks are observed in the above power spectra plots. The BModes frequencies are the direct outputs of BModes. The results of these two codes are similar with a difference of less than 10%. The difference is due to different modeling approaches of BModes and FAST, but does not affect the results of this study.

Damping analysis of the simulations is performed next. FAST-SC considers 1% damping of the structure in the simulations. However, there appears to be a discrepancy between this defined input and the actual free vibration results. Table 4.5 shows the damping ratio of the structures that are calculated by the logarithmic decrement method.

Thickness reduction (%)	**Tower-monopile structural damping (%)**
0	0.34
25	0.30
50	0.28

Table 4.5. Tower-monopile structural damping according to logarithmic decrement method

In this analysis, even though the structural damping ratio is defined as 1% in FAST-SC for all thicknesses, the structural damping ratio is significantly lower for the actual simulations. This may lead to some concerns about the accuracy of FAST-SC, but it is not expected to affect the results of this study.

4.1.3 Determining TMD parameters

Two translational orientations of the TMDs are used in this study: one translates in the fore-aft direction (TMD_x), and the other translates in the side-side direction (TMD_y).

The natural frequencies of the tower-monopile structures are calculated by BModes. Since the TMD mass affects the natural frequencies, each configuration has a different natural frequency. After obtaining the natural frequencies of the tower-monopile structures, the TMD spring stiffness and damping constants need to be calculated for the reduced thickness tower-monopile candidates. The change in natural frequency of the structure for different top mass configurations with respect to thickness can be seen in Figure 4.11.

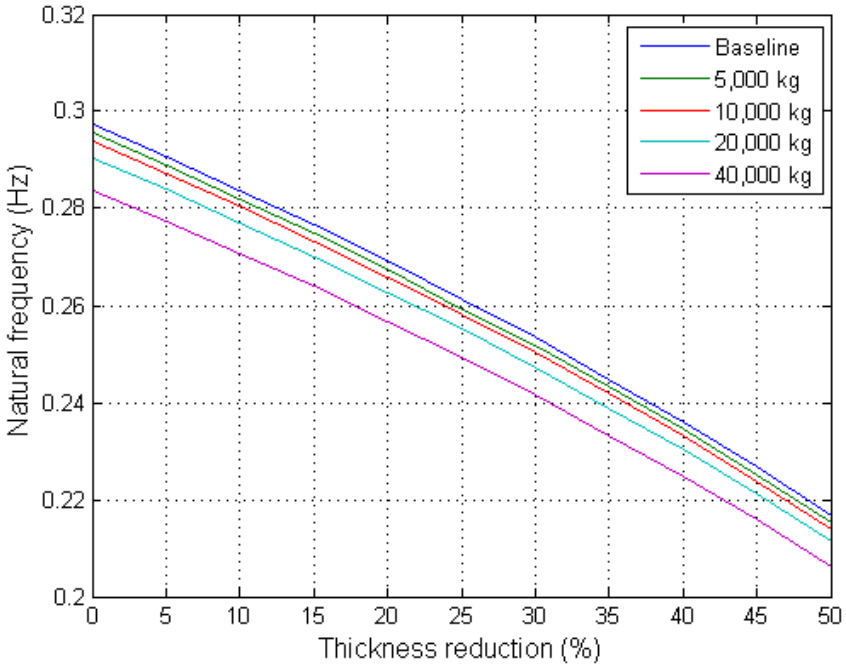

Figure 4.11. Tower-monopile structure natural frequencies according to tower-monopile top additional mass and thickness reduction

Once the tower-monopile's natural frequencies have been derived, one can calculate the TMD properties. For this research, the study of Stewart has been referenced to determine the TMD stiffness and damping properties. In Stewart's research, a genetic algorithm was implemented to find optimal TMD parameters for different offshore foundation substructures. Based on these results, optimal TMD configurations have natural frequencies that are approximately 93% of the tower natural frequency in the monopile case [44]. Equation 4.9 is used to obtain $\omega_{n_{TMD}}$. Equations 4.10 and 4.11 have been used to calculate stiffness and damping constants.

$$\text{Tuning ratio} = \frac{\omega_{n_{TMD}}}{\omega_{n_{Tower}}} = 0.93 \tag{4.9}$$

$$\omega_{n_{TMD}} = \frac{1}{2\pi}\sqrt{\frac{k_{TMD}}{m_{TMD}}} \tag{4.10}$$

$$\zeta = \frac{c}{2\sqrt{m_{TMD}k_{TMD}}} \tag{4.11}$$

k_{TMD} is the TMD spring stiffness, m_{TMD} is the TMD mass, c is the damping constant, and ζ is the damping ratio.

The reference work of Lackner suggested a 20,000 kg TMD mass, which is equal to 2% of the total mass of the monopile, a well-known ratio in civil engineering structures [29, 44]. In this study, 5,000 kg, 10,000 kg, and 20,000 kg values are chosen for TMD masses in the nacelle, with one TMD translating in the fore-aft direction and the other translating in the side-side direction. The mass values are respectively, 0.5%, 1%, and 2% of the monopile mass used in the simulations. For a certain TMD mass, the same damping ratio is used for the different thicknesses of the tower-monopile candidates. However, each TMD mass affects the damping ratio of the system. Stewart's research provides optimum TMD parameters for TMD masses of 10,000 kg, and 20,000 kg. By using the above equations with optimum TMD parameters that are obtained from Stewart's research, damping ratios can be calculated. Moreover, by implementing algebraic operations the damping ratio for a TMD mass of 5,000 kg can be calculated. As a result, the damping ratio, ζ , of 0.0582, 0.0824,and 0.1092 are calculated for TMD masses of 5,000 kg, 10,000 kg and 20,000 kg, respectively.

Tables 4.6, 4.7, and 4.8 show the tower-monopile overall mass, and the calculated values for the TMD masses of 5,000 kg, 10,000 kg, and 20,000 kg, respectively.

Thickness reduction (%)	$\omega_{\mathbf{n_{tower-monopile}}}$ **(Hz)**	$\omega_{\mathbf{n_{TMD}}}$ **(Hz)**	$\mathbf{k_{TMD}}$ **(N/m)**	$\mathbf{c_{TMD}}$ **(N - s/m)**	ζ **(-)**
0	0.2939	0.2733	14746.6988	999.5060	0.0582
5	0.2872	0.2671	14082.0055	976.7204	0.0582
10	0.2804	0.2608	13423.0639	953.5947	0.0582
15	0.2733	0.2542	12751.9001	929.4487	0.0582
20	0.2659	0.2473	12070.6960	904.2825	0.0582
25	0.2574	0.2394	11311.3053	875.3754	0.0582
30	0.2502	0.2327	10687.3553	850.8894	0.0582
35	0.2418	0.2249	9981.7855	822.3224	0.0582
40	0.2330	0.2167	9268.4579	792.3950	0.0582
45	0.2238	0.2081	8550.9783	761.1073	0.0582
50	0.2140	0.1990	7818.4954	727.7791	0.0582

Table 4.6. TMD parameters for a TMD mass of 5,000 kg

Thickness reduction (%)	$\omega_{\mathbf{n_{tower-monopile}}}$ **(Hz)**	$\omega_{\mathbf{n_{TMD}}}$ **(Hz)**	$\mathbf{k_{TMD}}$ **(N/m)**	$\mathbf{c_{TMD}}$ **(N - s/m)**	ζ **(-)**
0	0.2904	0.2701	28795.1177	2798.0730	0.0824
5	0.2839	0.2640	27520.5063	2735.4439	0.0824
10	0.2770	0.2576	26199.0276	2668.9608	0.0824
15	0.2700	0.2511	24891.6200	2601.5141	0.0824
20	0.2627	0.2443	23563.8245	2531.1769	0.0824
25	0.2543	0.2365	22080.9805	2450.2409	0.0824
30	0.2472	0.2299	20865.2007	2381.8307	0.0824
35	0.2389	0.2222	19487.5810	2301.8582	0.0824
40	0.2302	0.2141	18094.0703	2218.0317	0.0824
45	0.2211	0.2056	16691.7979	2130.3510	0.0824
50	0.2113	0.1965	15244.9017	2035.9257	0.0824

Table 4.7. TMD parameters for a TMD mass of 10,000 kg

Thickness reduction (%)	$\omega_{\mathbf{n_{tower-monopile}}}$ **(Hz)**	$\omega_{\mathbf{n_{TMD}}}$ **(Hz)**	$\mathbf{k_{TMD}}$ **(N/m)**	$\mathbf{c_{TMD}}$ **(N - s/m)**	ζ **(-)**
0	0.2839	0.2640	55041.0125	7243.0647	0.1092
5	0.2774	0.2580	52549.4945	7077.2319	0.1092
10	0.2707	0.2518	50041.7099	6906.2966	0.1092
15	0.2639	0.2454	47559.1857	6732.8100	0.1092
20	0.2567	0.2387	44999.4667	6549.1184	0.1092
25	0.2485	0.2311	42170.4675	6339.9140	0.1092
30	0.2415	0.2246	39828.1285	6161.3248	0.1092
35	0.2333	0.2170	37169.3620	5952.1204	0.1092
40	0.2248	0.2091	34510.2610	5735.2622	0.1092
45	0.2159	0.2008	31831.7792	5508.1989	0.1092
50	0.2063	0.1919	29063.9130	5263.2767	0.1092

Table 4.8. TMD parameters for a TMD mass of 20,000 kg

Figure 4.12 and 4.13 show the plots of the resulting TMD properties for all cases.

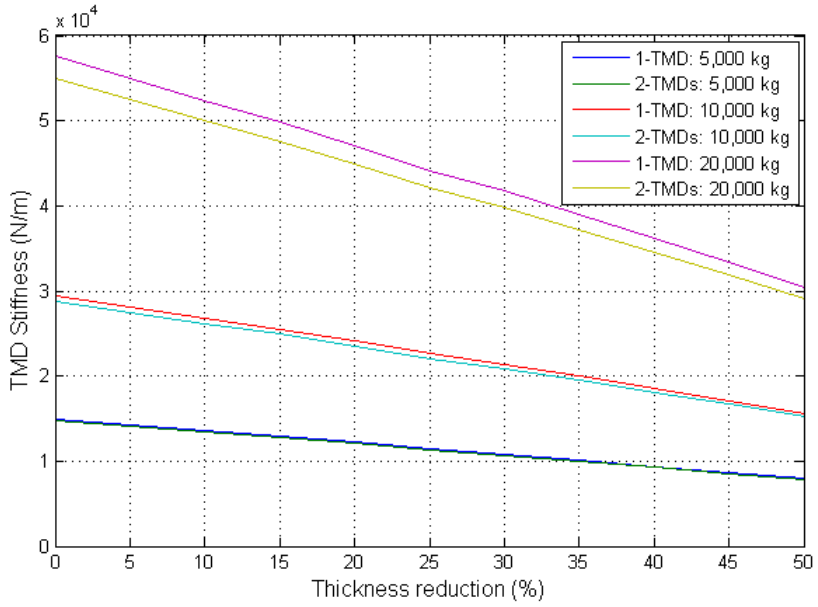

Figure 4.12. TMD spring stiffness versus thickness reduction

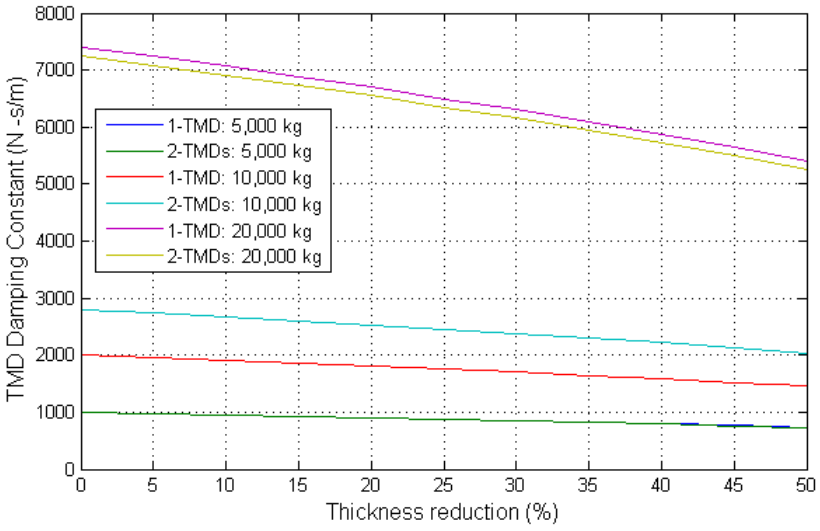

Figure 4.13. TMD damping constant versus thickness reduction

4.2 FAST-SC Simulations

4.2.1 Simulation outputs

Since the largest loads and stresses are expected to occur at the tower-monopile base, the main outputs of FAST-SC are chosen as the tower-monopile base forces and moments. Figure 4.14 shows the schematic of the reference wind turbine.

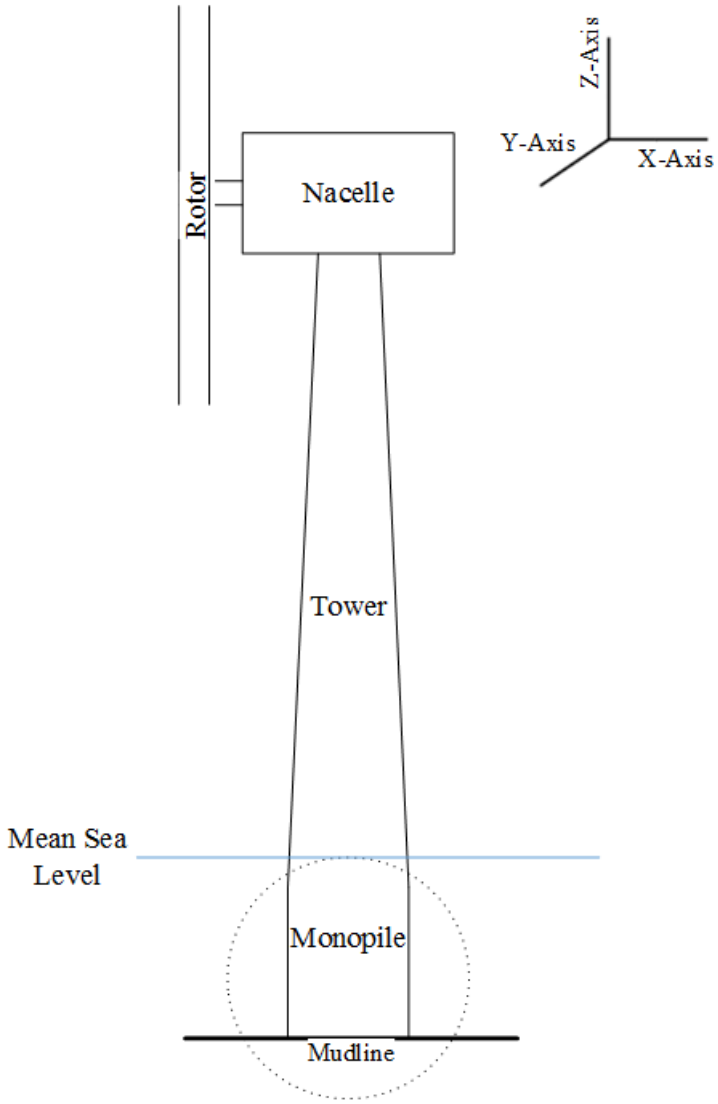

Figure 4.14. Schematic of the offshore wind turbine with a monopile substructure

By focusing on the tower-monopile base, Figure 4.15 presents the outputs of FAST-SC that are used in the post processing of the results.

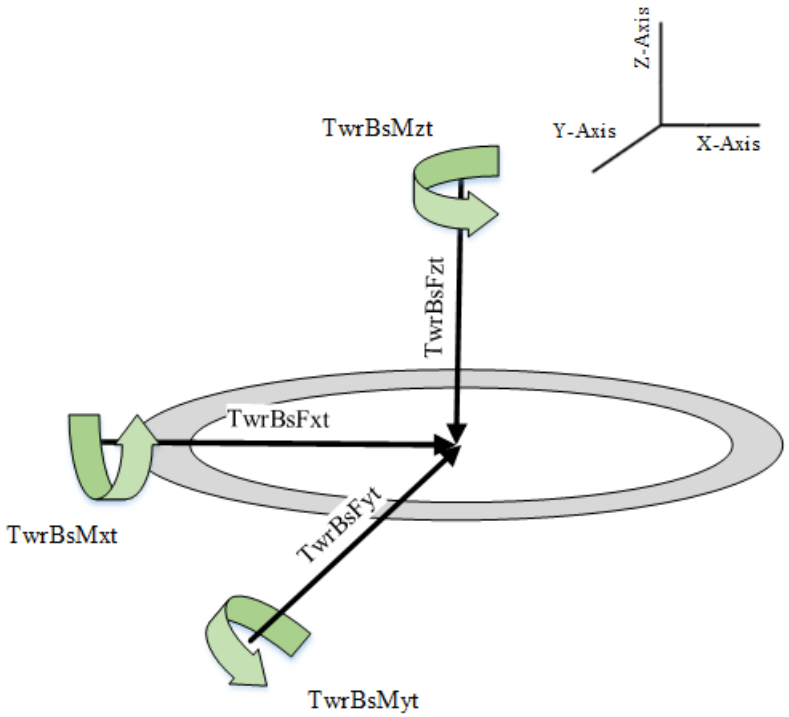

Figure 4.15. The forces and the moments for tower-monopile base

"TwrBsFxt", "TwrBsFyt", and "TwrBsFzt" are the forces that are measured at the base of the tower-monopile structure. "TwrBsMxt", "TwrBsMyt", and "TwrBsMzt" are the moments that are applied around the tower-monopile base axises. These entities are used to apply the design criteria steps, explained in the following section.

4.2.2 TMD configurations

A total of 10 configurations are considered in this study for each tower-monopile structure thickness: a no TMD case, 1-TMD cases: either in the fore-aft direction or in the side-side direction, 2-TMD cases: one in the fore-aft direction and one in the side-side direction resulting in 110 (10 configurations and 11 candidate thicknesses) different configurations.

The TMD configurations are:

- A baseline turbine (without any structural control system).

- A passive TMD in the x-direction (TMD_x case) with TMD masses of 5,000 kg, 10,000 kg, and 20,000 kg.
- A passive TMD in the y-direction (TMD_y case) with TMD masses of 5,000 kg, 10,000 kg, and 20,000 kg.
- Two passive TMDs in the x and y-direction (2 TMD case: TMD_x and TMD_y) with TMD masses of 5,000 kg, 10,000 kg, and 20,000 kg.

The simulations are performed in FAST-SC. The effect of the tower-monopile structure thickness and also the TMD mass are investigated in each case. The $2-TMD$ configurations are considered for all design load cases. However, the $1-TMD$ configurations are only used in the fatigue load case that is introduced in the next section.

4.2.3 Design load cases

A range of simulations are performed, including operational cases and extreme load cases. The various design load cases are taken from the IEC 61400-3 standards. Full field stochastic wind files generated using TurbSim are used to simulate the fatigue load case (DLC 1.2). On the other hand, the IECWind code is used in order to create IEC suggested wind files for the extreme load cases (DLC 1.4, 2.3, 4.2, 6.3a). The characteristics of the wind used in the simulations are described in the following sections.

4.2.3.1 Normal turbulence model (DLC 1.2)

This design load case is performed according to the following characteristics.

- Wind speed: Eleven wind speeds from 4 m/s to 24 m/s, in 2m/s increments.
- Wind seed: Six different random wind seeds are used for each wind speed, with full field stochastic wind files generated using TurbSim.

- Simulation time: The simulation time for each random seed is 600 seconds.
- IEC von Karman turbulence model with a turbulence characteristic level of "B" is used.
- The wind profile is assumed to follow the "Power Law" with a power law exponent of 0.1.
- The surface roughness is set to 0.03 m which is an approximate value for a fallow field [32]. It is known that this value is high to represent sea surface roughness, but the effect to the results of this study is assumed negligible.
- The significant wave height and the peak spectral period changes according to wind speed, as shown in Figure 3.2, and Figure 3.3, respectively.

4.2.3.2 Extreme coherent gust with direction change (DLC 1.4)

The following extreme event simulation is performed for 100 seconds for each event. The expected values of significant wave height and the peak spectral period are based on Figure 3.2 and Figure 3.3.

This analysis is performed for three different mean wind speeds. The wind turbine is assumed to be in the power production condition as suggested by IEC 61400-3 design standards.

- The wind speeds are 9.4 m/s ($V_{Rated} - 2\ m/s$), 11.4 m/s (V_{Rated}), and 13.4 m/s ($V_{Rated} + 2\ m/s$).
- The extreme direction change is -76.60 degrees for 9.4 m/s wind speed, and 53.73 degrees for 13.4 m/s wind speed. Two different direction change events are created for the rated wind speed of 11.4 m/s, -63.16 and 63.16 degrees.
- The maximum gust speed is 15 m/s for all cases.

4.2.3.3 Extreme operating gust during power production plus occurrence of a fault (DLC 2.3)

The extreme operating gust plus occurrence of a fault analysis is performed for three different wind speeds. These wind speeds are 9.4 m/s ($V_{Rated} - 2\ m/s$), 13.4 m/s ($V_{Rated} + 2\ m/s$), and 25 m/s (V_{Out}) as suggested by IEC 61400-3 design standards. The maximum gust speeds that are calculated by IECWind are 3.327 m/s, 4.116 m/s, and 6.404 m/s, respectively. This case is simulated by FAST-SC during power production. A fault is chosen to be the loss of grid that occurs at the time that the wind speed reaches a maximum value.

4.2.3.4 Extreme operating gust during normal shutdown (DLC 4.2)

The same wind configurations as DLC 2.3 case are chosen for this design load case. The difference is the special event is now a normal shutdown. A normal shutdown condition is simulated by employing the HSS (high-speed-shaft) brakes to decelerate the rotor at the time that the wind speed has the maximum value. The blades are set to the feather settings beginning at the same time.

4.2.3.5 Extreme wind model (DLC 6.3a)

The candidate designs of this research are tested with the extreme wind model with a recurrence period of 1-year (DLC 6.3a). The IECWind code calculation suggests a mean wind speed of 47.6 m/s for this analysis. As mentioned in Section 3.2.1, wind turbines are designed according to the wind classes. The hub-height reference wind speeds are 50 m/s, 42.5 m/s, and 37.5 m/s for wind turbine classes of I, II, and III, respectively. IEC 61400-1 defines the steady extreme wind speed as 1.4 times the hub-height reference wind speed. Therefore, a steady wind speed of 47.6 m/s generated by IECWind is assumed reasonable for this analysis. The extreme wave height is calculated according to the water depth, 20 m. In shallow waters, the wave height is limited by the 78% of the depth of the sea [2]. Therefore, a maximum wave height of

15.6 m is possible for this site. A general ratio of 1.5 can be used for the maximum wave height over the significant wave height [42]. Thus, the extreme significant wave height can be specified as 10 m. The peak spectral period of 18 s is used for this significant wave height. The turbine is modeled as "Parked" for all configurations. The blades are set to the feathered position (90 degrees) during the entire simulation time. The HSS brake is also applied in this special event. The simulation time for this extreme event is 600 seconds.

4.3 Post Processing

Post processing of the simulation results is performed in the following steps.

- MLife, a code developed by NREL, is used to obtain damage equivalent loads, maximum forces and maximum moments in the each simulation.
- The forces and the moments are then converted into the stress values and the design criteria (discussed below) are applied.

4.3.1 MLife

MLife is a MATLAB-based tool created to post process results from wind turbine tests, and aero-elastic dynamic simulations [17]. MLife performs fatigue calculations (lifetime damage-equivalent-loads, lifetime damage, time until failure) as well as statistical calculations (minimum, mean, maximum, etc.).

The concept of Damage-Equivalent-Loads (DELs) are crucial for this study. The limitations of practical test conditions for wind turbine components have led scientists to develop the concept of damage-equivalent-loads [12]. A damage-equivalent-load can be used to test a turbine component without waiting for the whole lifetime of the component. It can also be used to compare the effect of different design cases. In this study, the concept of DEL is used to evaluate the results.

The parameters that are processed in MLife are the tower-monopile base loads from Figure 4.15. The forces are "TwrBsFxt", "TwrBsFyt", and "TwrBsFzt". The moments are "TwrBsMxt", "TwrBsMyt", and "TwrBsMzt". MLife directly uses FAST-SC output files to evaluate the data.

The design load cases can be divided into two categories: the fatigue load case (DLC 1.2), and the extreme events (DLCs 1.4, 2.3, 4.2, and 6.3a).

For the DLC 1.2 load case:

- The 110 configurations of this load case have 66 files each, including six different random wind seeds and eleven wind speeds. MLife reads 66 files at a time for each configuration in DLC 1.2.
- The DELs of the tower-monopile base bending moments in the fore-aft and the side-side directions are calculated.
- The additional outputs are the maximum tower-monopile base forces and moments in the x, y, and z direction that occurred in each individual simulation (the maximum of 66 simulations for each configuration).

For the extreme load cases,

- MLife reads individual simulation outputs for each design load case.
- The simulations outputs with different wind speeds for a given load case are processed individually.
- The outputs are the maximum tower-monopile base forces and moments in the x, y, and z direction that occurred in each individual simulation.

4.3.2 Design criteria

The post processed MLife results are used in this section. The outputs are converted into the stress values using a set of formulations. The calculation step is

introduced in the following section. After obtaining the stress values, the design criteria, which are explained in this section, are applied in order to evaluate stress results.

4.3.2.1 Stress calculations

When a cylindrical shell is compressed axially, failure may occur by the yielding of the material, global buckling, or local buckling [7]. Therefore, the design criteria focus on these factors.

The critical point of the tower-baseline structure is the point at the base where the maximum stresses are expected. This point, which is located in the fore-aft direction, experiences the highest forces and moments rather than the side-side critical points. This conclusion is obtained from the results of Stewart's study [44].

Figure 4.16 shows the critical points along with the tower-monopile base loads.

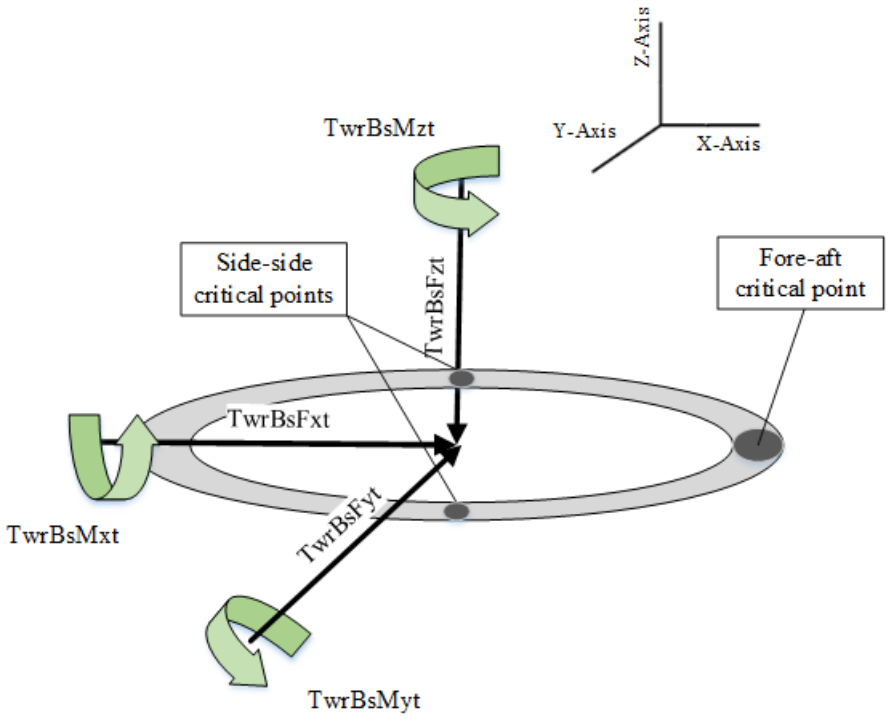

Figure 4.16. The critical points and loads for tower-monopile base

The fore-aft critical points are affected by the forces and moments in the y and z direction. The force and the moment in the x direction affect the side-side critical points according to basic principles of strength of materials [4].

- Equation 4.12 shows the shear stress created by "TwrBsFyt" at the fore-aft critical point

$$\tau_y = \frac{2(TwrBsFyt)}{A} \tag{4.12}$$

- "TwrBsFzt" creates a compressive bending stress at this point according to Equation 4.13.

$$\sigma_z = \frac{TwrBsFzt}{A} \tag{4.13}$$

  A is the cross sectional area at the base of the structure.

- "TwrBsMyt" is the critical moment that creates most of the bending. The stress associated with this moment is calculated by Equation 4.14.

$$\sigma_y = \frac{(TwrBsMyt)(r_o)}{I} \tag{4.14}$$

  r_o is the outer radius at the base of the structure, and I is the polar moment of inertia.

- "TwrBsMzt" is the torque along the tower-monopile structure. It creates a shear stress in the fore-aft critical point according to Equation 4.15.

$$\tau_z = \frac{(TwrBsMzt)(r_o)}{J} \tag{4.15}$$

  J is the torsional moment of inertia.

The combination of above stresses is performed according to the reference [4]. The maximum principle stress is calculated from Equation 4.16

$$\sigma_{max} = \frac{\sigma_y + \sigma_z}{2} + \sqrt{\left(\frac{\sigma_y + \sigma_z}{2}\right)^2 + (\tau_y + \tau_z)^2} \tag{4.16}$$

σ_{max} is calculated for the fatigue load case (DLC 1.2), and the extreme load cases (DLCs 1.4, 2.3, 4.2, and 6.3a).

The DELs of tower-monopile base bending moments are also converted into stress values. The DEL stress values are calculated according to Equation 4.17.

$$\sigma_{DEL} = \frac{(Moment)_{DEL}(r_o)}{I} \tag{4.17}$$

r_o is the outer radius, I is the polar moment of inertia. The combination of the fore-aft and the side-side DEL stresses is performed according to Miner's rule [16].

$$Combined\ DEL = \left(\left(DEL_{Fore-aft}\right)^m + \left(DEL_{Side-side}\right)^m\right)^{\frac{1}{m}} \tag{4.18}$$

m is the material coefficient that is equivalent to 3 for steel. This combined DEL is then converted to stress by using Equation 4.17. σ_{DEL} and $Combined_{DEL}$ are calculated only for the fatigue load case (DLC 1.2).

After obtaining the above stress values for each configuration, the following set of design criteria is applied.

4.3.2.2 Baseline equivalent stress method

It is known that the presence of the TMDs lowers tower-monopile base loads. On the other hand, the thickness reduction reduces the stiffness of the tower-monopile structure and increased loads are expected.

The baseline wind turbine without any structural control device, and also without any thickness reduction is simulated, and the loads are obtained. These loads are used to compare the results of different thickness reductions, and also TMD configurations.

This criteria aims to show the percentage of thickness reduction of the tower-monopile for a given configuration that yields the loads that are equivalent to the baseline turbine loads. It should be noted that the baseline turbine design includes a factor of safety. Therefore, no factor of safety is applied in this criteria.

The aim of this criteria is to create a new candidate turbine that is thinner and therefore less expensive, but with resulting fatigue and maximum stress values that are equivalent to the baseline values.

This criteria is applied to the results of the fatigue design load case (DLC 1.2) that contains the maximum operational stresses and the damage equivalent stresses. It is also applied to the extreme event load cases (DLC 1.4, 2.3, 4.2, and 6.3a), but only for maximum stresses.

4.3.2.3 Yield stress method

The maximum stress occurring in the simulations should be less than or equal to the yield stress of the material. A yield stress of 355 MPa for steel is used. A safety factor of 1.35 is applied in this method for DLC cases, as suggested by IEC 61400-1 [18].

4.3.2.4 Allowable local buckling stress method

The concept of the allowable local buckling stress method is described in this section [35]. This method consists of:

- Equation 4.20 is used to calculate the elastic critical buckling stress of a hollow cylinder made of steel.
- The critical stress reduction coefficients for bending and axial loading are determined with equations 4.21 and 4.22.
- Finally, the allowable local buckling stress calculation is performed with equation 4.19.

$$\sigma_{buckling} = \begin{cases} \sigma_{yield}[1 - 0.4123(\frac{\sigma_{yield}}{\alpha_B \sigma_{cr}})^{0.6}], & \alpha_B \sigma_{cr} \geq \sigma_{yield}/2 \\ 0.75\alpha_B \sigma_{cr}, & \alpha_B \sigma_{cr} \leq \sigma_{yield}/2 \end{cases} \tag{4.19}$$

$$\sigma_{cr} = 0.605 E_s \frac{t_w}{r_m} \tag{4.20}$$

$$\alpha_B = 0.1887 + 0.8113\alpha_0 \tag{4.21}$$

$$\alpha_0 = \begin{cases} \frac{0.83}{\sqrt{1+0.01\frac{r_m}{t_w}}}, & \frac{r_m}{t_w} \leq 212 \\ \frac{0.70}{\sqrt{1+0.01\frac{r_m}{t_w}}}, & \frac{r_m}{t_w} \geq 212 \end{cases} \tag{4.22}$$

where,

E_s	Modulus of elasticity
t_w	Tower wall thickness
r_m	Mean radius
α_0 and α_B	Stress coefficients
$\sigma_{buckling}$	Allowable local buckling
σ_{yield}	Material yield strength
$\sigma_{criticalelastic}$	Elastic critical buckling stress

Table 4.9. Term descriptions of allowable local buckling stress method

This method is considered for maximum stresses for all design load cases. The factor of safety of 1.35 is used for all DLC cases except for DLC 4.2. A modification factor is applied for this load case, and explained in the results of the DLC 4.2 case.

4.3.2.5 Euler's global buckling method

Euler's global buckling theory is utilized in this study. The theory assumes an ideal column (perfectly straight, homogeneous, and free from initial stress) with an

axial load. Equation 4.23 calculates the critical buckling load, P_{cr}[7].

$$P_{cr} = \frac{\pi^2 EI}{(kL)^2} \tag{4.23}$$

E is the Young's modulus, I is the polar moment of inertia, k is the column effective length factor (k=2 for one end fixed, and the other end free to move laterally), L is the length of the column.

Since the wind turbine tower is tapered, and not homogeneous (bolts, welding, rivets etc.), Euler's buckling theory might have some limitations. Therefore, a safety factor of 8 is picked in order to take the additional factors into account.

Since this criteria is mostly affected by the tower-monopile top mass, which is dependent to TMD configuration, the $2-TMD$ cases are chosen to maximize the mass. DLC 1.2 is preferred as the load case. The maximum vertical load ("TwrBsFzt"), which is shown in Figure 4.15, is used to compare with the critical buckling load.

CHAPTER 5

RESULTS

The results are shown in this chapter. The design load cases are separated into two categories; the first is the normal operational load case, DLC 1.2, and the second is the extreme load cases, DLCs 1.4, 2.3, 4.2, and 6.3a.

5.1 Operational Loads

This section contains the results of the DLC 1.2 simulations. The results are organized according to the load types. The fatigue loads subsection contains the damage equivalent loads and damage equivalent stresses for different TMD configurations. Maximum operational stresses and global buckling loads are presented in the next subsections.

Detailed illustrations of the 5,000 kg TMD mass cases are presented in this section. On the other hand, the $2-TMD$ cases are chosen to compare the TMD mass effect for all cases. A summary table for all TMD configurations is presented at the end of the section.

5.1.1 Fatigue loads

The damage equivalent loads and the corresponding stress values are presented in this section.

5.1.1.1 Damage equivalent loads

The following results are presented for a passive TMD mass of 5,000 kg with different configurations.

Damage equivalent loads of the tower-monopile base bending moment in the fore-aft direction can be seen in Figure 5.1.

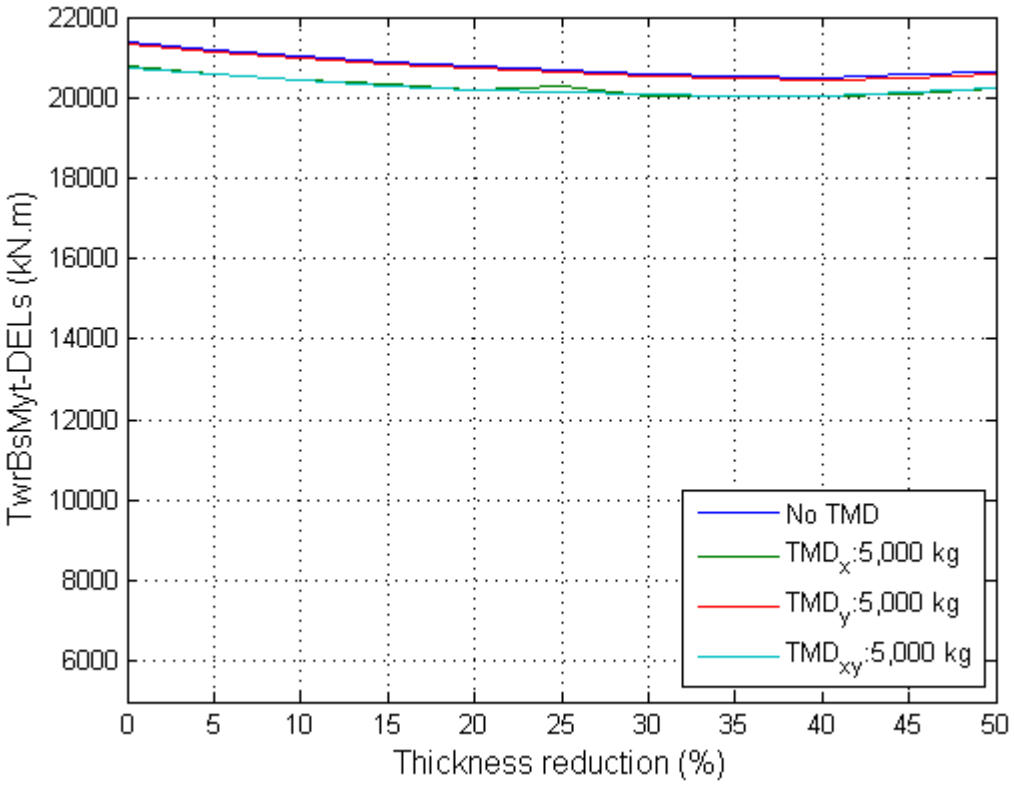

Figure 5.1. Damage equivalent loads in the fore-aft direction for TMD mass of 5,000 kg

The presence of a passive TMD only in the x-direction causes a 3% reduction of the DEL for a 0% thickness. On the other hand, a passive TMD in the y-direction has a 0.23% reduction of the DEL for a 0% thickness reduction. When combined with one TMD in the x-direction and the other in the y-direction, a 3.13% reduction is accomplished.

Damage equivalent loads of the tower-monopile base bending moment in the side-side direction can be seen in Figure 5.2.

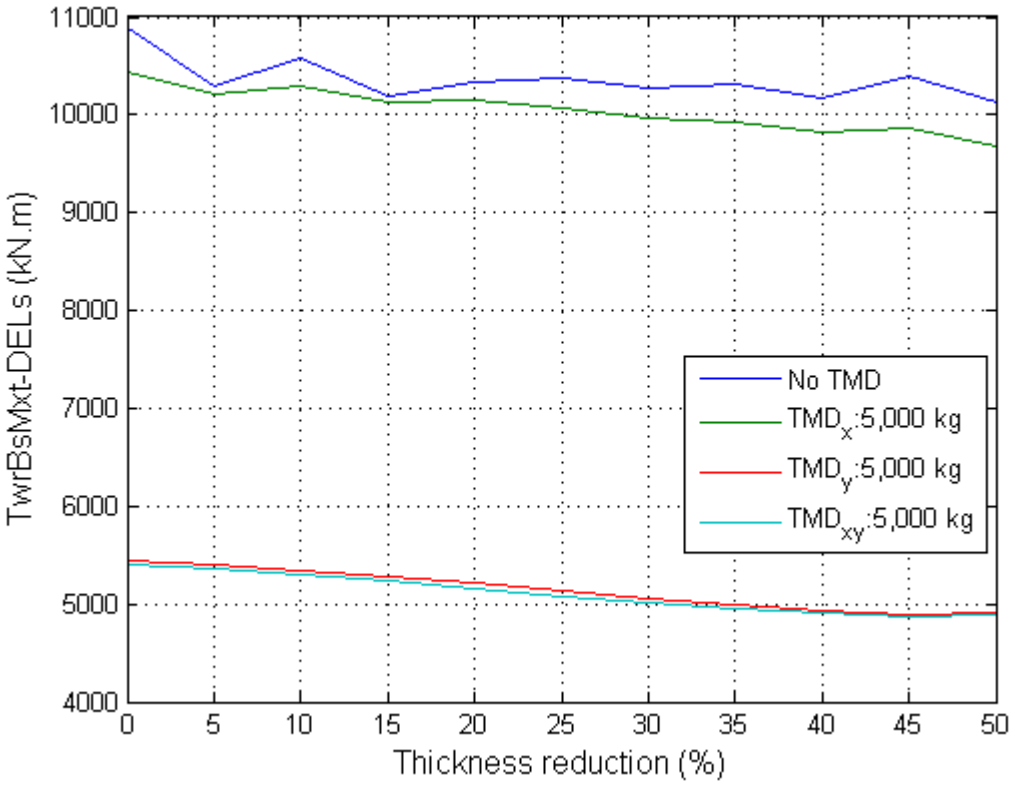

Figure 5.2. Damage equivalent loads in the side-side direction for TMD mass of 5,000 kg

The presence of a passive TMD only in the x-direction causes a 4.2% reduction of the DEL for a 0% thickness. On the other hand, a TMD in the y-direction has a 50% reduction of the DEL for a 0% thickness reduction. The combination of these two cases yields a reduction of 50.5%.

Larger reductions in the DEL in the side-side direction compared to the fore-aft direction are observed in the above results. The higher damping of the wind turbine in the fore-aft direction due to the aerodynamic damping of the rotor causes less reduction of the damage equivalent loads in this direction.

The effectiveness of the translational direction of the TMDs can be concluded from this analysis. The TMD_x, which translates in the fore-aft direction has lower

effects on reducing the DEL in the side-side direction. Likewise, the TMD_y, which translates in the side-side direction, has negligible effects on the fore-aft DEL.

The effect of the thickness reduction of the tower-monopile on the fore-aft loads is less noisy for the $No\,TMD$ case. An explanation for this currently not available, but a further investigation is warranted. It can be observed that the plot of the fore-aft loads decreases slightly across the thickness reduction, and eventually bends up for all TMD mass values. This trend shows that a possible optimum may be in this region. Likewise, the plot of the side-side loads yields a decreasing trend across all the thickness reduction values except for the last section in the plot (between 40% and 50% thickness reduction).

Next, the $2 - TMD$ cases with TMD masses of 5,000 kg, 10,000 kg, and 20,000 kg are analyzed. The damage equivalent loads in the fore-aft direction for these configurations can be seen in Figure 5.3. The four lines represent the TMD mass values including the $No\,TMD$ case.

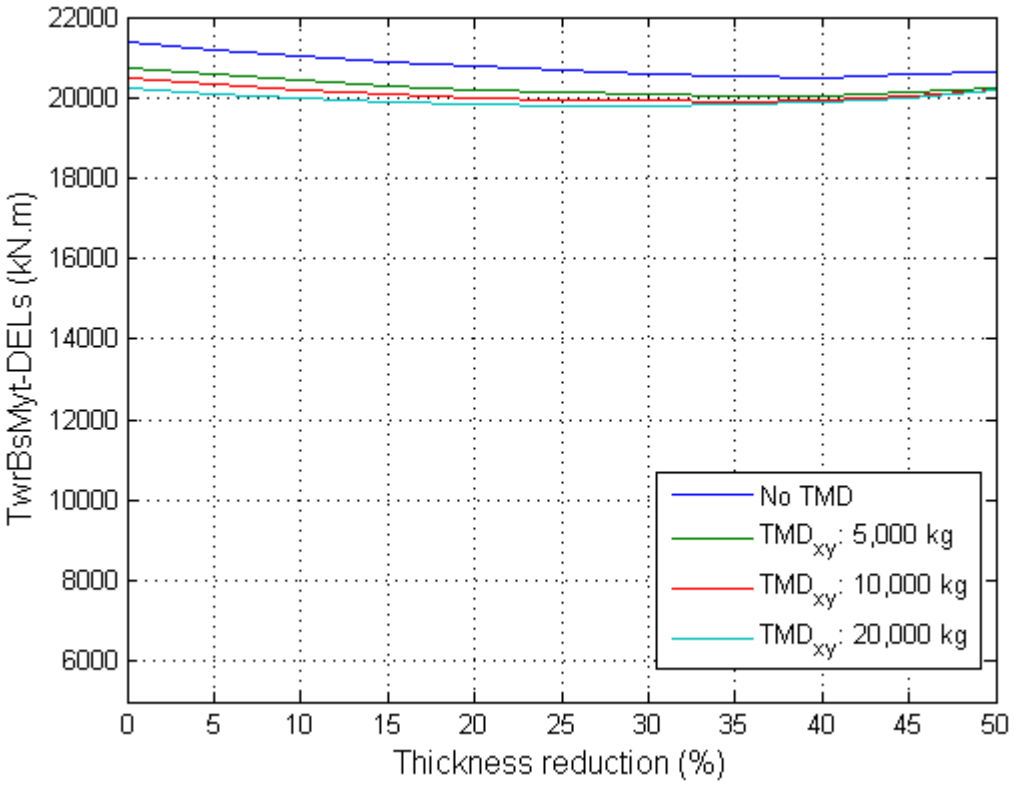

Figure 5.3. Damage equivalent loads in the fore-aft direction for different TMD configurations

The following results are compared to the $No\ TMD$ case with 0% thickness reduction. The $TMDxy$ case with 5,000 kg provides a reduction of 3.1% of DEL in the-fore-aft direction, while the mass of 10,000 kg yields a reduction of 4.2%. Finally, a 5.4% reduction is achieved by using a mass of 20,000 kg.

Figure 5.4 illustrates the DEL in the side-side direction for different TMD mass configurations.

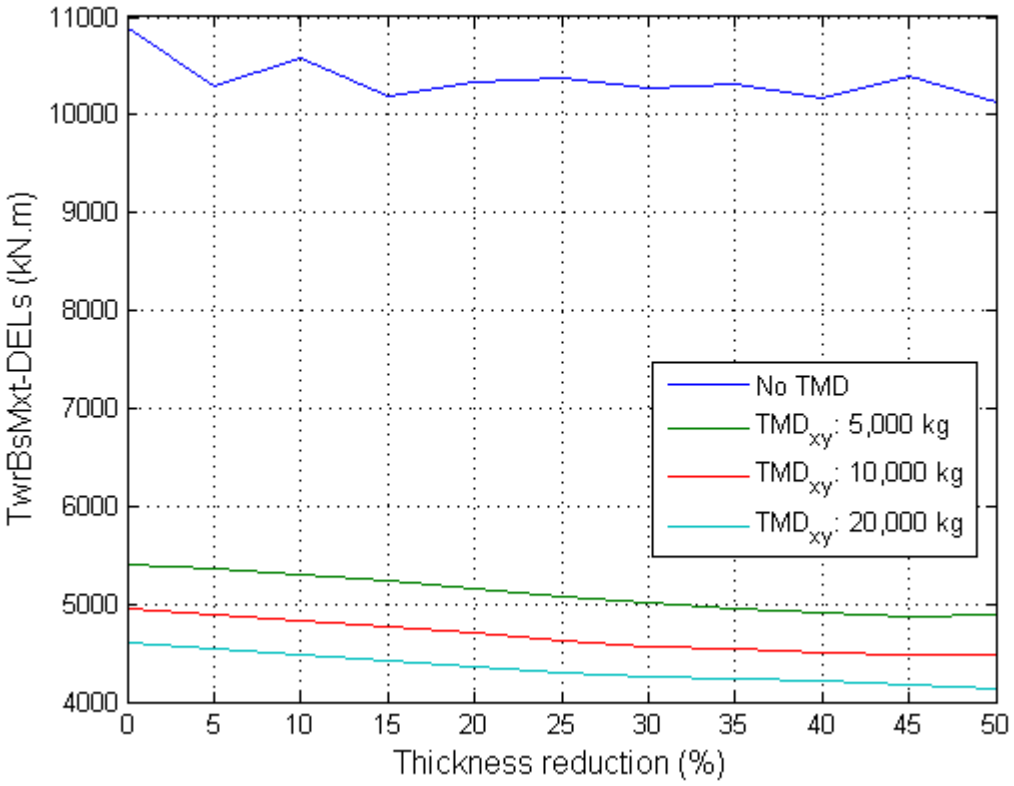

Figure 5.4. Damage equivalent loads in the fore-aft direction for different TMD configurations

The 5,000 kg TMD causes a reduction of 50.5% of the DEL in the side-side direction. The 10,000 kg and 20,000 kg configurations provide 54.5% and 57.7% reductions of the side-side DEL for 0% thickness reduction.

A general conclusion can be obtained from this analysis, as the TMD mass increases, the fatigue load reduction increases. Another conclusion is that the increase of TMD mass value has lower effects as the mass values increase. A higher decrease can be observed from the $No\,TMD$ case to the $TMD_{xy} : 5,000\ kg$ compared to the other TMD mass values. The thickness reduction reduces the DEL in the fore-aft direction, but it should be noted that these are not the stress values - the physical

properties (cross sectional area, polar moment of inertia, etc.) of the structure are not taken into account.

5.1.1.2 Damage equivalent stresses

The damage equivalent loads from the previous section are converted into stresses using Equation 4.17. Figure 5.5 shows the combined DEL stresses according to Equation 4.18.

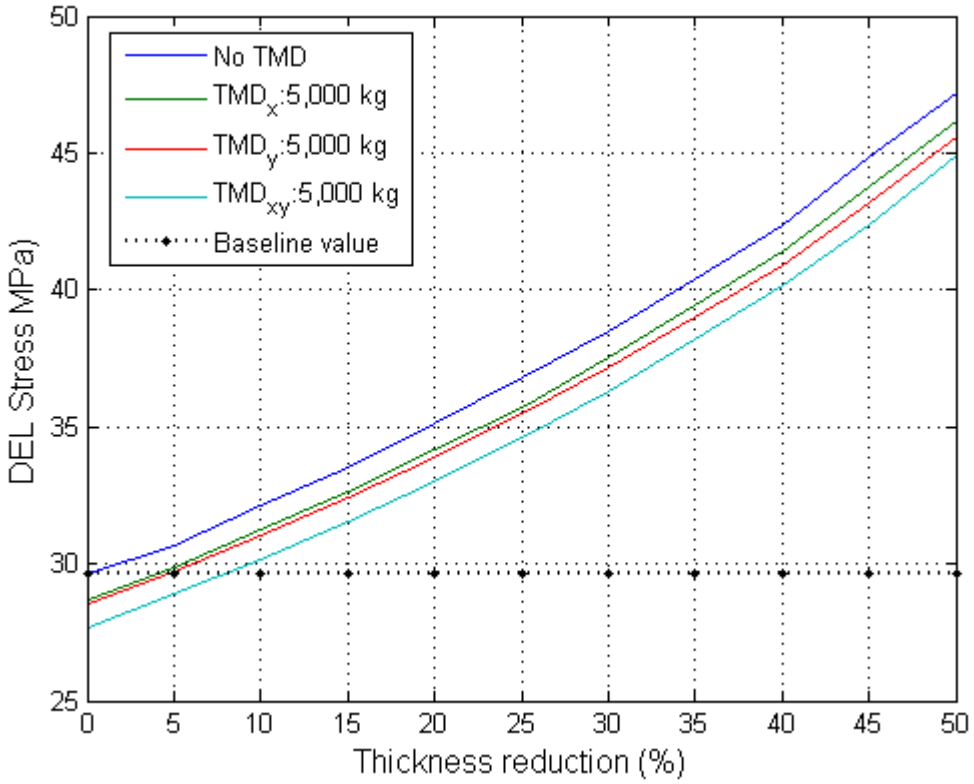

Figure 5.5. Damage equivalent stresses for TMD mass of 5,000 kg

The effect of the thickness reduction as well as the TMD translational direction can be seen in this analysis. The stress values that are equivalent to the baseline turbine are obtained at 4.9%, 5%, and 8% tower-monopile thickness reductions for the TMD_x, TMD_y, and TMD_{xy} cases, respectively. The TMD_x and TMD_y have

close results, but the TMD_{xy} case yields lower DEL stress values as the thickness reduction increases. Therefore, it is concluded that the use of the TMD_{xy} case is more effective in reduction of the DELs and DEL stress values as the thickness reduction is applied.

The DEL stress for different TMD mass values for the TMD_{xy} configuration can be seen in Figure 5.6.

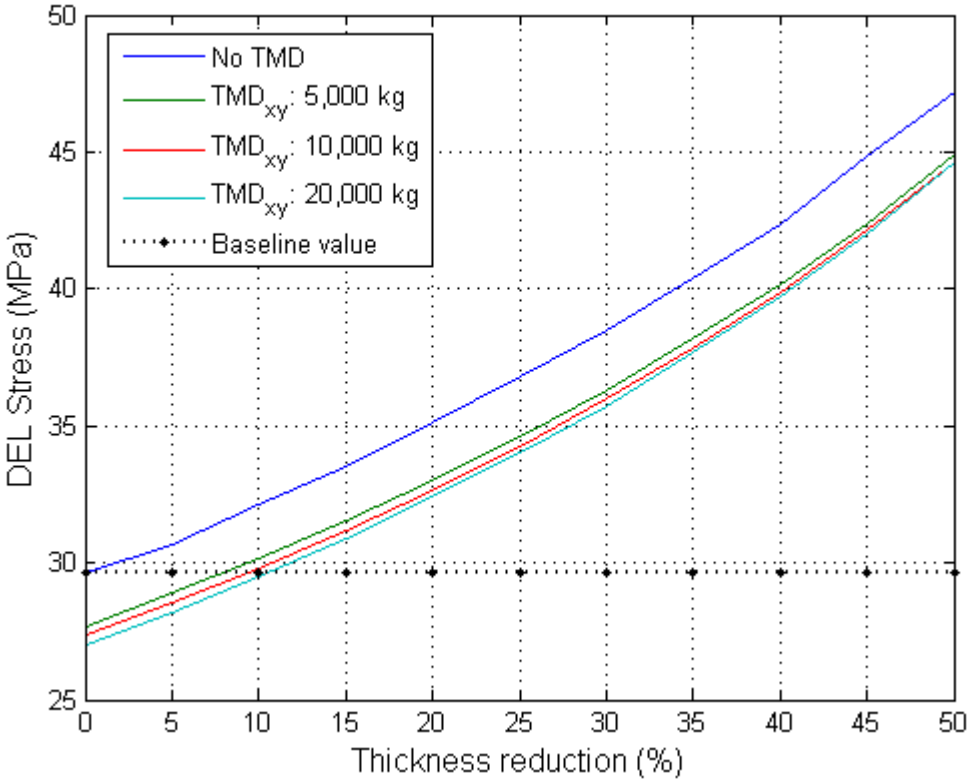

Figure 5.6. DEL Stresses for different TMD configurations

The stress values that are equivalent to the baseline turbine are obtained at 8%, 10%, and 11% tower-monopile thickness reductions for the 2-TMD cases of $5,000\ kg$, $10,000\ kg$, and $20,000\ kg$ cases, respectively. The use of the higher TMD mass values causes more reductions in DEL stress than was previously observed in the damage equivalent loads.

5.1.2 Maximum operational loads

Maximum operational load results are presented in this section.

The maximum operational stresses for DLC 1.2 case are combined using Equation 4.16 and presented in Figure 5.7 for a TMD mass of 5000 kg.

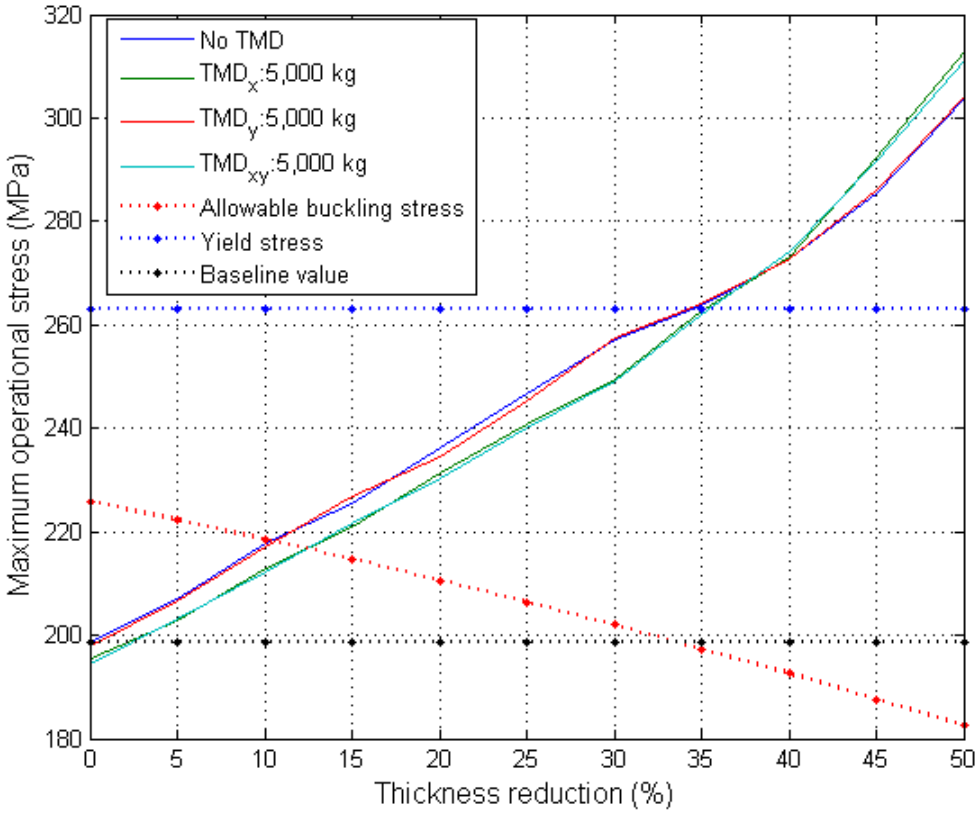

Figure 5.7. Maximum operational stresses for TMD configurations with 5,000 kg mass

Although, Stewart suggests that the TMD is not specifically designed to reduce the maximum operational loads in the structure, the following reductions are obtained due to the reduction in the amplitude of the bending moment [44]. The effect of the use of different translational directions of the TMDs can be concluded from these results. TMD_x and TMD_{xy} allow approximately 3% thickness reduction of the

tower-monopile structure before exceeding the baseline stress value for a 0% thickness reduction. The $No\,TMD$ and TMD_y cases have nearly equal results. The allowable local buckling curve crosses the results of the simulations at 10% for the $No\,TMD$ and TMD_y cases, and 13% for the TMD_x, and TMD_{xy} cases. Considering the yield stress of the steel with a factor of safety of 1.35, the yielding occurs at 263 MPa. Therefore, the yielding is not a design driver in this case. It can be concluded that the limiting criteria is the baseline turbine stress comparison (not local buckling, nor yielding of the material).

In Figure 5.7, it is observed that the use of the TMD_x and TMD_{xy} reduces the maximum stresses until a thickness reduction of approximately 35% when the results are compared to the $No\,TMD$ and TMD_y cases.

Next, the effect of the TMD mass value on the maximum operational stresses for DLC 1.2 case can be seen in Figure 5.8.

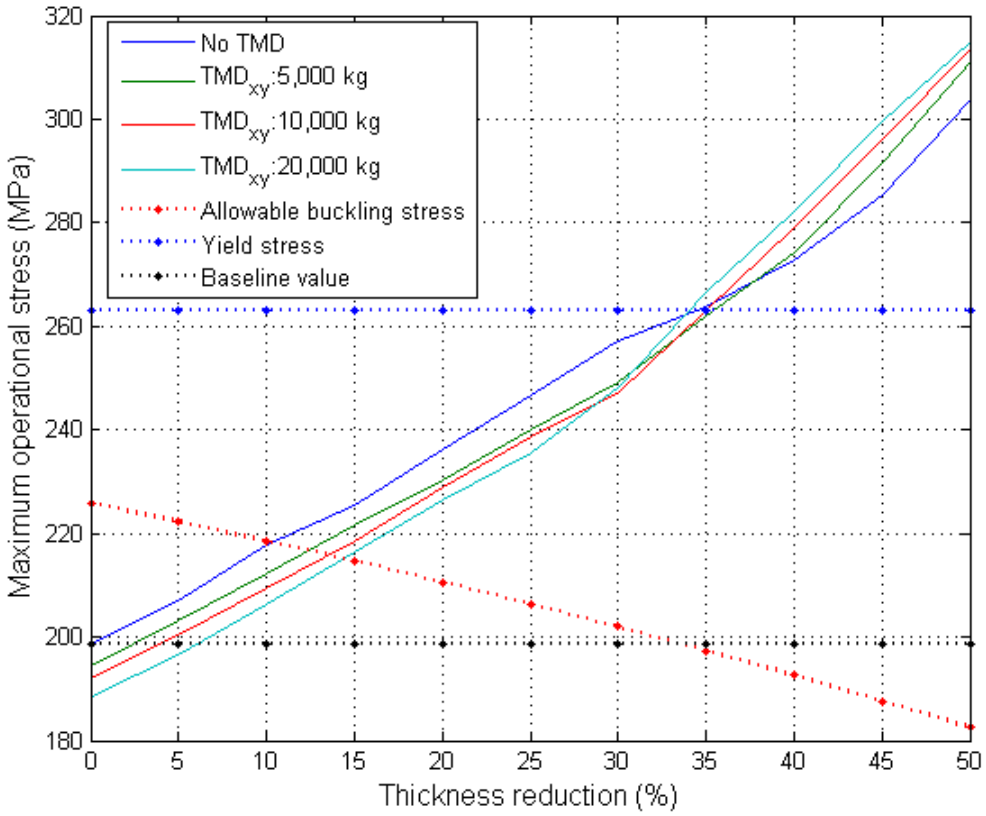

Figure 5.8. Maximum operational stresses for different TMD configurations

Generally, lower stress values are obtained as the TMD mass increases. The TMD masses of 5,000 kg, 10,000 kg, and 20,000 kg allows 3%, 4.9%, and 6.2% thickness reduction according to the baseline equivalent stress method, respectively. The buckling occurs at 10% thickness reduction for the $No\ TMD$ case, at 13% for the TMD mass configuration of 5,000 kg. The 10,000 kg and the 20,000 kg follows with 14.2% and 14.5% thickness reduction. The yielding of the material exceeds the buckling criteria since it is expected to occur at 263 MPa (including the factor of safety, 1.35). This analysis concludes that the use of 20,000 kg TMD mass value provides higher allowable thickness reductions for the baseline equivalent stress method which is the limiting criteria among the other methods.

An example time series of tower-monopile base bending moment in the fore-aft direction is illustrated in Figure 5.9, for a wind speed of 12 m/s, significant wave height of 2 m and peak spectral period of 7.5 s, for a 10 second window of the simulation. Identical wind and wave seeds are used for both thickness values.

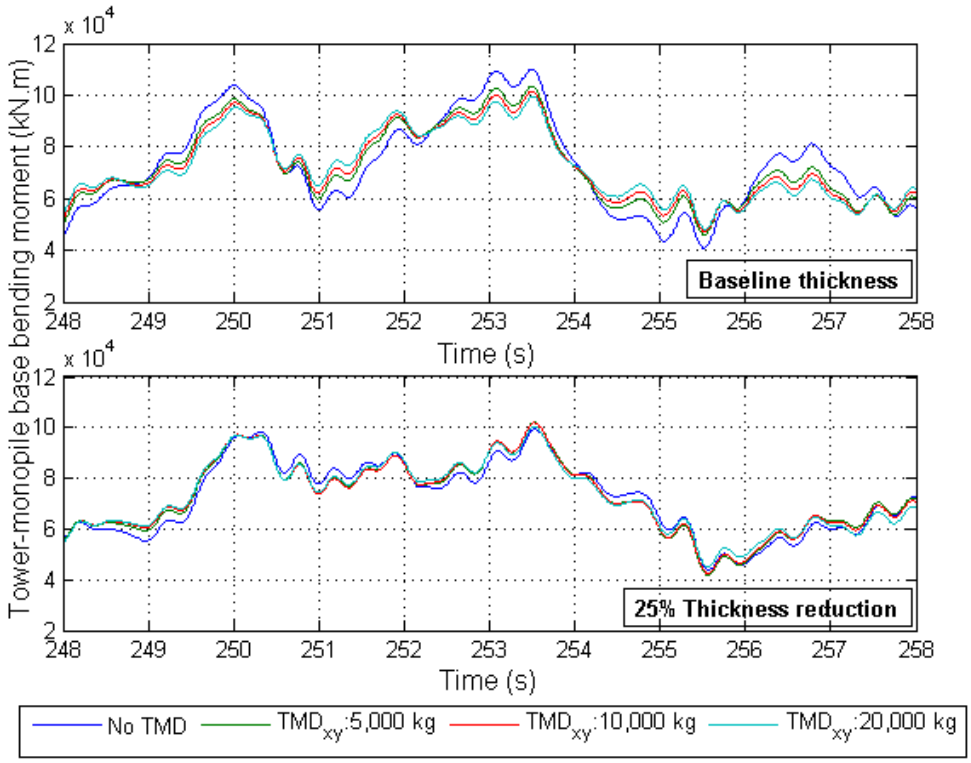

Figure 5.9. Time series of tower-monopile base bending moment in the fore-aft direction for DLC 1.2

The upper plot shows the bending moment in the fore-aft direction for the baseline thickness. Higher amplitudes are observed for the *No TMD* case, with reduced amplitudes for the TMD cases. The lower plot illustrates the base bending moment for a 25% thickness reduction. In this case, the loads are reduced due to the decreased inertia of the structure. However, higher stress values occur when the cross-sectional area of the tower-monopile base is taken into account, as shown in Figure 5.8. The effect of the TMD is not as clear in this case.

The time series of tower-monopile base bending moment in the side-side direction is shown in Figure 5.10. The same wind and wave characteristics are used as Figure 5.9.

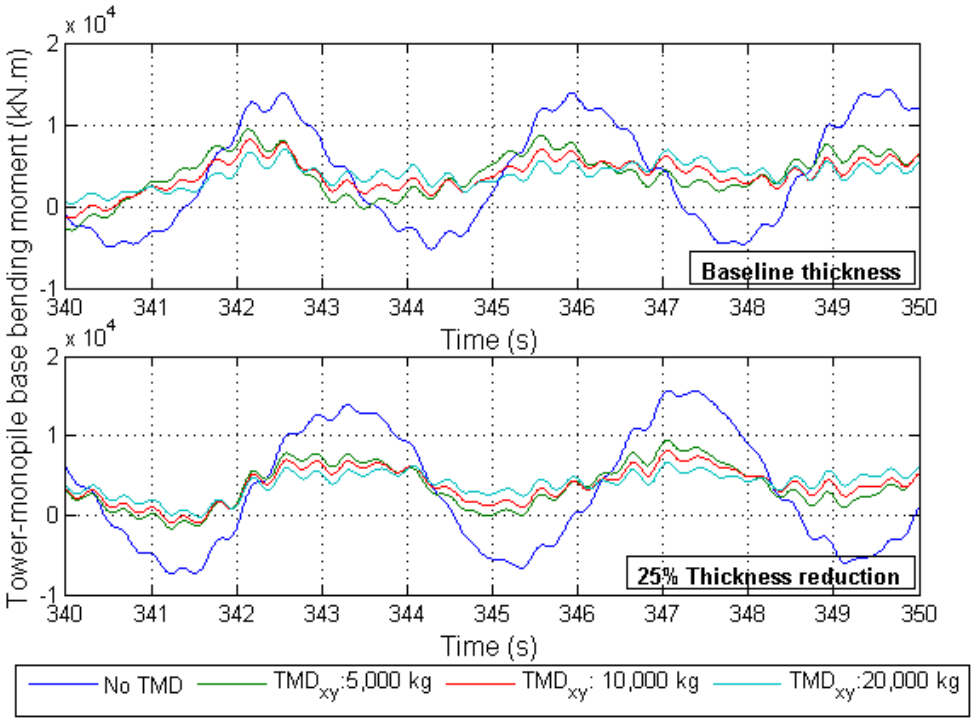

Figure 5.10. Time series of tower-monopile base bending moment in the side-side direction for DLC 1.2

The effect of the TMD is now clear. The use of the TMD is more effective in the side-side direction due to the lower damping of the rotor in this direction. The upper plot illustrates the bending moment in the side-side direction for the baseline thickness. Much higher amplitudes are observed for the $No\ TMD$ case, with reduced amplitudes for the TMD cases. The reduction increases, as the TMD mass is increased. The lower plot shows the base bending moment for a 25% thickness reduction. Again, the loads are reduced due to the decreased inertia of the structure. However, Figure 5.8 shows that the stress values are higher when the cross-sectional area of the tower-monopile base is taken into account.

5.1.3 Global buckling loads

Euler's global buckling method is applied to the results according to Equation 4.23. The $2 - TMD$ configurations are considered for this analysis, since the tower-monopile mass reduction is maximized for these cases. Figure 5.11 shows the global buckling conditions for the configurations.

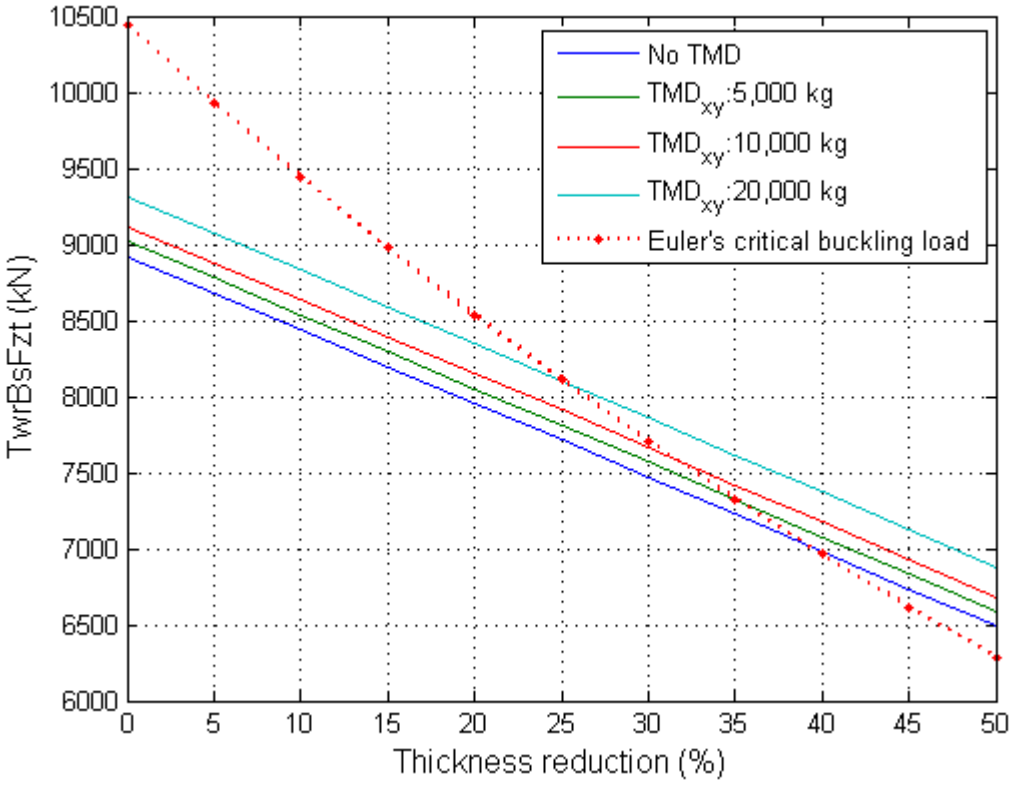

Figure 5.11. Global buckling loads with respect to thickness reduction

According to Figure 5.11, global buckling occurs approximately at 40% thickness reduction for a $No\ TMD$ case. Global buckling occurs at 35%, 32%, and 25% for the TMD_{xy} cases of 5,000 kg, 10,000 kg, and 20,000 kg, respectively.

As the tower-monopile top mass is increased, the global buckling becomes a more important consideration. However, the previous analysis indicated that tower-

monopile thickness can be reduced up to 15% at most; therefore, the global buckling is not a limiting criteria for this research.

5.1.4 Summary of the results of DLC 1.2

The use of the $1-TMD$ cases with different TMD masses are also simulated and the results are obtained. Table 5.1 indicates the allowable thickness reduction across the specified design criteria, and TMD configurations for the DLC 1.2 case.

Load Type	**Design Criteria**	**No TMD**	**TMD Mass: 5,000 kg**			**TMD Mass: 10,000 kg**			**TMD Mass: 20,000 kg**		
			TMD_x	TMD_y	TMD_{xy}	TMD_x	TMD_y	TMD_{xy}	TMD_x	TMD_y	TMD_{xy}
DEL Stress	Baseline equivalent stress method	N/A	5.0%	4.9%	8.0%	5.0%	5.0%	10.0%	7.0%	5.0%	11.0%
Maximum Operational Stress	Baseline equivalent stress method	N/A	3.0%	0.0%	3.0%	4.9%	0.0%	4.9%	6.0%	0.0%	6.2%
	Yield stress method	34.0%	35.0%	34.0%	35.0%	35.0%	34.0%	35.0%	37.0%	34.0%	33.0%
	Allowable buckling stress method	10.0%	13.0%	10.0%	13.0%	14.0%	10.0%	14.2%	14.5%	14.0%	14.5%
Vertical Load	Euler's method	40.0%	37.0%	37.0%	35.0%	35.0%	35.0%	32.0%	32.0%	32.0%	25.0%

Table 5.1. Allowable percent reductions according to design criteria and TMD configuration for DLC 1.2 case

In the results of this section, it can be concluded that the yielding of the material and the global buckling method are not design drivers when they are compared to the other methods listed in the design criteria. The baseline equivalent stress method indicates more conservative results depending on the load type. Using the baseline equivalent stress method, it can be seen that nearly double allowable thickness reductions are obtained for the DEL fatigue stress compared to the maximum operational stress. The maximum operational stress criteria yields the limiting allowable thickness reductions, which are 3.0%, 4.9%, and 6.2% for the $2-TMD$ cases with the mass values of 5,000 kg, 10,000 kg, and 20,000 kg, respectively. Especially for DEL stress values, the higher effectiveness of the $2-TMD$ cases than the $1-TMD$ cases are concluded. The extreme loads section includes only the $2-TMD$ cases, based on this conclusion.

These load reductions are obtained according to the FAST-SC configurations that are used for DLC 1.2 case. The expected values of the significant wave height and peak spectral period are used. Additionally, the multi directionality of the wind and waves are not taken into account. The realistic conditions are expected to be more complicated which requires a further study using more detailed wind and wave directionality configurations for this design load case.

5.2 Extreme Loads

This section contains the results of the DLC 1.4, 2.3, 4.2, and 6.3a simulations. The results are organized according to the design load cases:

- Extreme operating gust during power production plus occurrence of a fault
- Extreme operating gust analysis during a normal shutdown
- Extreme coherent gust analysis with direction change
- Extreme wind model with a recurrence period of 1 year

The maximum stresses are used to compare the results of these discrete events.

5.2.1 Extreme operating gust

5.2.1.1 Power production plus occurrence of a fault

The maximum stresses for an EOG during power production plus occurrence of a fault can be seen in Figure 5.12.

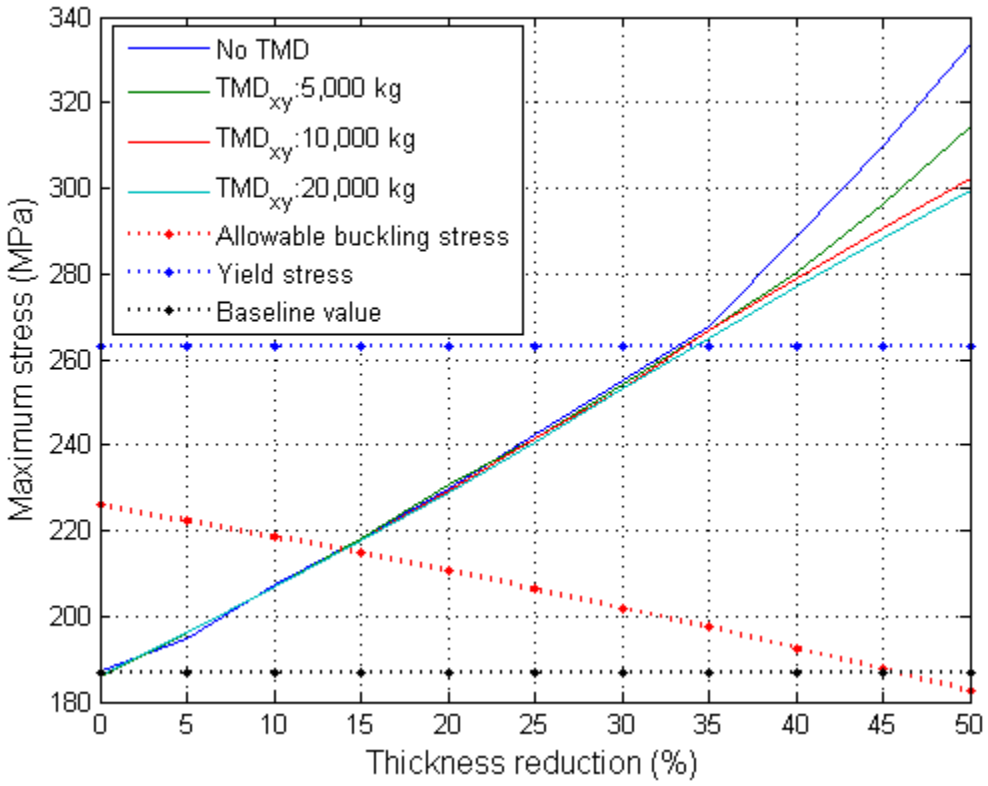

Figure 5.12. Maximum stresses for extreme operating gust analysis during power production plus occurrence of a fault

The $No\,TMD$ case has slightly higher maximum stresses, but it should be noted that the stress values are quite low compared to the maximum operational stress values, shown in Figure 5.8. The allowable local buckling curve crosses the results approximately at 14% for all configurations. Therefore, the yielding of the material (263 MPa, with a factor of safety of 1.35) is not a limiting criteria, since it crosses the results at approximately 33% thickness reduction. There are negligible differences between the TMD cases. This makes the baseline equivalent method questionable for this analysis.

A time series of the tower-monopile base bending moment in the fore-aft direction can be seen in Figure 5.13.

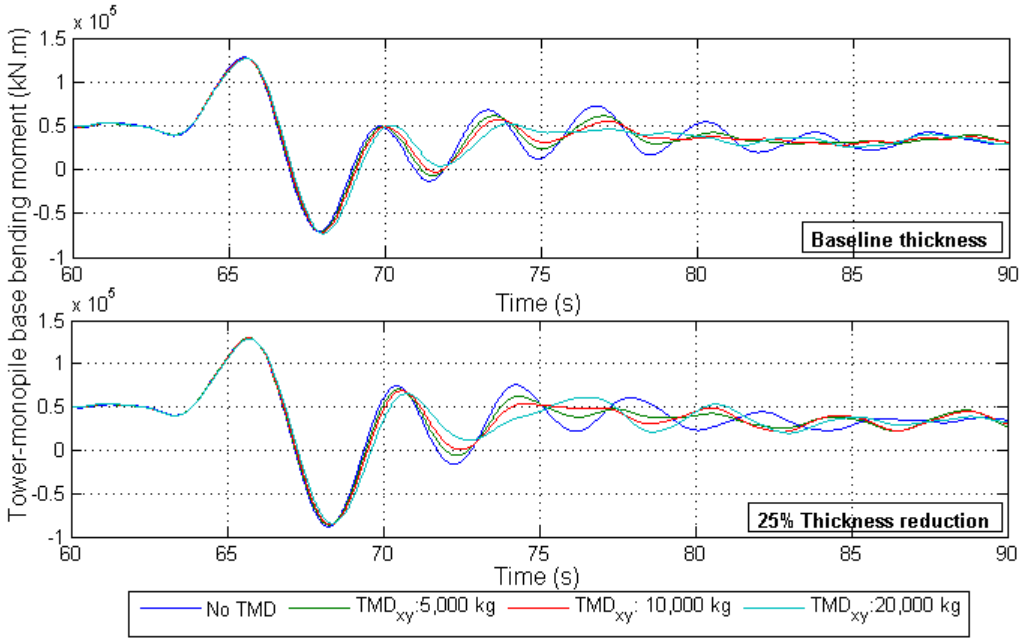

Figure 5.13. Time series of tower-monopile base bending moment in the fore-aft direction for DLC 2.3

The loss of grid connection is simulated with a generator shutdown in 65^{th} second. The HSS brake is then employed to stop the generator. The use of the TMDs has negligible effects on the highest peaks for both thicknesses. However, later peaks are observed to be higher for the 25% thickness reduced candidate. The effect of the TMDs can be seen in these peaks. The highest peaks are observed for a $No\ TMD$ case. The increase of the TMD mass also reduces the amplitudes of these peaks. It should be noted that the fluctuation of the base bending moment of the structure caused by the generator shutdown event seem to be stabilized in a short time period for all cases.

5.2.1.2 Normal shutdown

The maximum stresses for the DLC 4.2 load case are shown in Figure 5.14.

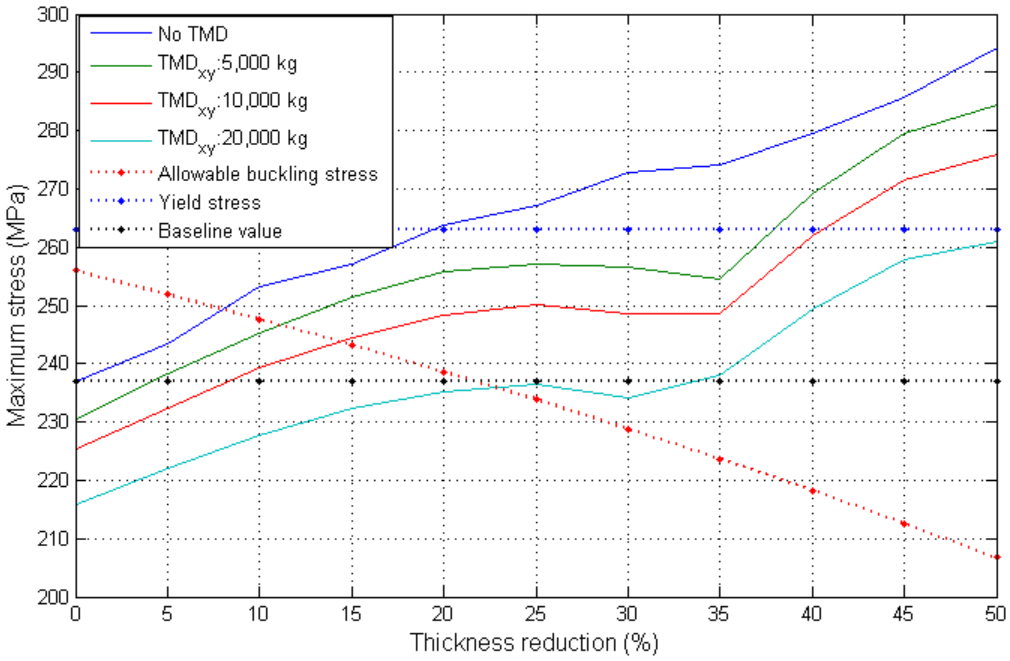

Figure 5.14. Maximum stresses for extreme operating gust analysis during a normal shutdown

The extreme operating gust analysis during normal shutdown clearly shows the effect of the usage of the TMDs during an extreme event. The use of TMDs decreases the maximum stress values, as the thickness is reduced. The baseline equivalent stress method yields a 4%, 9%, and 25% allowable thickness reductions for the $2-TMD$ case with a TMD mass of 5,000 kg, 10,000 kg, and 20,000 kg, respectively. For the allowable local buckling stress method, the allowable thickness reduction is 8% for a $No\ TMD$ case. The $2-TMD$ cases follows with the 11%, 14%, and 23% allowable thickness reductions for the TMD mass values of 5,000 kg, 10,000 kg, and 20,000 kg, respectively. Because the local buckling limit is already exceeded even for a $No\,TMD$ case at 0% thickness reduction, a multiplication factor of 1.15 is applied to the limiting value. This method is considered based on the result of the baseline configuration with 0% thickness reduction, considering that it is designed including

the factor of safety. This discrepancy may also result from limitations of the local buckling theory explained in Section 4.3.2.4. The yielding occurs at nearly 19.0% thickness reduction for the $No\ TMD$ case. The TMD mass values of 5,000 kg, and 10,000 kg yield 38.0%, and 40.0% thickness reductions, respectively. The yield stress method allows thickness reductions greater than 50% with the use of a TMD mass of 20,000 kg. The design driver method is the baseline equivalent method for this analysis.

Some conclusions can be drawn in this analysis. As a general trend, as the TMD mass increases, larger allowable thickness reductions resulted. Another conclusion is that the highest stress values are obtained in this extreme event analysis. This suggests that the simulation of DLC 4.2 is the design driver across the applied extreme load cases so far.

The time series of the tower-monopile base bending moment in the fore-aft direction can be seen in Figure 5.15.

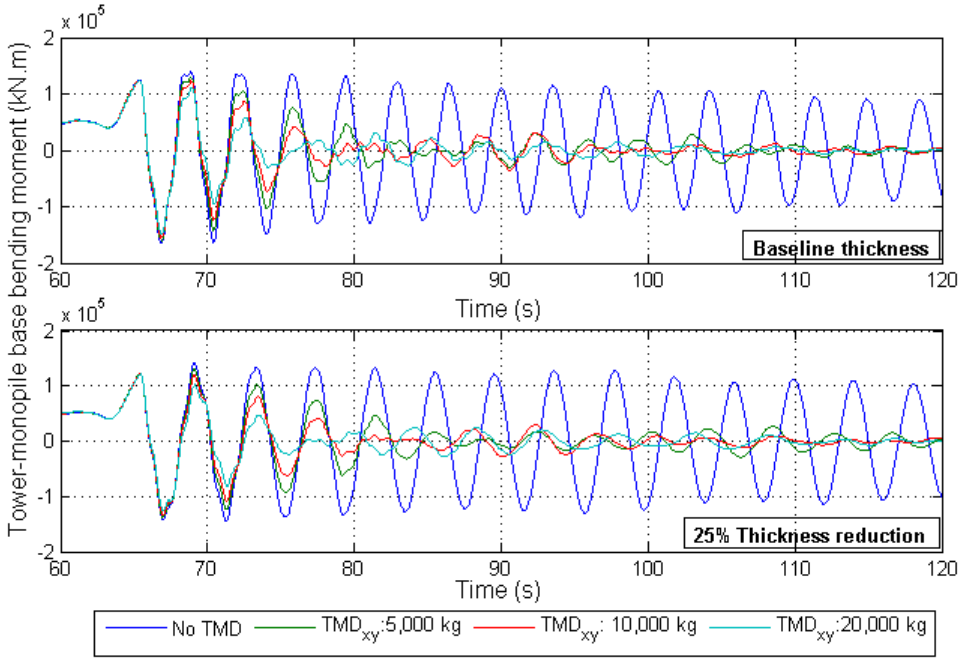

Figure 5.15. Time series of tower-monopile base bending moment in the fore-aft direction for DLC 4.2

The use of the TMDs reduces the amplitude of the tower-monopile base bending moment for both thicknesses. A *No TMD* case has a very slow decay, while the TMD cases yield more damping of the tower vibrations. The increase of the TMD mass value causes higher reductions, especially after the first highest peaks. The thickness reduction seems to produce lower loads, but it should be noted that the the stress values for these loads increase due to the decreased wall thickness of the overall structure.

5.2.2 Extreme coherent gust with direction change

The maximum stresses for the DLC 1.4 case can be seen in Figure 5.16.

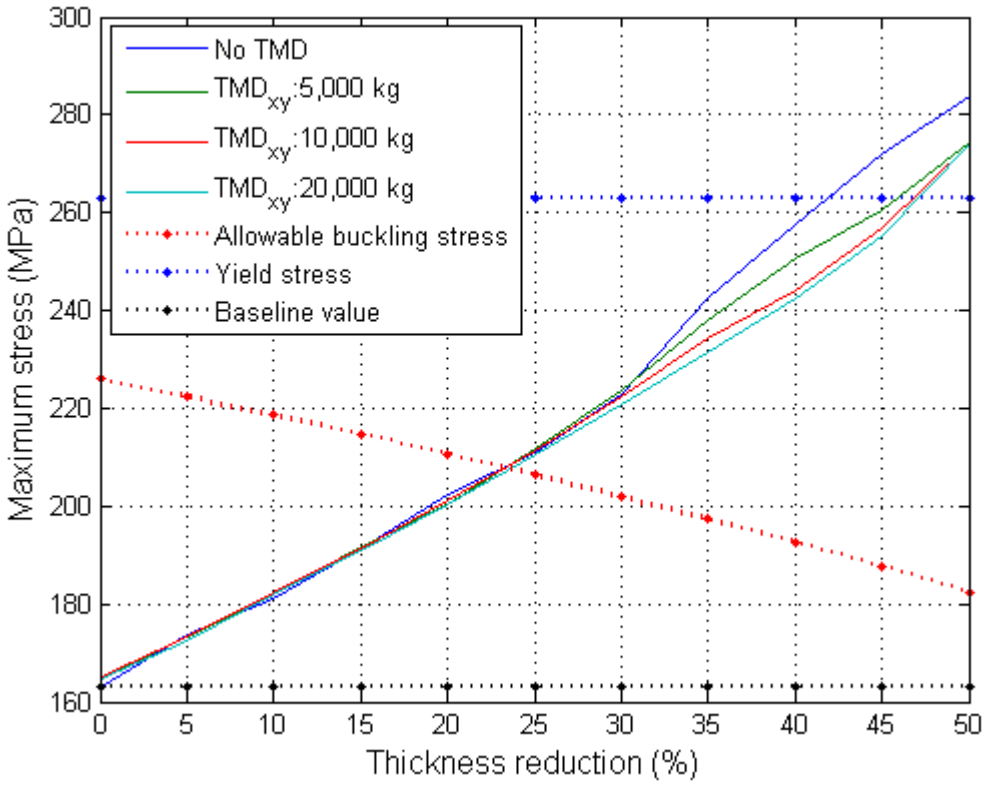

Figure 5.16. Maximum stresses for extreme coherent gust analysis

This analysis yields lower stress values compared to the previous extreme event cases. This enables higher thickness reductions, but these reductions are already limited by the previous analysis. It can be concluded that the extreme operating gust analysis yields higher maximum stress values than the extreme coherent gust with direction change analysis. This may be expected when the wind speed profiles of these events shown in Figures 3.4 and 3.5 are considered. The EOG profile has a more severe change in the wind speed that might cause higher aerodynamic loads than the ECD profile.

The time series of the tower-monopile base bending moment in the fore-aft direction is illustrated in Figure 5.17.

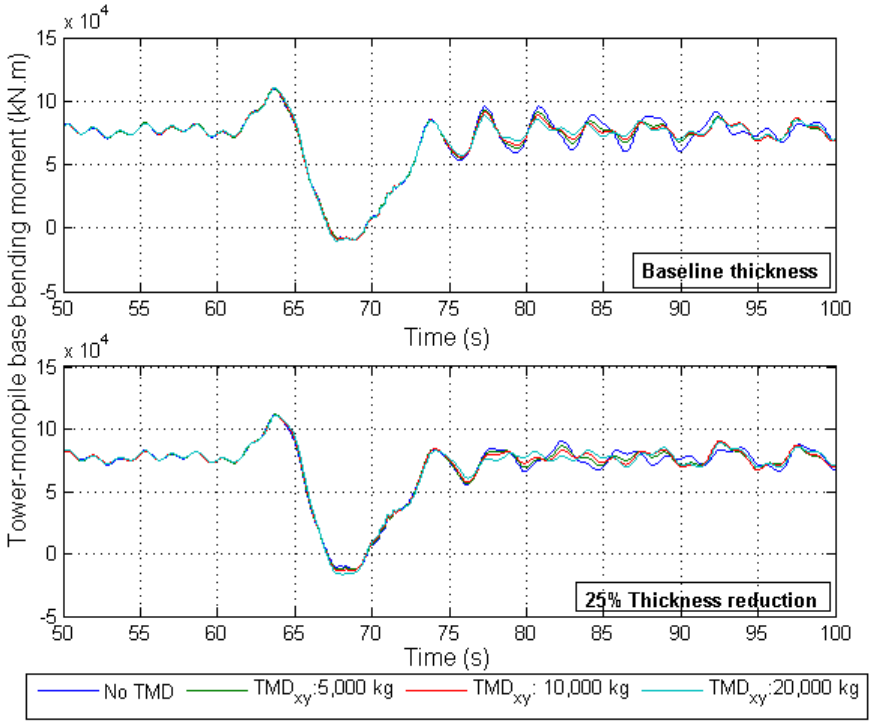

Figure 5.17. Time series of tower-monopile base bending moment in the fore-aft direction for DLC 1.4

It can be observed that the use of the TMDs has negligible effects in this analysis. Lower loads occur in this event compared to the previous extreme events. Again, lower loads are obtained for a 25% thickness reduction, but the stress values increase according to the previous section.

5.2.3 Extreme wind model

The maximum stresses that are combinations of all loads at the tower-monopile base are presented in Figure 5.18 for DLC 6.3a case.

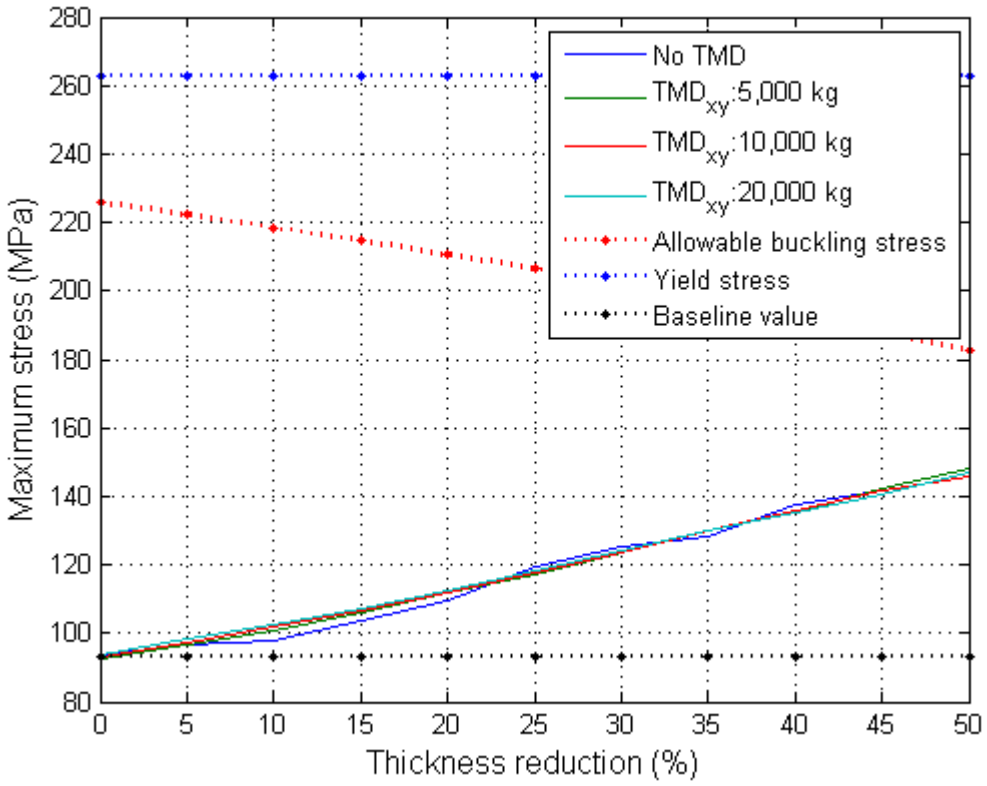

Figure 5.18. Maximum stresses for extreme wind model analysis

The lowest stress values are obtained in this analysis. The use of the TMDs has negligible effects on the results. The baseline equivalent method is not applicable due to the low stress values. The allowable local buckling limit and yield stress limit is far from the resulting stress values. Therefore, this analysis is not a design driver for this study.

It can be concluded that parking the turbine (the blades are in feathered position, HSS brake is applied during entire simulation) during an extreme wind condition yields lower stress values than other extreme events simulated in this research.

Parking the turbine aerodynamically reduces the extreme wind forces allowing the turbine to survive in this event.

The time series of the tower-monopile base bending moment in the fore-aft direction can be seen in Figure 5.19.

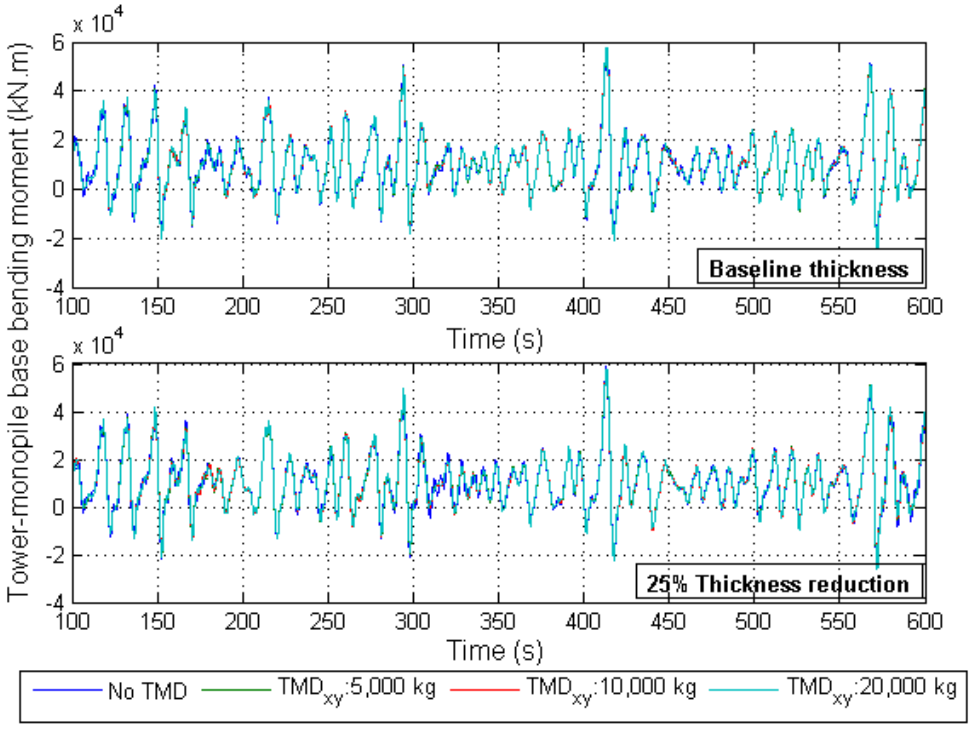

Figure 5.19. Time series of tower-monopile base bending moment in the fore-aft direction for DLC 6.3a

It can be seen that the tower-monopile base bending moment is nearly independent of the TMD configuration. The thickness reduction now causes a slight increase in the peaks of the plot.

5.2.4 Comparison of the results of all design load cases

This section presents the results of the $2-TMD$ cases with different TMD mass configurations. Table 5.2 shows the allowable thickness reduction percentage for a given TMD configuration, and the design criteria.

Design Load Case	Design Criteria		No TMD	TMD_{xy} 5,000kg	TMD_{xy} 10,000 kg	TMD_{xy} 20,000 kg
DLC 1.2	Baseline equivalent stress method	DEL stress	N/A	8.0%	10%	11.0%
		Maximum operational stress	N/A	3.0%	4.9%	6.2%
	Yield stress method		34.0%	35.0%	35%	33.0%
	Allowable local buckling method		10.0%	13.0%	14.2%	14.5%
	Euler's global buckling method		40.0%	35.0%	32.0%	25%
DLC 1.4	Baseline equivalent stress method		N/A	N/A	N/A	N/A
	Yield stress method		42.5%	46.0%	47.0%	48.0%
	Allowable local buckling method		23.0%	23.0%	23.0%	23.0%
DLC 2.3	Baseline equivalent stress method		N/A	N/A	N/A	N/A
	Yield stress method		34.0%	34.0%	34.0%	34.0%
	Allowable local buckling stress method		14.0%	14.0%	14.0%	14.0%
DLC 4.2	Baseline equivalent stress method		N/A	4.0%	9.0%	25.0%
	Yield stress method		8.0%	11.0%	14.0%	23.0%
	Allowable local buckling stress method		19.0%	38.0%	40.0%	50.0%
DLC 6.3a	Baseline equivalent stress method		N/A	N/A	N/A	N/A
	Yield stress method		N/A	N/A	N/A	N/A
	Allowable local buckling stress method		N/A	N/A	N/A	N/A

Table 5.2. Allowable percent reductions according to design criteria and TMD configuration for all design load cases

In the results of the extreme load cases, the highest maximum stress values are observed in the DLC 4.2 simulations rather than the DLC 1.4, 2.3, and 6.3a. Therefore, DLC cases 1.2 and 4.2 are chosen to make some final conclusions.

For all TMD configurations, the maximum operational stress in DLC 1.2 is the limiting factor for how much the tower-monopile thickness may be reduced. For TMD masses of 5,000 kg, 10,000 kg and 20,000 kg, the allowable thickness reductions are 3.0%, 4.9% and 6.2%, respectively. If the maximum operational stresses in DLC were not design driving, then the either the fatigue stresses in DLC 1.2 or maximum

stresses in DLC 4.2 would limit the thickness reductions with values of 4.0%, 9.0% and 11.0% for the TMD configurations.

Since the larger allowable thickness reductions of the tower-monopile structure are obtained for the DEL stress analysis, one can conclude that the use of the TMDs are more effective in reducing the fatigue loads rather than the maximum operational loads in the structure.

5.3 Spectral Analysis

The following section presents the spectral analysis of some of the configurations. In order to avoid resonance of the support structure and the rotor of the NREL 5 MW offshore wind turbine, the first natural frequency range of the tower-monopile system should be between 0.20 Hz and 0.34 Hz according to the Campbell Diagram in Figure 5.20 [1].

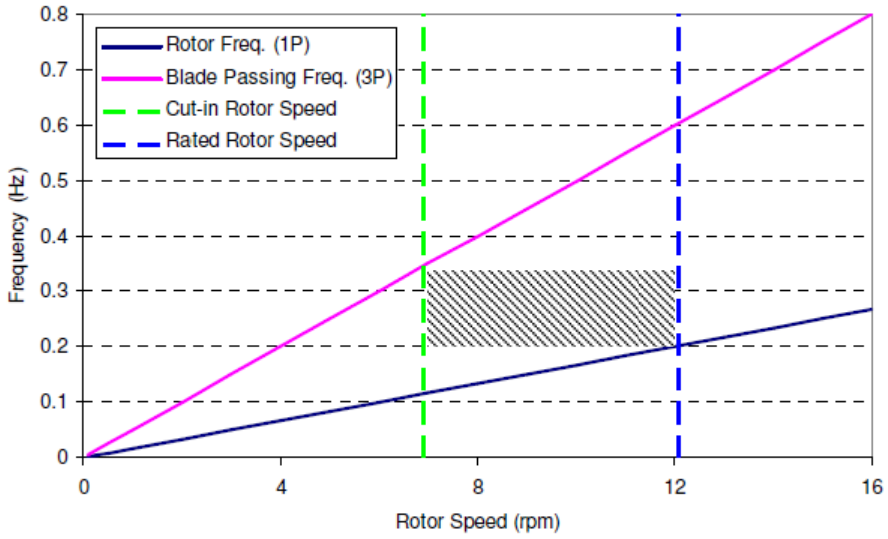

Figure 5.20. Campbell diagram of NREL 5MW offshore wind turbine [1]

The lower limit of the frequency range is the rotor rotating frequency (1P) at the rated rotor speed, and the upper limit is the blade passing frequency (3P) at the cut-in rotor speed [1].

The following analysis is performed for a wind speed of 12 m/s. The same random seed is used for all cases in order to observe the effect of the TMD, and the thickness reduction only. The selected configurations are the baseline thickness, 25% reduced thickness, and 50% reduced thickness. The TMD configurations are the $No\ TMD$ case, and the $2 - TMD$ cases with TMD masses of 5,000 kg, 10,000 kg, and 20,000 kg.

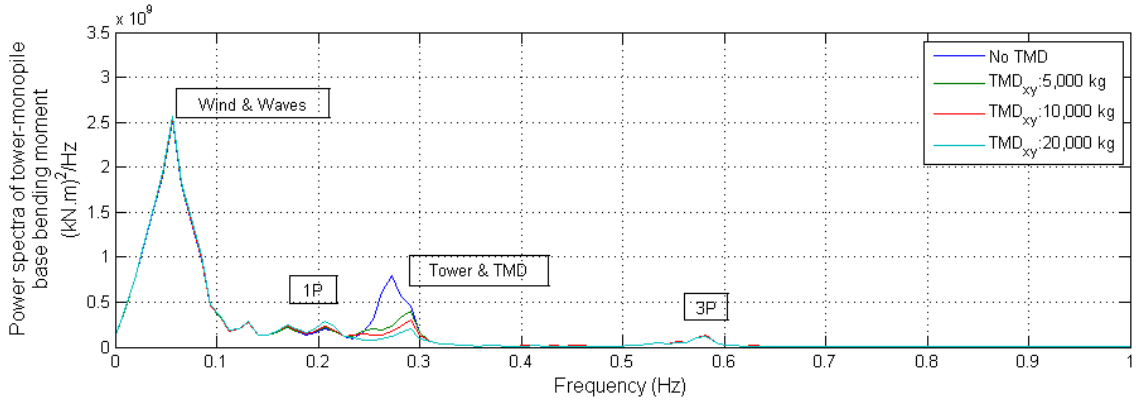

Figure 5.21. Power spectral density of tower-monopile base bending moment in the fore-aft direction for 0% thickness reduction

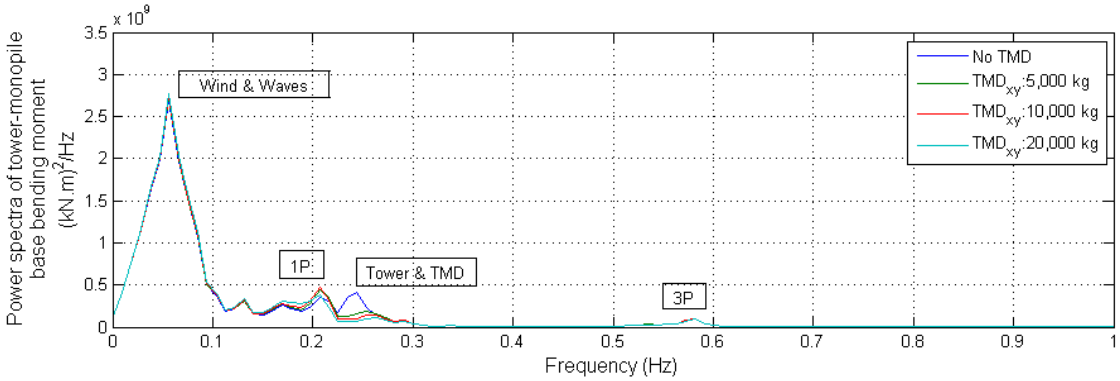

Figure 5.22. Power spectral density of tower-monopile base bending moment in the fore-aft direction for 25% thickness reduction

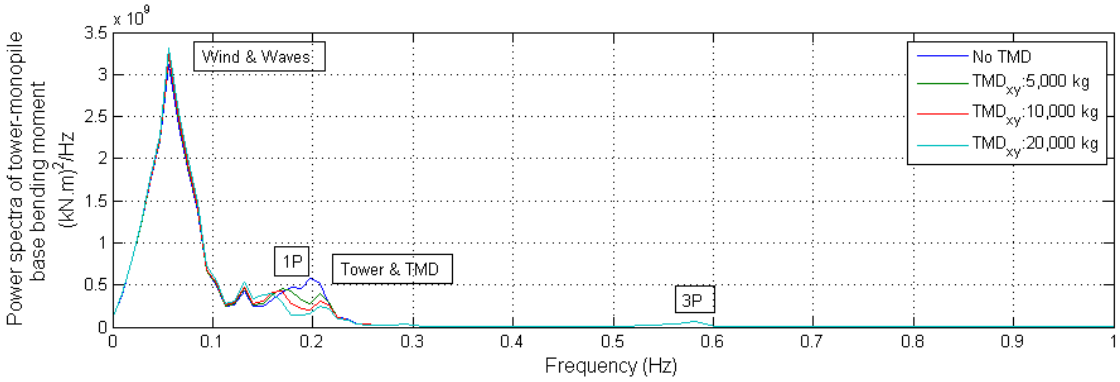

Figure 5.23. Power spectral density of tower-monopile base bending moment in the fore-aft direction for 50% thickness reduction

It can be seen that the presence of the TMD affects the power spectrum of the tower-monopile base bending moment in the fore-aft direction. The tower-monopile vibrational frequency and the TMD first natural frequency, tuned to the tower-monopile vibrational frequency, can be seen in the peak named "Tower & TMD". As the TMD mass increases, the amplitude of the "Tower & TMD" peak decreases for all thickness cases. This is due to the presence of the TMD in the structure. Likewise, the thickness reduction of the tower-monopile structure also causes a reduction of the power at the given frequency value of the "Tower & TMD". On the other hand, the amplitude of the power spectra, and the overall motion of the structure increases as the thickness is reduced. Especially, the loads caused by the wind and waves increases, as the thickness reduced. The previous study of Lackner and Rotea suggests using active tuned mass dampers instead of passive tuned mass dampers in this case to lower the wind and wave loads by tuning the dampers to the natural frequency of the waves. Another conclusion from this analysis is that the critical values of the first natural frequencies are observed for the $No\ TMD$ case for 50% thickness reduction. This is eliminated in the $1-TMD$ and the $2-TMD$ cases, but the previous results suggest that this thickness reduction is not applicable and limited by the design criteria of the study.

The maximum thickness reduction allowable is 6.2%, as concluded from the previous analysis. According to the Campbell Diagram in Figure 5.20, the frequency of this configuration is in the "safe region" since it is in the frequency range of 0.20 Hz and 0.34 Hz.

5.4 Cost Calculation

A simple cost calculation is applied to the results of this study. The cost of the implementation of structural control devices may vary depending on the selected type. A tuned mass damper may require higher manufacturing and construction cost than

a tuned liquid damper, or a tuned liquid columns damper. Assuming a tuned liquid columns damper provides equal load reductions compared to TMDs, the cost of the implementation may be minimized, since the mass in TLCDs is just water.

A tower is constructed by fan-shaped plate segments that are cut from rectangular parent steel plates and roll-formed and welded into cone sections [50]. A monopile is constructed through a similar process, but with different wall thickness. Steel is the core material of a tower-monopile structure. The NREL 5MW offshore monopile wind turbine tower has an overall mass of 522,617 kg [24]. A maximum of 6.2% thickness reduction is allowable determined by the design criteria of this research. The cold-rolled steel price can be assumed to be \$900 per metric tonne from Figure 5.24.

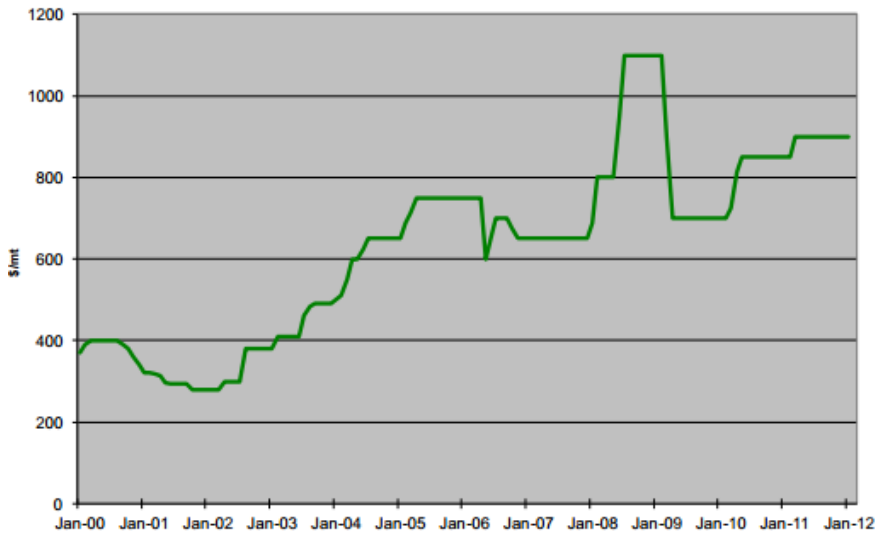

Figure 5.24. Cold-rolled steel prices [37]

Considering the overall mass of the reference wind turbine, the tower-monopile raw material cost is \$470,340. This cost is reduced to \$437,417 for a 6.2% thickness reduction. Additionally, the cost of the manufacturing process of the tower-monopile structure might decrease, as the thickness reduction is applied. The thickness re-

duction may also reduce the transportation cost due to lighter structures. However, it should be noted that this calculation is based on calculations that take only raw material into account. A detailed study may be performed to investigate the implementation cost of various structural control devices.

CHAPTER 6

CONCLUSION

This research examines if the usage of TMDs allows a thickness reduction of a tower-monopile structure of an offshore wind turbine.

The NREL 5MW monopile offshore wind turbine is chosen as the reference, and 5% thickness reduction is applied until a 50% thickness reduction increments are achieved. These 11 candidates are then processed to obtain structural properties. The modal shapes of these candidates are calculated by BModes, NREL's preprocessor. The tower-top monopile mass are changed according to the additional TMD mass. Passive mass damper devices that contains a mass, a spring, and a damper are selected as the structural control mechanism. The properties of the passive TMD are decided according to the previous study of Stewart. The TMD parameters are adjusted by considering $1-TMD$, and $2-TMD$ configurations with the translational directions in the fore-aft, and side-side directions.

The simulations are carried out using FAST-SC (FAST Structural control) which is a modified version of NREL's design code, FAST. Tower-monopile base loads are taken as the outputs of these simulations. Design criteria which consists of base-line equivalent method, maximum principle stress method, Euler's global buckling method, and allowable local buckling method is explained.

The assumptions that should be recalled are that the multi-directionality of the waves are not taken into account, and general approximations are used for the significant wave height, and the peak spectral period. The thickness reduction is only applied for the above mudline portion of the tower-monopile structure. Additionally,

the portion of the tower-monopile structure under the mudline is simulated assuming a rigid foundation. The outer radii are kept constant for all configurations, and inner radii are reduced. The same additional material on the outer surface of the structure is assumed for all configurations. The tower-monopile top mass affects the natural frequencies, and the modal displacements of the structure. Hence, each configuration has unique modal displacements. The TMD parameters are assumed to be optimum according to the previous research of Stewart. The design criteria focuses on the fatigue loads, and the maximum operational loads.

The first analysis is performed with a 5,000 kg TMD mass. The results of the fatigue load simulations (DLC 1.2) show that the use of passive TMDs reduces the tower-base loads allowing for 3.0% thickness reduction for the $2-TMD$ case. The limiting criteria is the baseline equivalent stress method with the maximum operational stresses. However, the damage equivalent stress comparison allows a thickness reduction of 8% before exceeding the baseline DEL stress for 0% thickness reduction. This indicates that the use of TMDs are more effective at reducing fatigue loads than ultimate loads. Finally, it is observed that the $2-TMD$ case yields lower loads than the $1-TMD$ cases.

Next, the analysis includes the effect of larger TMD mass values while still considering the thickness reduction of the tower-monopile structure. In this case, higher allowable thickness reductions are obtained at the end of the design criteria steps. The 10,000 kg mass configuration of the $2-TMD$ case provides a 4.9% thickness reduction before exceeding the baseline turbine's maximum operational stress value. On the other hand, a 6.2% thickness reduction is achieved for the 20,000 kg mass configuration according to the same criteria. The DEL stresses provide less conservative results up to 10% and 11% thickness reduction of the tower-monopile structure for 10,000 kg, and 20,000 kg in the $2-TMD$ mass configurations, respectively. To

conclude, the trend of increasing TMD mass value provide higher allowable thickness reductions for DLC 1.2 case.

Extreme event simulations are presented in the next section of this research. The simulations are performed according to IEC 61400-3 Design Standards. The extreme operating gust plus occurrence of a fault and extreme coherent gust with direction change analysis (DLC 1.4 and 2.3) is carried out. It is concluded that the use of the TMDs has negligible effects on the stress values; therefore, the baseline equivalent stress method is decided to be "not applicable" in these cases. The extreme wind model with a recurrence period of 1-year (DLC 6.3a) is presented as another extreme event. It is noted that also this event does not cause critical loads in the tower-monopile base. On the other hand, the extreme operating gust during a normal shutdown (DLC 4.2) yields the highest loads compared to the other extreme event simulations. The design driver is the baseline equivalent method for the TMD masses of 5,000 kg and 10,000 kg in this load case, allowing 4.0% and 9.0% thickness reductions, respectively. The yield stress method is the design driver with 23.0% thickness reduction for the TMD mass value of 20,000 kg.

The overall allowable thickness reduction for the $2 - TMD$ case with a TMD mass of 5,000 kg is 3.0% according to the baseline equivalent stress method. The use of the TMD masses of 10,000 kg, and 20,000 kg allows 4.9% and 6.2% thickness reductions. The design driver for these cases is the baseline equivalent stress method that is applied to the maximum operational stresses in DLC 1.2 case. If this criteria were not design driving, then the either the fatigue stresses in DLC 1.2 or maximum stresses in DLC 4.2 would be utilized to make a final decision.

It can be concluded that the performance of the given design criteria depends on the design load case. The baseline equivalent stress method is more applicable to the fatigue load case, since the larger differences for the DEL and maximum stresses are obtained in the results of this load case. This method is concluded to be not applicable

for the extreme load cases in which the use of the TMDs yields negligible effects on the stress values. The allowable local buckling method yields larger allowable thickness reductions than the baseline equivalent method. On the other hand, the yield stress method generally allows more allowable thickness reductions than the other methods.

Spectral analysis is performed in order to determine the safe first natural frequencies of the tower-monopile candidates. The power spectra of various time series are compared by considering the different TMD configurations and thickness reduction effects. The first natural frequencies of the candidate structures, which have the allowable thickness reductions determined in the previous analysis, are in the "safe region" according to the Campbell diagram of the NREL 5MW offshore wind turbine.

6.1 Concluding Remarks

Considering the allowable thickness reduction achieved in this study, the use of tuned mass dampers have an important effect on decreasing the dynamic loads in the structure. However, the practical use of tuned mass dampers still needs to be improved. Since the design and construction processes of tuned mass dampers are more complicated than its alternatives, tuned liquid dampers and tuned liquid columns dampers, the use of these structures may be considered. The raw material cost of the tower-monopile structures may be reduced through implementing these systems, but a further study should be performed in order to evaluate the economic analysis of the use of these systems individually.

APPENDIX

DETAILED RESULTS

The detailed results are presented in this appendix chapter. First section shows the outputs of FAST-SC for the $No\ TMD$ case, and the $2 - TMD$ cases. In the second section, the maximum stress values for each extreme event can be found.

A.1 Operational Loads (DLC 1.2)

The outputs listed below represent the maximum of 11 wind speeds and 6 wind seeds. Stress calculation tables are also included for different TMD mass values.

A.1.1 No TMD

Thickness Reduction (%)	Maximum Operational Loads						Damage Equivalent Loads (DELs)		
	TwrBsFxt (kN)	TwrBsFyt (kN)	TwrBsFzt (kN)	TwrBsMxt (kN.m)	TwrBsMyt (kN.m)	TwrBsMzt (kN.m)	TwrBsMxt (kN.m)	TwrBsMyt (kN.m)	Combined DEL (kN.m)
0	2721	-554	-8920	58460	130600	-12400	10900	21400	22304
5	2731	-572	-8679	54720	129300	-12500	10290	21200	21979
10	2717	-533	-8438	55610	129800	-12610	10580	21030	21887
15	2713	-450	-8197	45680	127700	-12650	10200	20890	21671
20	2707	-468	-7954	44780	127400	-12640	10340	20780	21601
25	2670	-445	-7711	48850	126800	-12580	10370	20670	21506
30	2638	-524	-7468	55230	125500	-12570	10270	20580	21399
35	2630	-424	-7224	46510	122300	-12630	10310	20510	21344
40	2617	-463	-6980	47070	120100	-12560	10170	20460	21265
45	2608	-432	-6734	43800	119600	-12720	10400	20560	21411
50	2596	-408	-6487	42870	121600	-12800	10140	20620	21407

Table A.1. Results of DLC 1.2 for a $No\,TMD$ case

Thickness reduction (%)	Stress Calculation									
	Outer Radius (m)	Base Thickness (m)	Area (m^2)	Second moment of area (m^4)	Bending stress due to TwrBsMyt (MPa)	Bending stress due to TwrBsFzt (MPa)	Shear stress due to TwrBsMzt (MPa)	Shear stress due to TwrBsFyt (MPa)	Maximum combined stress (MPa)	Damage Equivalent Stress (MPa)
0	3	0.0270	0.5066	2.2595	173.40	17.61	36.71	2.19	198.63	29.61
5	3	0.0257	0.4814	2.1480	180.59	18.03	38.95	2.38	206.87	30.70
10	3	0.0244	0.4575	2.0419	190.71	18.45	41.35	2.33	217.91	32.16
15	3	0.0231	0.4347	1.9410	197.38	18.86	43.65	2.07	225.50	33.50
20	3	0.0220	0.4130	1.8450	207.16	19.26	45.91	2.26	236.24	35.12
25	3	0.0209	0.3924	1.7537	216.91	19.65	48.08	2.27	246.83	36.79
30	3	0.0198	0.3729	1.6669	225.87	20.03	50.57	2.81	256.98	38.51
35	3	0.0189	0.3543	1.5843	231.58	20.39	53.47	2.40	263.80	40.42
40	3	0.0179	0.3366	1.5058	239.27	20.73	55.97	2.75	272.65	42.37
45	3	0.0170	0.3198	1.4312	250.70	21.05	59.65	2.70	285.38	44.88
50	3	0.0162	0.3039	1.3602	268.20	21.35	63.18	2.68	303.82	47.21

Table A.2. Stress calculation for the $No\,TMD$ cases

A.1.2 TMD_{xy}: 5,000 kg

Thickness Reduction (%)	Maximum Operational Loads						Damage Equivalent Loads (DELs)		
	TwrBsFxt (kN)	TwrBsFyt (kN)	TwrBsFzt (kN)	TwrBsMxt (kN.m)	TwrBsMyt (kN.m)	TwrBsMzt (kN.m)	TwrBsMxt (kN.m)	TwrBsMyt (kN.m)	Combined DEL (kN.m)
0	2706	-376	-9017	30860	127300	-12540	5393	20730	20851
5	2708	-334	-8777	30410	126600	-12470	5358	20570	20690
10	2699	-353	-8535	31790	126000	-12500	5296	20420	20538
15	2688	-354	-8295	31270	125100	-12580	5230	20290	20405
20	2674	-351	-8052	29210	123700	-12590	5154	20190	20301
25	2666	-351	-7810	30850	122600	-12590	5079	20130	20237
30	2655	-371	-7566	31910	120900	-12590	5012	20070	20174
35	2634	-359	-7322	33450	121300	-12640	4945	20060	20160
40	2602	-349	-7076	29510	120800	-12710	4913	20050	20148
45	2594	-335	-6833	28210	122700	-12680	4875	20120	20215
50	2590	-303	-6586	29050	125200	-12700	4898	20260	20355

Table A.3. Results of DLC 1.2 for a $2-TMD$ case with 5,000 kg TMD mass

Thickness reduction (%)	Stress Calculation									
	Outer Radius (m)	Base Thickness (m)	Area (m^2)	Second moment of area (m^4)	Bending stress due to TwrBsMyt (MPa)	Bending stress due to TwrBsFzt (MPa)	Shear stress due to TwrBsMzt (MPa)	Shear stress due to TwrBsFyt (MPa)	Maximum combined stress (MPa)	Damage Equivalent Stress (MPa)
0	3	0.0270	0.5066	2.2595	169.02	17.80	37.13	1.48	194.48	27.68
5	3	0.0257	0.4814	2.1480	176.82	18.23	38.85	1.39	203.03	28.90
10	3	0.0244	0.4575	2.0419	185.12	18.66	40.99	1.54	212.30	30.18
15	3	0.0231	0.4347	1.9410	193.36	19.08	43.41	1.63	221.60	31.54
20	3	0.0220	0.4130	1.8450	201.14	19.50	45.72	1.70	230.40	33.01
25	3	0.0209	0.3924	1.7537	209.73	19.90	48.12	1.79	240.01	34.62
30	3	0.0198	0.3729	1.6669	217.59	20.29	50.65	1.99	249.01	36.31
35	3	0.0189	0.3543	1.5843	229.69	20.67	53.51	2.03	262.12	38.17
40	3	0.0179	0.3366	1.5058	240.67	21.02	56.63	2.08	274.25	40.14
45	3	0.0170	0.3198	1.4312	257.20	21.36	59.47	2.09	291.56	42.37
50	3	0.0162	0.3039	1.3602	276.14	21.67	62.69	1.99	311.25	44.89

Table A.4. Stress calculation for the $2-TMD$ cases with the TMD mass of 5,000 kg

A.1.3 TMD_{xy}: 10,000 kg

Thickness Reduction (%)	Maximum Operational Loads						Damage Equivalent Loads (DELs)		
	TwrBsFxt (kN)	TwrBsFyt (kN)	TwrBsFzt (kN)	TwrBsMxt (kN.m)	TwrBsMyt (kN.m)	TwrBsMzt (kN.m)	TwrBsMxt (kN.m)	TwrBsMyt (kN.m)	Combined DEL (kN.m)
0	2697	-349	-9114	31220	125300	-12550	4949	20490	20586
5	2691	-340	-8874	31900	124400	-12510	4895	20340	20434
10	2684	-367	-8633	32440	123800	-12510	4838	20200	20292
15	2675	-354	-8393	29030	123000	-12550	4772	20090	20179
20	2670	-351	-8150	28500	122600	-12580	4701	20000	20086
25	2666	-356	-7908	28550	121700	-12590	4628	19950	20033
30	2655	-361	-7664	31250	119600	-12660	4573	19920	20000
35	2629	-324	-7419	31340	121600	-12700	4533	19910	19988
40	2600	-323	-7175	28190	123200	-12700	4504	19930	20006
45	2600	-300	-6931	28370	124900	-12730	4488	20020	20095
50	2595	-309	-6683	28780	126100	-12670	4480	20170	20243

Table A.5. Results of DLC 1.2 for a $2-TMD$ case with 10,000 kg TMD mass

Thickness reduction (%)	Stress Calculation									
	Outer Radius (m)	Base Thickness (m)	Area (m^2)	Second moment of area (m^4)	Bending stress due to TwrBsMyt (MPa)	Bending stress due to TwrBsFzt (MPa)	Shear stress due to TwrBsMzt (MPa)	Shear stress due to TwrBsFyt (MPa)	Maximum combined stress (MPa)	Damage Equivalent Stress (MPa)
0	3	0.0270	0.5066	2.2595	166.37	17.99	37.16	1.38	192.08	27.33
5	3	0.0257	0.4814	2.1480	173.75	18.43	38.98	1.41	200.32	28.54
10	3	0.0244	0.4575	2.0419	181.89	18.87	41.02	1.60	209.44	29.81
15	3	0.0231	0.4347	1.9410	190.11	19.31	43.31	1.63	218.66	31.19
20	3	0.0220	0.4130	1.8450	199.35	19.73	45.69	1.70	228.90	32.66
25	3	0.0209	0.3924	1.7537	208.19	20.15	48.12	1.82	238.78	34.27
30	3	0.0198	0.3729	1.6669	215.25	20.55	50.93	1.94	247.11	36.00
35	3	0.0189	0.3543	1.5843	230.25	20.94	53.77	1.83	262.95	37.85
40	3	0.0179	0.3366	1.5058	245.45	21.31	56.59	1.92	279.03	39.86
45	3	0.0170	0.3198	1.4312	261.81	21.67	59.70	1.87	296.28	42.12
50	3	0.0162	0.3039	1.3602	278.12	21.99	62.54	2.03	313.42	44.65

Table A.6. Stress calculation for the $2-TMD$ cases with the TMD mass of 10,000 kg

A.1.4 TMD_{xy}: 20,000 kg

Thickness Reduction (%)	Maximum Operational Loads						Damage Equivalent Loads (DELs)		
	TwrBsFxt (kN)	TwrBsFyt (kN)	TwrBsFzt (kN)	TwrBsMxt (kN.m)	TwrBsMyt (kN.m)	TwrBsMzt (kN.m)	TwrBsMxt (kN.m)	TwrBsMyt (kN.m)	Combined DEL (kN.m)
0	2679	-345	-9310	29260	122300	-12510	4608	20240	20319
5	2671	-350	-9070	28310	121400	-12510	4545	20110	20187
10	2668	-352	-8830	30480	121300	-12540	4485	20000	20075
15	2667	-350	-8588	28770	121200	-12570	4419	19910	19982
20	2667	-317	-8346	29180	120800	-12580	4357	19850	19920
25	2659	-313	-8104	27240	119500	-12640	4301	19810	19877
30	2640	-305	-7860	27870	119800	-12750	4260	19790	19856
35	2618	-296	-7616	27770	123400	-12710	4234	19820	19884
40	2601	-278	-7372	28100	124600	-12750	4209	19870	19933
45	2602	-293	-7126	28320	126400	-12680	4178	19980	20041
50	2635	-292	-6880	28320	126400	-12760	4127	20190	20247

Table A.7. Results of DLC 1.2 for a $2-TMD$ case with 20,000 kg TMD mass

Thickness reduction (%)	Stress Calculation									
	Outer Radius (m)	Base Thickness (m)	Area (m^2)	Second moment of area (m^4)	Bending stress due to TwrBsMyt (MPa)	Bending stress due to TwrBsFzt (MPa)	Shear stress due to TwrBsMzt (MPa)	Shear stress due to TwrBsFyt (MPa)	Maximum combined stress (MPa)	Damage Equivalent Stress (MPa)
0	3	0.0270	0.5066	2.2595	162.38	18.38	37.04	1.36	188.58	26.98
5	3	0.0257	0.4814	2.1480	169.56	18.84	38.98	1.45	196.71	28.19
10	3	0.0244	0.4575	2.0419	178.22	19.30	41.12	1.54	206.34	29.49
15	3	0.0231	0.4347	1.9410	187.33	19.76	43.38	1.61	216.44	30.89
20	3	0.0220	0.4130	1.8450	196.42	20.21	45.69	1.53	226.48	32.39
25	3	0.0209	0.3924	1.7537	204.42	20.65	48.31	1.59	235.65	34.00
30	3	0.0198	0.3729	1.6669	215.61	21.08	51.29	1.64	247.99	35.74
35	3	0.0189	0.3543	1.5843	233.66	21.50	53.81	1.67	266.70	37.65
40	3	0.0179	0.3366	1.5058	248.24	21.90	56.81	1.65	282.25	39.71
45	3	0.0170	0.3198	1.4312	264.96	22.28	59.47	1.83	299.77	42.01
50	3	0.0162	0.3039	1.3602	278.78	22.64	62.98	1.92	314.80	44.66

Table A.8. Stress calculation for the $2-TMD$ cases with the TMD mass of 20,000 kg

A.2 Extreme Events

The maximum stress values for each extreme design load case are presented in this section. The stress values are calculated with the same method used for the operational design load case.

A.2.1 Extreme coherent gust with direction change (DLC 1.4)

Thickness reduction (%)	Maximum Stresses (MPa)			
	No TMD	**TMD_{xy} : 5,000 kg**	**TMD_{xy} : 10,000 kg**	**TMD_{xy} : 20,000 kg**
0	163.12	164.64	164.97	164.76
5	173.62	173.40	173.47	172.68
10	181.24	182.04	182.11	181.73
15	191.20	191.89	191.19	190.94
20	202.20	200.17	201.05	200.46
25	210.93	211.86	211.26	210.64
30	222.90	223.52	222.53	220.61
35	242.55	238.10	234.40	231.63
40	257.68	250.81	244.33	242.40
45	271.85	260.42	256.75	255.14
50	283.71	274.56	274.00	274.07

Table A.9. Maximum stresses for DLC 1.4

A.2.2 Extreme operating gust during power production plus occurrence of a fault (DLC 2.3)

Thickness reduction (%)	Maximum Stresses (MPa)			
	No TMD	**TMD_{xy} : 5,000 kg**	**TMD_{xy} : 10,000 kg**	**TMD_{xy} : 20,000 kg**
0	187.26	185.46	186.05	186.44
5	194.82	196.00	196.20	196.47
10	207.65	206.69	206.90	206.74
15	218.06	218.13	217.89	218.03
20	229.97	230.53	229.30	228.96
25	242.35	241.58	241.31	241.13
30	255.06	254.42	253.78	253.22
35	267.86	267.00	267.09	265.37
40	283.51	281.01	279.31	277.69
45	300.90	292.61	291.45	288.91
50	323.97	304.44	302.78	299.89

Table A.10. Maximum stresses for DLC 2.3

A.2.3 Extreme operating gust during normal shutdown (DLC 4.2)

Thickness reduction (%)	Maximum Stresses (MPa)			
	No TMD	**TMD_{xy} : 5,000 kg**	**TMD_{xy} : 10,000 kg**	**TMD_{xy} : 20,000 kg**
0	236.91	230.49	225.24	215.68
5	243.30	238.32	232.25	221.91
10	253.35	245.20	239.39	227.64
15	257.19	251.37	244.50	232.45
20	263.78	255.75	248.20	235.20
25	267.02	257.18	250.25	236.59
30	272.16	256.45	248.46	234.26
35	274.38	254.62	248.67	237.89
40	279.60	269.16	261.90	249.36
45	285.64	279.48	271.41	257.80
50	294.27	284.44	275.96	260.98

Table A.11. Maximum stresses for DLC 4.2

A.2.4 Extreme wind model with a recurrence period of 1-year (DLC 6.3a)

Thickness reduction (%)	Maximum Stresses (MPa)			
	No TMD	**TMD_{xy} : 5,000 kg**	**TMD_{xy} : 10,000 kg**	**TMD_{xy} : 20,000 kg**
0	93.45	92.59	93.00	93.76
5	96.39	96.72	97.23	98.23
10	98.00	100.80	101.82	102.73
15	103.75	105.82	106.46	107.42
20	109.69	111.59	111.76	112.66
25	119.35	117.39	117.76	118.26
30	125.46	123.78	123.81	123.91
35	128.07	130.18	129.85	129.82
40	137.48	135.52	135.65	135.42
45	141.70	142.35	141.67	140.33
50	145.58	147.88	145.69	146.75

Table A.12. Maximum stresses for DLC 6.3a

BIBLIOGRAPHY

[1] American Bureau of Shipping, Corporate Offshore Technology, Renewables. Design standards for offshore wind farms, 2011.

[2] American Society of Civil Engineers, Ed. *Minimum Design Loads for Buildings and Other Structures*. ASCE Publications - Technology & Engineering, 2013.

[3] Banerji, et. al. Tuned liquid dampers for controlling earthquake response of structures. *Earthquake Engineering and Structural Dynamics 29*, 5 (April 2000), 587–602.

[4] Beer, et.al., Ed. *Mechanics of Materials*. McGraw-Hill Higher Education, 2012.

[5] Bir, G. S. User's guide to BModes (software for computing rotating beam coupled modes). Tech. Rep. NREL/TP-500-39133, National Renewable Energy Laboratory, 2005.

[6] Calderon, B. E. Design and optimization of a wind turbine tower by using a damper device. Master's thesis, Stuttgart University, 2009.

[7] Chantharasenawong, et. al. Preliminary design of 1.5-MW modular wind turbine tower. In *The* 2^{nd} *TSME Conference on Mechanical Engineering* (2011), TSME.

[8] Colwell, S., and Basu, B. Tuned liquid column dampers in offshore wind turbines for structural control. *Engineering Structures 31* (2009), 358–368.

[9] der Temple, J.V. *Offshore Wind Power*. In Twidell and Gaudiosi [48], 2009, ch. Offshore Turbines: Dynamics and Fatigue.

[10] Enevoldsen, I. Effects of a vibration mass damper in a wind turbine tower. *Mechanics of Structures and Machines 24*, 2 (1996), 155–187.

[11] European Wind Energy Association. Upwind: Design limits and solutions for very large wind turbines. `http://www.upwind.eu/~/media/UpWind/Documents/Home/21895_UpWind_Report_low_web.ashx`, March 2011.

[12] Freebury, G., and Musial, W. Determining equivalent damage loading for full-scale wind turbine blade fatigue tests. In *the* 19^{th} *Wind Energy Symposium* (2000), American Society of Mechanical Engineers, NREL.

[13] Global Wind Energy Council. Annual Market Update, 2012 Annual Report. `http://www.gwec.net/wp-content/uploads/2012/06/Annual_report_2012_LowRes.pdf`, April 2013.

[14] Gsanger, S., and Pitteloud, J.D. World Wind Energy Association, 2012 Annual Report. `http://www.wwindea.org/webimages/WorldWindEnergyReport2012_final.pdf`, May 2013.

[15] Guerrero-Lemus, R., and Martinez-Duart, J.M., Eds. *Lecture Notes in Energy 3 - Renewable Energies and CO_2*. Springer-Verlag, London, 2013.

[16] Hayman, G.J. MLife theory manual for version 1.00. Tech. Rep. NREL/TP-XXXXX, National Renewable Energy Laboratory, 2012.

[17] Hayman, G.J., and Buhl, Jr. M. MLife user's guide for version 1.00. Tech. Rep. NREL/TP-XXXXX, National Renewable Energy Laboratory, 2012.

[18] International Electrotechnical Commission. IEC 61400-1 Ed.3: Wind turbines - Part 1: Design requirements, 2005.

[19] International Electrotechnical Commission. IEC 61400-3 Ed.1: Wind turbines - Part 3: Design requirements for offshore wind turbines, 2009.

[20] Jamil, F., Zia, S., Abbasi, P.A., Ansari, M. To study of wind resistant stability of tubular wind turbine tower. Master's thesis, NED University of Engineering & Technology, 2012.

[21] Jonkman, B. J., and Kilcher, L. TurbSim user's guide: Version 1.06.00 (Draft Version). Tech. rep., National Renewable Energy Laboratory, 2012.

[22] Jonkman, J.M. Dynamics modeling and loads analysis of an offshore floating wind turbine. Tech. Rep. NREL/TP-500-41958, National Renewable Energy Laboratory, 2007.

[23] Jonkman, J.M., and Buhl, M.L. Fast user's guide. Tech. Rep. NREL-EL-500-38230, National Renewable Energy Laboratory, 2005.

[24] Jonkman, J.M., and Musial, W. Offshore code comparison collaboration (OC3) for IEA task 23 offshore wind technology and deployment. Tech. Rep. NREL/TP-5000-48191, National Renewable Energy Laboratory, 2010.

[25] Jonkman, J.M., Butterfield, S., Musial, W., and Scott, G. Definition of a 5-MW reference wind turbine for offshore system development. Tech. Rep. NREL/TP-500-38060, National Renewable Energy Laboratory, 2009.

[26] Kaldellis, J.K., and Zafirakis, D. The wind energy (r)evolution: A short review of a long history. *Renewable Energy 36*, 7 (2011).

[27] Kobor, et. al. Seismic response controlled structure with active mass driver system - part 1: Design. *Earthquake Engineering and Structural Dynamics 20* (1991), 133–149.

[28] Korkmaz, S. A review of active structural control: Challenges for engineering informatics. *Computers and Structures 89* (August 2011).

[29] Lackner, M. A., and Rotea, M.A. Passive structural control of offshore wind turbines. *Wiley Online Library 14*, 10 (2010).

[30] Lee, K., and Bang, H. A study on the prediction of lateral buckling load for wind turbine tower structures. *International Journal of Precision Engineering and Manufacturing 13*, 10 (October 2012), 1829–1836.

[31] Lynch, J. P. Active structural control research at Kajima Corporation. *The National Science Foundation's Summer Institute in Japan Program* (1998).

[32] Manwell, J., McGowan J., and Rogers, A., Eds. *Wind Energy Explained (Theory, Design and Application)*. John Wiley and Sons LTD, West Sussex, United Kingdom, 2009.

[33] Musial, W., and Ram, B. Large-scale offshore wind power in the united states: Assessment of opportunities and barriers. Tech. rep., National Renewable Energy Laboratory, Energetics, 2010.

[34] Navigant Consulting, Inc. Offshore wind market and economic analysis, 2012 annual market assessment. `http://www1.eere.energy.gov/wind/pdfs/offshore_wind_market_and_economic_analysis.pdf`, February 2013.

[35] Nicholson, J. C. Design of wind turbine tower and foundation systems: Optimization approach. Master's thesis, University of Iowa, 2011.

[36] Nixon, N. Timeline: The history of wind power. `http://www.theguardian.com/environment/2008/oct/17/wind-power-renewable-energy`, October 2008.

[37] NREL. Wind Energy Update: Wind Powering America. `http://www.windpoweringamerica.gov/pdfs/wpa/wpa_update.pdf`, January 2012.

[38] NREL. IECWind by Marshall Buhl. `http://wind.nrel.gov/designcodes/preprocessors/iecwind/`, March 2014.

[39] NREL. Wind maps. `http://www.nrel.gov/gis/images/offshore_wind/US-offshore-windmap-90-dpi600.jpg`, March 2014.

[40] Palazzo, B., and Petti, L. Aspects of passive control of structural vibrations. *Meccanica 32* (1997), 529–544.

[41] Pastia, et. al. Structural control systems implemented in civil engineering. *The Bulletin of the Polytechnic Institute of Iasi 51*, 1 (2005).

[42] Pelinovsky, Efim N., Kharif, C, Ed. *Extreme Ocean Waves*. Springer, 2008.

[43] Soong, T.T., and Spencer, Jr. B. F. Active, semi-active and hybrid control of structures. In *12 WCEE 2000: 12TH World Conference on Earthquake Engineering*.

[44] Stewart, G. M. Load reduction of floating wind turbines using tuned mass dampers. Master's thesis, University of Massachusetts, Amherst, 2012.

[45] Tamura, Y., Fujii, K., Ohtsuki, T., Wakahara, T., and Kohsaka, R. Effectiveness of tuned liquid dampers under wind excitation. *Engineering Structures 17*, 9 (1995), 609–621.

[46] Tegen S., Hand M., Maples B., Lantz E., Schwabe P., and Smith A. 2010 cost of wind energy review. Tech. Rep. NREL/TP-5000-52920, National Renewable Energy Laboratory, 2012.

[47] Tsouroukdissian, A.R., Fischer, T., Carcangiu, C.E., Kuhnle, B., Amo, I.P., Scheu M., and Martin M. Wind turbine tower load reduction using passive and semi-active dampers. In *Conference Proceedings* (2011), European Wind Energy Association, EWEA, pp. 102–105.

[48] Twidell, J., and Gaudiosi, G., Eds. *Offshore Wind Power*. Multi-Science Publishing Co. Ltd, Brentwood, Essex, UK, 2009.

[49] US Department of Energy. 20% Wind Energy by 2030 - Increasing Wind Energy's Contribution to U.S. Electricity Supply. `http://www.nrel.gov/docs/fy08osti/41869.pdf`, July 2008.

[50] World Steel Association. Steel Solutions in the Green Economy, Wind Turbines. `https://www.worldsteel.org/dms/internetDocumentList/bookshop/worldsteel-wind-turbines-web/document/Steel%20solutions%20in%20the%20green%20economy:%20Wind%20turbines.pdf`, 2012.